

INFRARED AND OPTICAL STAR COUNTS
IN THE PLANE OF THE GALAXY

A THESIS SUBMITTED FOR THE
DEGREE OF DOCTOR OF PHILOSOPHY

by

NICHOLAS EATON

Department of Astronomy
University of Leicester

1982

UMI Number: U328022

All rights reserved

INFORMATION TO ALL USERS

The quality of this reproduction is dependent upon the quality of the copy submitted.

In the unlikely event that the author did not send a complete manuscript and there are missing pages, these will be noted. Also, if material had to be removed, a note will indicate the deletion.



UMI U328022

Published by ProQuest LLC 2015. Copyright in the Dissertation held by the Author.
Microform Edition © ProQuest LLC.

All rights reserved. This work is protected against
unauthorized copying under Title 17, United States Code.



ProQuest LLC
789 East Eisenhower Parkway
P.O. Box 1346
Ann Arbor, MI 48106-1346



THESIS
647492
9 .8 .82

X752931813

SUMMARY

Infrared and optical star counts have been obtained to investigate the stellar distribution in the plane of the Galaxy. The discovery of an obscured infrared cluster of sources is presented and a search technique for finding such obscured sources using visible and near-infrared plates is discussed. The techniques and mathematical treatment of star counting are described and, as an introduction, a literature review of the galactic structure is given.

Optical star counts in a strip across the dark rift of the Galaxy, containing the line of sight to the galactic centre, indicate that the extinction in this direction starts to increase significantly at a distance of about 1500 pc, approximately at the distance of the Sagittarius arm. Counting the stars into reseau squares shows that the direction of the thickest extinction in the visible, for star counts to $18^m.0$, is not coincident with the plane of the Galaxy but about $+1^\circ$ in latitude away.

Infrared star counts at 2.2 microns have been obtained for seven regions, spaced at 10° intervals, in the galactic plane. Away from the nucleus the star counts seem to fit a simple exponential disc model. At a longitude of 30° where the line of sight is tangential to a ring of molecular clouds, the disc population appears to be supplemented by an increase in density of late-type giants. Towards the galactic centre the extinction at 2.2 microns is low enough for the dense core to be seen in the star counts, these dominating the star counts from the disc population.

C O N T E N T S

Page No.

CHAPTER 1 - A SKETCH OF GALACTIC STRUCTURE

Introduction	1.1
Disc galaxies	1.1
The spheroid	1.3
The disc	1.5
Spiral arms	1.7
Spiral arm tracers	1.8
HII regions	1.9
Young stars and young clusters	1.11
Radio evidence for galactic structure	1.12
Comparison of optical and radio structure	1.14
The CO molecule	1.15
Interstellar extinction	1.17
The extinction law	1.19
Cosmic dust	1.21
Polarisation of starlight	1.22
Interstellar absorption lines	1.23
Association of gas and dust	1.24
Dark nebulae in external galaxies	1.25
Dark nebulae in our Galaxy	1.26
Mapping dark clouds	1.28
The far infrared	1.29
The galactic centre	1.31
Radio features of the galactic nucleus	1.31
The infrared core	1.33
Star counts	1.35
References	1.37

CHAPTER 2 - METHODS OF STAR COUNTING AND ANALYSIS

The pioneers	2.1
The equation of star counts	2.3
Special solution	2.4
The luminosity function	2.6
The effect of interstellar extinction	2.8
Accuracy of the star counts	2.11

Instabilities of the integral equation	2.11
Methods of star counting	2.12
Reseau square analysis	2.13
Analysis of star counts	2.14
Studies of localised clouds of extinction	2.15
Star counts at two wavelengths	2.16
Methods of solving the integral equation	2.17
Model fitting	2.19
References	2.20

CHAPTER 3 - OPTICAL STAR COUNTS

Introduction	3.1
Proposal of project	3.2
The operation of COSMOS	3.3
The output produce of COSMOS	3.4
COSMOS analysis of field 455	3.5
Calibration of COSMOS sources	3.6
UBV photometry of COSMOS sources	3.6
The star counts	3.12
The solution for the relative distribution of distance moduli	3.13
Improvement by trial and error	3.15
The solution for extinction	3.17
The line of sight distribution of extinction	3.19
Analysis by reseau squares	3.21
Simple models to simulate the star counts	3.25
Conclusion	3.27
References	3.28

CHAPTER 4 - INFRARED STAR COUNTS

1. OBSERVATIONS	4.1
Preamble	4.1
Literature guide	4.2
Observing technique	4.3
The observations	4.4
Reduction	4.9
Confusion	4.11

Page No.

2. DISCUSSION	4.15
The star counts	4.15
A model galaxy	4.18
The plane fit	4.20
The centre fit	4.23
Conclusions	4.27
References	4.28

CHAPTER 5 - OBSCURED SOURCES IN THE GALACTIC PLANE

Discovery	5.1
Photometry	5.1
Discussion	5.3
The V-I overlay	5.7
The obscured cluster in V-I	5.9
The galactic centre in V-I	5.10
References	5.11

1

CHAPTER 1

A SKETCH OF GALACTIC STRUCTURE

INTRODUCTION

It must be that every popular astronomy book has a stunning picture of a large spiral galaxy, more often than not M31. There are certainly plenty to choose from. Since the beginning of this century, when these spiral nebulae were definitely identified as separate 'island universes', the science of galactic astronomy has advanced rapidly. Theories for the formation of these galaxies, and the persistence of their spiral arms are now well accepted. Studies of the spiral structure, and the distribution of stars and stellar populations in these galaxies, can be used to classify them into groups. Similar studies in our Galaxy show that it can now be firmly placed within this family of spiral galaxies. Star counting gave the first evidence that the Galaxy is a flattened system of limited extent; this topic will be discussed in the next chapter. This chapter contains a review of some of the more recent work used to study the structure of the Galaxy.

DISC GALAXIES

It is now well known that the gross photometric properties of galaxies can be resolved into two major components: 1 - a spheroidal component obeying the $r^{\frac{1}{4}}$ law of luminosity distribution, typical of elliptical galaxies,¹ and 2 - a disc component obeying the exponential law of late type spirals and Magellanic irregulars.^{1,2}

Secondary structural details such as a bar, spiral arms, or rings usually only contain a small proportion of the total blue luminosity of a galaxy, and tend to be inconspicuous in yellow or red light.³

It is thought that the elliptical and exponential components of a typical disc galaxy form from a rotating protogalactic cloud, in

which star formation accompanies gravitational collapse.⁴ It is currently thought^{5,6} that the relative prominence of the bulge and disc is determined by the efficiency of star formation during collapse. Systems in which star formation is highly efficient at an early age form large spheroidal components (since the stellar system undergoes an essentially dissipationless collapse). When the initial star-forming efficiency is low, the collisions between gas clouds in the protogalaxy lead to the dissipation of energy in the gas, and the eventual formation of a thin disc, stars begin to form in the disc when the average gas density is sufficiently large.

The star forming history of a protogalactic cloud also determines the degree of element formation, and the distribution of heavy elements in the collapsing cloud. In 1944 Baade⁷ first introduced the concept of stellar populations in galaxies. He noted that galaxies could be thought of as consisting of two distinct population components: population I and population II. According to Baade elliptical galaxies consist of pure population II whereas irregulars constitute pure population I. Baade defined population II as consisting of stars that lie on colour-magnitude diagrams similar to those of galactic globular clusters, and population I as comprising stars that lie on colour-magnitude diagrams similar to those of young, or old, metal-rich open clusters. Hubble's classification sequence for galaxies E-Sa-Sb-Sc-Ir may then be understood in terms of changes in the relative importance of populations I and II.

These two populations can, as described earlier, be represented by two photometric components; the $r^{\frac{1}{4}}$ spheroid law and the exponential disc law. The equations governing these two laws are given by de Vaucouleurs and Pence⁸ as

$$\log J_{II}(R_{II}) = -3.3307(R_{II}^{\frac{1}{4}} - 1) \quad \text{spheroid}$$

$$\log J_I(R_I) = -0.7290(R_I - 1) \quad \text{disc}$$

which are dimensionless. The scale factors or normalizing units are the effective radii re^{II} , re^I and specific intensities $Ie^{II} = I^{II}(re^{II})$, and $Ie^I = I^I(re^I)$, so that $R = r/re$ and $J = I/Ie$. The effective radius is defined for a face-on galaxy, as the radius of the circle enclosing half the total luminosity at a specific wavelength, that is

$$L(re) = \frac{1}{2}L_T = \pi \int_0^{\infty} I(r)dr$$

$$\text{with } L_T^{II} = 7.268 \pi Ie^{II} (re^{II})^2 \quad \text{spheroid}$$

$$\text{and } L_T^I = 3.803 \pi Ie^I (re^I)^2 \quad \text{disc}$$

THE SPHEROID

It has been shown by Kormendy⁹ from a study of SO galaxies, that the surface brightness distribution for the spheroidal component of disc systems can be well represented by the de Vaucouleurs $r^{\frac{1}{4}}$ law. In this respect the spheroid component resembles elliptical galaxies.

In our Galaxy a large proportion of the spheroid component, especially towards the galactic centre, is hidden behind local interstellar dust clouds. This makes it difficult to study the gross properties of the bulge of our Galaxy. There is an absorption window in Sagittarius (Baade's window) that allows one to see within 4° of the nucleus, and this defines the inner limit to which the spheroid component can be studied. Whitford¹⁰ showed, from spectrophotometric analysis in this window, that the integrated light from patches of the nuclear bulge has characteristics very similar to those observed for comparable regions of other galaxies.

The stellar content of the bulge is not solely identifiable with Baade's population II classification. Nassau and Blanco¹¹ were able to show that the globular cluster like RR Lyrae in Baade's window are outnumbered two to one by M-type giants. Because M giants do not occur in halo-type globular clusters it follows that the stellar population in the nuclear bulge cannot be pure population II. Colour magnitude diagrams of the bulge component at a galactocentric distance of 0.6 kpc, show that the dominant stellar population resembles that in the old metal-rich cluster NGC 188.¹² Metal poor halo stars in this direction, account for at most a few percent of all giant stars. At a galactocentric distance of 1.2 kpc, the nuclear bulge is seen to have a larger fraction of metal poor population II giants than it does at 0.6 kpc.¹³

The conclusion that emerges from these results is that the dominant stellar population in the nuclear bulge of the Galaxy consists of old metal-rich stars, and that these regions contain only a fraction of true globular cluster stars. A similar population mixture is also seen in the bulge of M31. To describe these populations, subdivisions of Baade's original I and II types have been made. There have also been observed young globular clusters and old galactic clusters in antithesis to Baade's classification.

The shape of the nuclear bulge may be implied from studies of various bulge constituents. Unfortunately conflicting results arise from these various studies. The distribution of globular clusters in the Galaxy shows no measurable flattening towards the galactic plane and this suggests that the stellar population should be similarly spheroidal.¹⁴ The 2.4 micron distribution¹⁵ shows a prominent flattening of the nuclear bulge with major and minor semi-axes of 2.5 kpc and 1.3 kpc respectively, but in this case the disc contribution

may be extending the contours of emission along the galactic plane. The true spheroid is expected to have an ellipticity between these two limits.⁸

From the distribution of surface brightness, e.g. the de Vaucouleurs $r^{\frac{1}{4}}$ law, the spatial density of stars can be deduced. Young¹⁶ has found an asymptotic expansion for this density which is accurate for $r/re \gtrsim 0.2$ or $r \gtrsim 500$ pc,

$$\rho_s(r) = \frac{c \exp(-b(r/re)^{\frac{1}{4}})}{(r/re)^{7/8}}$$

where ρ_s is the space density of spheroid stars, c is a normalization constant and b is a constant equal to 7.669. De Vaucouleurs and Buta¹⁴ find that the effective radius $r_e \approx r_0/3$, where r_0 is the distance of the Sun from the centre of the Galaxy. Throughout this thesis a value of $r_0 = 8$ kpc will be adopted.¹⁷

THE DISC

As mentioned earlier both de Vaucouleurs¹ and Freeman² showed that the disc light distribution for spirals and SO galaxies can be well fitted by an exponential law. In the same paper Freeman made a more controversial statement. He claimed that the extrapolated central surface brightnesses (obtained by evaluating the best-fit exponential law at a galactocentric distance of zero) for most disc galaxies are approximately constant at 21.6 ± 0.3 B mag arc sec⁻². More recent faint photometry of disc galaxies, he claims, tends to confirm this result,¹⁸ except for dwarf systems which have a lower central brightness.

Kormendy⁹ argued differently. After subtracting a best-fit de Vaucouleurs profile for the bulge light, he found that very few disc components can be represented by an exponential law. He found in many cases that the disc components contribute insignificantly to the

system light near the galactic nucleus, and also it is not clear to what extent a disc component exists in the near nuclear regions of some of the galaxies.

Freeman riposted¹⁸ by claiming that Kormendy mostly looked at systems with prominent bulges, and that he did not always go faint enough to define the exponential disc properly. Other opponents to Freeman's claim show that the result does not hold for spiral galaxies with low surface brightness, and even go as far as saying that this constancy of mean surface brightness may just be a selection effect, associated with only choosing galaxies above a certain photographic sky background. This topic may be resolved from studies of deep sky survey plates of the UK Schmidt Survey.

The variation of star density ρ_d with distance x within the plane for disc galaxies is approximated by an exponential¹⁷

$$\rho_d \propto \exp(-(x - r_0)/h)$$

where r_0 is the distance of the Sun from the galactic centre, and h is the scale length of the disc which varies with galaxy type.²

The projection of the surface brightness law to this density law assumes the disc is of constant thickness. De Vaucouleurs and Pence⁸ suggest a value for $h \approx 3.5$ kpc for the Galaxy. The value of $h = 3.5 \pm 0.5$ kpc is also the mean for Sbc galaxies in the Freeman² sample.**

The distribution of disc stars perpendicular to the plane of the Galaxy varies with luminosity. The typically younger and more massive stars are found relatively close to the plane, whereas the older and less massive stars are not as localised. The variation in

** The Galaxy is of morphological type SAB(rs)bc⁸ where SAB implies an intermediate stage between barred and spiral, rs is an intermediate between ringed and spiral and bc is an intermediate between bulge to disc type galaxies b and c.

star density ρ_d , with perpendicular distance z from the plane is given to a good approximation by an exponential function

$$\rho_d(z, M) \propto \exp(-z/H(M))$$

where H is the scale height, which varies with the absolute magnitude M of the stars. Bahcall and Soneira¹⁷ use an approximate step function for the scale height with $H \approx 100$ pc for $M < 4$ and $H \approx 300$ pc for $M > 4$, for our Galaxy.

The star density of the disc is obtained by combining these two equations

$$\rho_d(r, M) = \exp(-z/H(M) - (x - r_o)/h) .$$

As Kormendy⁹ shows, this relation may not hold near the galactic centre.

SPIRAL ARMS

An important question raised in the study of spiral galaxies is why the spiral arms do not wrap themselves up due to the differential rotation of the disc. If the spiral arms were composed always of the same stars then, after a few revolutions, these arms would be wound very tightly and practically disappear. This should occur on time-scales of $\sim 5 \times 10^8$ yrs which is much less than the age of the Galaxy. It was suggested many years ago by Lindblad, that spiral patterns could be maintained for a long period by density wave propagation. In this system stars move through the spiral arms, but stay there longer on the average, so that the spiral arms are, at every moment, the maxima of density; they are not stable arms but spiral waves. Lin, Shu and Yuan¹⁹ have shown how such a density wave causing a spiral pattern can be sustained by its own spiral gravitational field. These theories do not, unfortunately, describe how the initial spiral density wave is

formed. At the moment this part of the theory is left to speculation.

The density wave theory not only explains the persistence of spiral arms, but also suggests how the continuing process of star formation, seen in our and other galaxies, may occur. Interstellar gas coming into the influence of a spiral arm may be induced into a shocked state by even a small wave potential. The compression of material at this shock front may be sufficient to initiate gravitational collapse which results in the birth of stars. Hence the birth places of most young objects should be close to the shock front.

Observational evidence of density waves can probably best be obtained from external galaxies. Mathewson et al.²⁰ have produced a high resolution radio continuum map of M51 showing how the radio emission follows the inner edge of the optical arms. This is perhaps the best evidence for the existence of spiral shock fronts.

SPIRAL ARM TRACERS

It was stated earlier that the spiral arms usually contain only a small fraction of the total blue luminosity of a galaxy, and that they tend to be inconspicuous in yellow or red light. So what makes the spiral arms stand out so prominently in our 'popular astronomy book' pictures? The types of object that in most cases are confined to the spiral arms are called spiral tracers. Spiral tracers must necessarily be quite young, since stars of population I have peculiar speeds of the order of 10 kms^{-1} , and so such stars can diffuse from their birth places to distances of about 1 kpc in 10^8 years. The best optical tracers appear to be

HII regions

O-associations and young open clusters

Wolf-Rayet stars and early type emission B-stars

High luminosity supergiants

Dark cloud complexes.

In external galaxies which are face-on it is easy to follow the pattern of these tracers. In our Galaxy the spiral arms are seen edge-on and since there may be more than one spiral arm or offshoot in the line of sight, the distances of these tracers are needed to describe any spiral structure. An additional problem at optical wavelengths is that interstellar extinction limits the view of the Galaxy, in the plane, to a few kiloparsecs at most.

HII REGIONS

An HII region is formed when there is a combination of a hot star (O5 - B0) surrounded by a cloud of hydrogen atoms with a density of the order of 1 to 10 per cubic centimetre.²¹ The strong ultraviolet emission from these stars ionises the hydrogen in the cloud which results in the large regions of emission. The exciting stars of HII regions are excellent indicators of spiral structure since these objects lie on or very close to the zero age main sequence. The location of these objects at the zero age main sequence indicates that there is little scattering in the absolute magnitudes and, as a consequence, little uncertainty in the determination of distance.

The close association of HII regions with the spiral arms of a galaxy was first recognised by Baade in a study of HII regions in M31. A photographic survey of HII regions in our Galaxy led to the first detection of spiral structure. Morgan et al.²² found that HII regions north of -10° declination occurred in two long narrow belts. The first of these was found to extend from $l^{II} = 40^\circ$ to $l^{II} = 190^\circ$ passing near the Sun on the side opposite to the galactic centre. A second arm was traced from $l^{II} = 70^\circ$ to $l^{II} = 140^\circ$ parallel to the first but with a distance of about 2000 pc from the Sun in the anticentre direction. There was also some evidence for another arm located at a distance of

about 1500 pc in the direction of the galactic centre.

The visual identifications of HII regions was improved by taking photographs in a wavelength narrowly defined around the $H\alpha$ line. By 1959 approximately 400 HII regions had been found, most of which were situated close to the galactic plane.²³

Crampton and Georgelin²⁴ re-analysed data giving the distances to HII regions to produce a definitive map of the spiral structure in the local sector of the Galaxy. For HII regions too distant ($\gtrsim 4$ kpc) to use spectrophotometric data of the exciting stars, they obtained the distances by measuring the $H\alpha$ radial velocities and applying these to a rotation model of the Galaxy. The major features found by this survey were:

Perseus Arm - situated at a distance of about 2500 pc from the Sun between galactic longitudes 100° and 198° identified with Morgan et al.'s second arm.

Local Arm - extending in two directions, $l^{II} \sim 70^\circ$, $l^{II} \sim 230^\circ$, away from the Sun, with the Sun situated on the inside edge of this arm.

Sagittarius-Carina Arm - a major arm is seen stretching from $l^{II} \sim 290^\circ$ to $l^{II} \sim 40^\circ$ at a distance of about 1500 pc in the direction of the galactic centre. In the direction of Carina this arm can be traced to a distance of about 8000 pc.

Norma-Centaurus Arm - situated at a distance of about 4000 pc behind the Sagittarius-Carina arm.

There are very few optical identifications of HII regions beyond 4000 pc and so investigators have turned to radio emission of HII regions to trace spiral structure at increased distances. The $H109\alpha$ line has been used to obtain radial velocities of 'invisible' HII regions. Georgelin and Georgelin²⁵ have produced a map of HII regions obtained in this way. As with other radio analysis the agreement

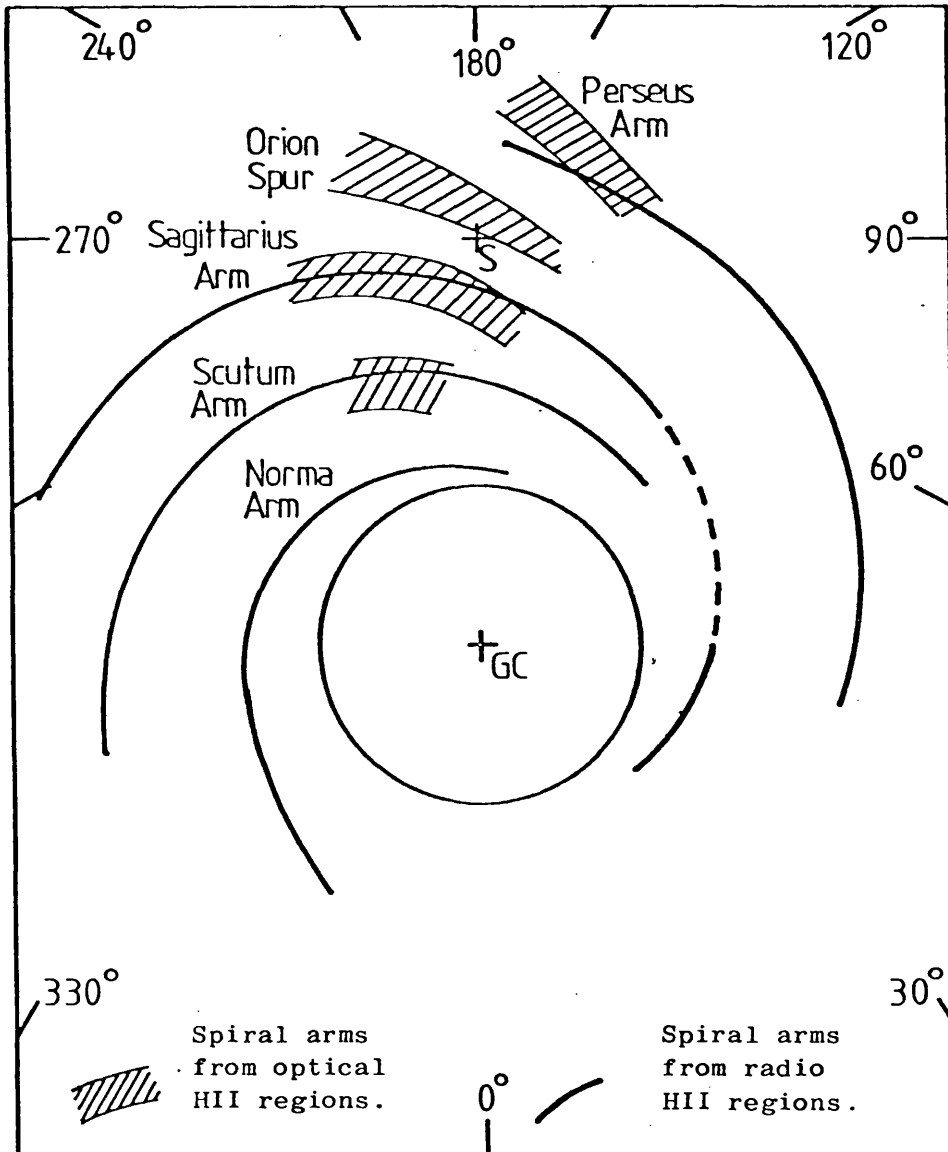


Fig. 1A Spiral structure from optical and radio HII regions (refs. 24,25).

between the radio and optical structures is not exceptionally good, but the major spiral arms can be traced to much greater distances. The Perseus arm is seen round to a longitude of 40° and the Sagittarius arm is tentatively traced to 30° . The Norma-Centaurus arm seen in the optical is well defined in the radio, and renamed as an intermediate Scutum-Crux arm. A new arm about 4000 pc from the galactic centre inside the Scutum-Crux arm becomes the Norma arm. These arms can be interpreted as two symmetrical pairs with a pitch angle of 12° . On this plan the local arm becomes an inter-arm feature. No arm is observed to go all the way around the Galaxy, in agreement with observations of spiral structure in similar external galaxies.

YOUNG STARS AND YOUNG CLUSTERS

Like HII regions young stars and young open clusters are good spiral tracers. Associations of 0 stars, not gravitationally bound in a cluster, are necessarily young since differential galactic rotation and tidal effects would disrupt the aggregation on a timescale of the order of 10^7 years.²³ The members of these young associations and young clusters are identified on the basis of spectral and luminosity classifications. Once the probable members have been identified their individual spectroscopic parallaxes can be determined and the mean distance of the association is thus the average of these. When these young objects are projected onto the galactic plane, their distribution is seen to be very similar to that of the optical HII regions. The three local spiral features, the Sagittarius-Carina arm, the Local arm and the Perseus arm are clearly defined with distinct gaps between the three features.²⁶

Long period Cepheid variables, although supposedly good spiral tracers, are too few in the local sector, to usefully be used to plot

out the arms.

RADIO EVIDENCE FOR GALACTIC STRUCTURE^{27,28}

It has already been mentioned that ionized hydrogen can be observed by both optical and radio means in the form of HII regions. Optical observations are, however, severely limited by interstellar absorption. Radio observations can detect these individual regions, but with less detail, throughout most of the Galaxy. The bulk of atomic hydrogen is in the neutral form (HI or H₂) which cannot be observed optically at all. Radio observations of the hyperfine transition line at 21 cm of HI can cover almost the whole Galaxy, and at present provides the only method available for tracing out the large-scale structure of the entire system.

While observations in the radio continuum can only give the integrated emission along the line of sight, the 21 cm line observations give discrimination in distance, although they cannot by themselves provide actual distances. The distance distribution in a given direction has to be inferred from radial velocity calibrations. For longitudes 90° to 270°, that is for directions outside the Sun's orbital circle, this procedure is unambiguous since a given rotation velocity only occurs at one distance. Looking in toward the centre, however, there are two distances 'near' and 'far' that give rise to the same line of sight rotation velocity. It is therefore necessary to decide whether a given feature in the profile is due to the 'near' or 'far' region. To overcome this problem it is assumed that the neutral hydrogen layer has a constant thickness, so that the angular width of a feature in latitude can be used as a crude distance indicator.

The rotation curves used to deduce the distances are also obtained from the radio data. If the hydrogen distribution is uniform, and all

motions are circular, the highest velocity on a line profile gives the rotational velocity at the point where the line of sight is tangential to a circle around the galactic centre, after making allowance for the velocity dispersion of the hydrogen clouds. A set of tangential-point observations up to plus or minus 90° of longitude around the galactic equator then leads to the variation of the rotational velocity with distance from the centre. This method for deriving the rotation curve can only be used for orbits within the Sun's radius. Beyond the Sun the curve is generally extrapolated using a mass distribution model for the Galaxy.

An embarrassment for the radio investigators is that there is a clear difference of about 10 kms^{-1} between the apparent rotation curves for the two sides of the Galaxy in the radius range 5 to 8 kpc. This disparity implies that the hydrogen cannot be moving in circular orbits, and it can also give rise to large differences in the derived distances, for the mapping of the HI distribution onto the galactic plane. The apparent discrepancy between these two curves can also be explained if the solar neighbourhood has an outward motion of about 7 kms^{-1} , if the Galaxy is symmetrical and the velocity field axisymmetric.

The completed HI map of the galactic plane²⁸ has many irregularities, and although these are seen in the line profiles their positions in the galactic plane are by no means certain. The broad scale structure of the HI map does, however, show similarities to the optical and radio HII region distributions.

The Sun lies on the inner side of the local arm (Orion arm). About 2 kpc outside the Sun is the Perseus arm. These two arms can be followed through a large range of longitude. Inside the Sun, about 2 kpc distant, lies the prominent Sagittarius arm, and inside this an arm sometimes called the 'Scutum-Norma arm', which must be a mixture of

the Norma and Scutum-Crux arms seen in the HII region distribution.

COMPARISON OF OPTICAL AND RADIO STRUCTURE

When the distribution of the young spiral tracers is superimposed on an HI map of the local region, at first sight the agreement appears to be poor.²³ The optically mapped spiral arms have a markedly different slope from the more circular radio arms. Moreover, in places the optical arms cross the radio arms and pass through regions where there is no evidence of HI at all. It is conceivable that not all the arms indicated by the 21 cm survey need contain young objects since the presence of neutral hydrogen is no proof that star formation has recently taken place. In regions where hot supergiants and HII regions are observed optically, on the other hand, one should expect to observe significant amounts of neutral hydrogen, since these objects are too young to have moved significantly from their respective origins.

This discrepancy may not, however, be real. It could be due to the different ways in which the optical and radio maps are constructed. The optical maps depend on distances determined from absolute and apparent magnitudes, with the largest uncertainty arising from lack of knowledge about the interstellar absorption. The radio map, in contrast, depends on measured radial velocities and a postulated rotation law for the Galaxy. Fletcher²⁹ found that if the optical tracers are reconstructed in the same way as the radio map, then a good correlation between stars and gas is achieved. The resulting maps may not properly reflect the real situation but any errors should affect equally the positions of the stars and gas.

THE CO MOLECULE

Millimetre wave observations of emission from the CO molecule have become the chief method for determining the physical properties of dense interstellar clouds, composed primarily of molecular hydrogen. The usefulness of CO as a tracer of molecular hydrogen is based on two related premises. First the CO to H₂ abundance ratio is assumed to be reasonably constant and therefore a measure of the CO column density will imply a measure of the hydrogen column density, and secondly the photons emitted by CO, and consequently the line intensity, result from collisions between H₂ and CO.

Two isotopes of this molecule can be measured. ¹²CO is the commonest, but the high intensity of emission, due to a high ubiquitous opacity, makes this isotope less easy to interpret in quantitative terms. The much less abundant ¹³CO isotope (¹²CO/¹³CO ≈ 40) can also be observed throughout the Galaxy.

One of the great expectations of the CO line is that its distribution will delineate the spiral structure of the Milky Way with a definition not obtained in either 21 cm line studies or radio observations of HII regions. The line is highly selective towards the densest interstellar clouds, and there is excellent agreement between the distribution of giant HII regions and CO emission with similar radial velocities.

The most striking large scale characteristics of the molecular clouds in the Galaxy are their concentrations, in the galactic centre region, and in a ring at a galactocentric distance extending from 4 - 8 kpc.³⁰ Figure 1B shows the radial distribution of the CO emission. Both of these features are unlike the flat atomic hydrogen distribution. The extremely good agreement of the radial distribution between ¹³CO and ¹²CO shows that either isotope can be used as an

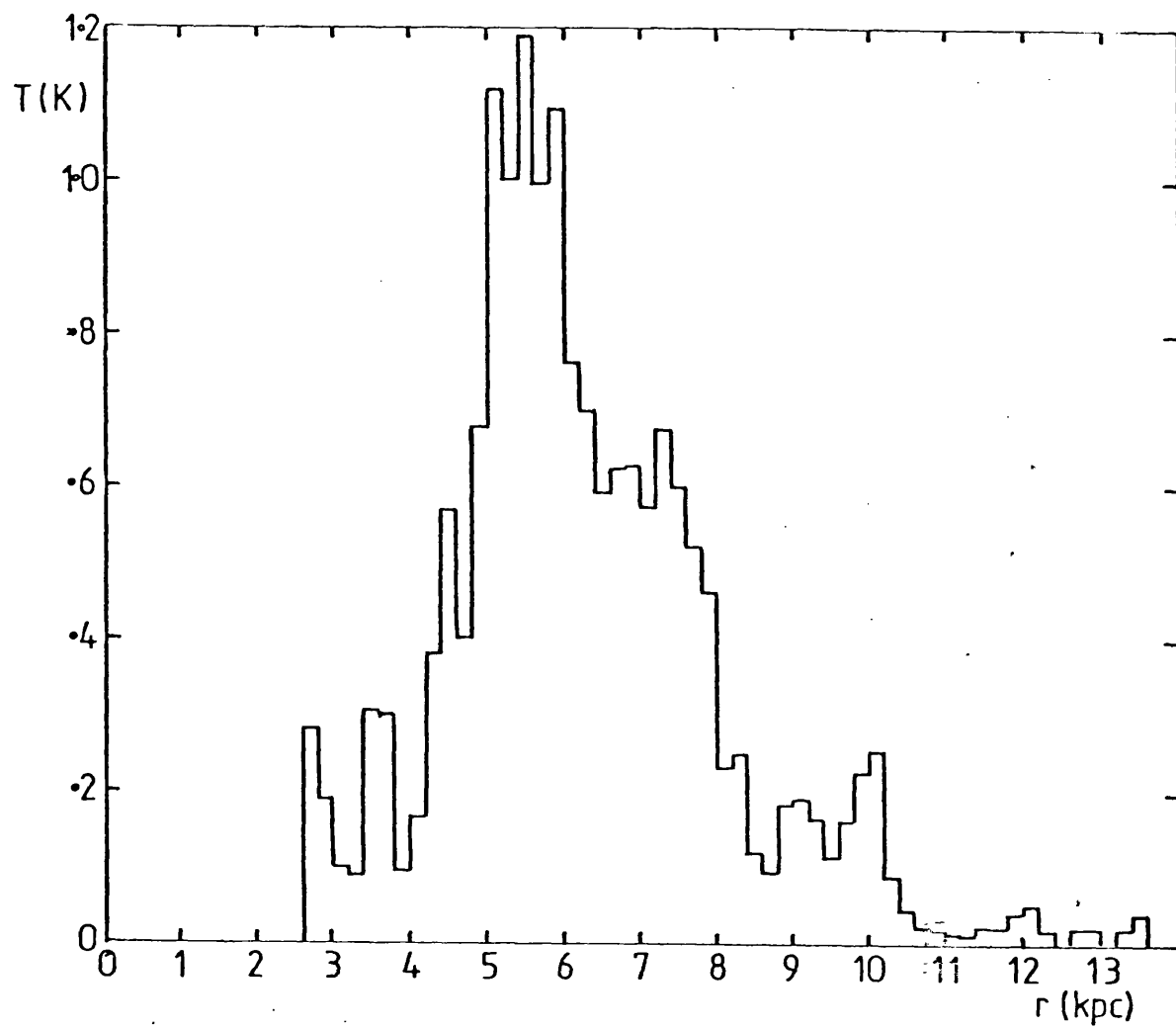


Fig. 1B Radial distribution of CO emission in the Galaxy (ref. 30).
($r_0 = 10$ kpc)

indication of the relative mass distribution in the Galaxy despite the ^{12}CO emission being saturated.

When the emission data is plotted in the velocity longitude plane, a clear breakup into individual clouds is seen. The average cloud size is 40 pc, and with a mean H_2 density of 300 cm^{-3} the mass per cloud is therefore about $5 \times 10^5 M_{\odot}$. These objects can best be described as giant molecular clouds or possibly giant molecular cloud complexes and represent a class of objects which are among the most massive in the Galaxy. From an estimation of the fraction of the Galaxy seen in their survey, Solomon et al.³⁰ estimate that there should be 4000 giant molecular clouds in the Galaxy.

The evolutionary history of the giant molecular clouds and the role played by the spiral shock in initiating star formation will be strongly influenced by whether the clouds are situated only within spiral arms or whether they are also found just as frequently in interarm regions. Scoville et al.³¹ show that there is no recognizable spiral form in the distribution of CO clouds, and so most of the clouds cannot be situated within a regular pattern of spiral arms. The Sagittarius and Scutum arms are, however, observed at their tangential points at a distance of about 7 kpc from the Sun.

The fact that these molecular clouds are seen in interarm regions means that they cannot just represent a brief compression phase of the interstellar medium, each time a galactic shock passes by. Since the clouds continue well into the interarm regions, their ages are at least 10^8 years. The giant molecular clouds are probably not formed solely from compression by density waves since the time scale for spiral density waves to turn atomic hydrogen into the total amount of observed molecular hydrogen is calculated to be a significant fraction of the age of the Galaxy.³⁰ More likely is that the giant molecular clouds

are formed by cloud collisions. The timescale for cloud collisions in the galactic ring is $\sim 3 \times 10^8$ years³¹, and it can be expected that they can double their masses within such a time.

This mass buildup via accretion cannot go unchecked, otherwise there would be an excess of massive clouds which is not observed. There must be one or more processes which remove H_2 from the clouds at a similar rate to that provided by collisions. The most important of these are probably the ionization of hydrogen by O-stars and the accumulation of H_2 into newly formed stars.

The evidence of the CO emission is that star forming clouds are not the result of compression by a galactic density-wave travelling through the low density interstellar medium. Except for the higher rate of star formation which clearly does occur when these clouds pass through a spiral arm, the large scale cloud structure may be affected very little.

INTERSTELLAR EXTINCTION³²

In 1930 Trumpler³³ compared the diameters of galactic clusters with their distances determined from spectral types and photographic photometry. He noticed that according to the apparent distances, the linear diameters of the clusters increased with increasing distance. To resolve this dilemma he proposed the existence of interstellar extinction which would reduce the brightness of an object and so make it appear more distant. The method of estimating cluster distances from their apparent diameters is an effective way of investigating interstellar extinction because the apparent angular diameter of clusters, being in principle a linear function of only the true distance, should be independent of the amount of extinction.³⁴

Other evidence for interstellar extinction²⁵ are the many areas

in rich Milky Way star fields that are completely or nearly starless. These 'dark nebulae' are regions where the light of distant stars is obscured by clouds of dark matter. In the vicinity of bright hot stars this dark matter becomes luminous by reflection or excitation, producing bright diffuse galactic nebulae. In many extragalactic nebulae, the existence of dark matter between the stars is plainly noticeable. Also the distribution of these extragalactic systems on the celestial sphere, has a marked 'zone of avoidance' along the Milky Way.

A crude estimate of the amount of interstellar material in the Galaxy can be made on the basis of gravitational arguments. Since, on the whole, excessive velocities are not observed for stars in the vicinity of interstellar clouds, then the total mass of a cloud must be limited. Oort concluded that the average density of interstellar matter in the galactic plane is of the same order of magnitude as the space density of known stars.³⁵

Another quantitative measure of extinction can be made by use of the variable-extinction method.³² This method requires two colour photometric data, and the absolute magnitudes and intrinsic colours of individual stars. Suppose there is a cluster of stars (at a constant distance from the Earth) with all the stars having exactly the same absolute magnitude and intrinsic colour. If the reddening and the extinction are variable across the face of the cluster, then a straight-line relationship exists between the observed magnitudes and observed colours. The slope of this line is the ratio of total to selective extinction, which in the B and V wavebands is $R = A_V/E_{B-V}$, where A_V is the total extinction at V, and E_{B-V} is the difference between the colour indices B-V of the absolute magnitude and the observed magnitude. This method only applies to the component of the extinction which is

variable across the face of the cluster, and is 'blind' to any additional extinction which may exist between the cluster and the Earth.

More evidence for extinction is that distant stars of a specified spectral type in our Galaxy are redder in colour than nearby stars of the same spectral type. This result shows that the interstellar extinction varies with wavelength. By comparing the differences between magnitudes at various colours for the nearby and extinguished star, the amount of extinction can be found. In contrast to the variable extinction method, the colour difference method applies to the total mass of interstellar material to the reddened star.

THE EXTINCTION LAW

Light passing through the interstellar medium can suffer extinction by three processes.³⁵

- 1 - direct obscuration by solid particles .
- 2 - scattering by small particles or grains.
- 3 - absorption by atoms, ions, molecules or metallic grains.

Direct obscuration or blocking of light by solid particles is not wavelength dependent, and therefore the observed variation with wavelength indicates that only a small amount of interstellar extinction, if any, can be due to light blocking.

The scattering process consists of the interstellar material acting as a centre for a secondary, divergent, wave of the impinging radiation. Only some of this divergent wave travels forward in the direction of the original beam, and so the intensity of radiation is reduced. The amount of radiation lost to the observer by scattering depends upon the size, shape, and composition of the scattering particle, and upon the wavelength of the incident radiation. Scattering is

wavelength dependent, it alters the observed colour of a star.

Scattering by electrons in the astronomical wavelength range is slight, and its wavelength dependence is small. For scattering by interstellar grains, two cases must be considered: dielectric particles which, except for direct blocking, cause extinction solely by scattering, and metallic particles, which can cause extinction by scattering or by absorption.

Absorption occurs when the incident radiation is converted into energy of free electrons or of bound electrons in metallic solids. The effects of atomic or molecular absorption are evident in the form of interstellar lines in the spectra of stars. The absorption of light occurs at well defined wavelengths and has little effect on the total brightness of a source.

It therefore seems that the effect of interstellar extinction on starlight is mainly due to the wavelength dependent, scattering of light by grains.

To obtain the wavelength dependence of the extinction the colour-difference method is used. The star's magnitude is measured at as many wavelengths as possible, especially towards the long infra-red and the colour differences are compared with those of a similar unreddened star. Johnson³² shows these extinction curves for many dark regions. It is important to obtain the colours at long wavelengths since at $1/\lambda = 0$ the extinction by scattering will be zero, and therefore the total extinction at any wavelength can be found from this baseline. From the value of the total extinction at V, A_V the ratio of the total to selective extinction $R = A_V/E_{B-V}$ can be determined.

For most of the local neighbourhood of the Galaxy the value of R is fairly constant at $R \approx 3.1$.³⁶ There is controversy as to whether this value changes considerably, up to $R \approx 6$, in certain directions.

The value of R is dependent on the composition of the interstellar medium, and so a constant galactic value would imply that the interstellar mix is fairly uniform throughout the Galaxy.

The wavelength variation of interstellar extinction can be predicted theoretically by considering various mixtures for the interstellar medium. A famous theoretical evaluation of the extinction law is van de Hulst's curve No. 15 which is shown by Johnson³² (p.193) and is reproduced in Figure 1C.

COSMIC DUST^{37,38}

After the solid particle nature of interstellar grains had been established it became important to establish what elements made up the material. Initially, iron particles were considered, because of the belief that meteorites were of cosmic origin. Subsequently at the suggestion of Lindblad that the grains could condense out of the interstellar medium, van de Hulst considered that ices of water (H_2O), methane (CH_4) and ammonia (NH_3) would be likely constituents. Other investigators suggested that graphite and silicates formed part of the interstellar medium, these constituents being formed in the atmospheres of stars.

In recent years observations in the far-infrared and the far-ultraviolet have enabled theoretical models to be properly tested. Greenberg³⁸ proposes that two kinds of particle widely disparate in size are needed to explain the wavelength dependence in the visual and in the ultraviolet. The larger size particles consist of silicate cores with mantles of accreted ices, comprising mixtures of oxygen, carbon and nitrogen, with hydrogen. These core-mantle particles have sizes of the order of 0.1 microns. The composition of the small particles is probably of graphite or silicates with sizes of the order

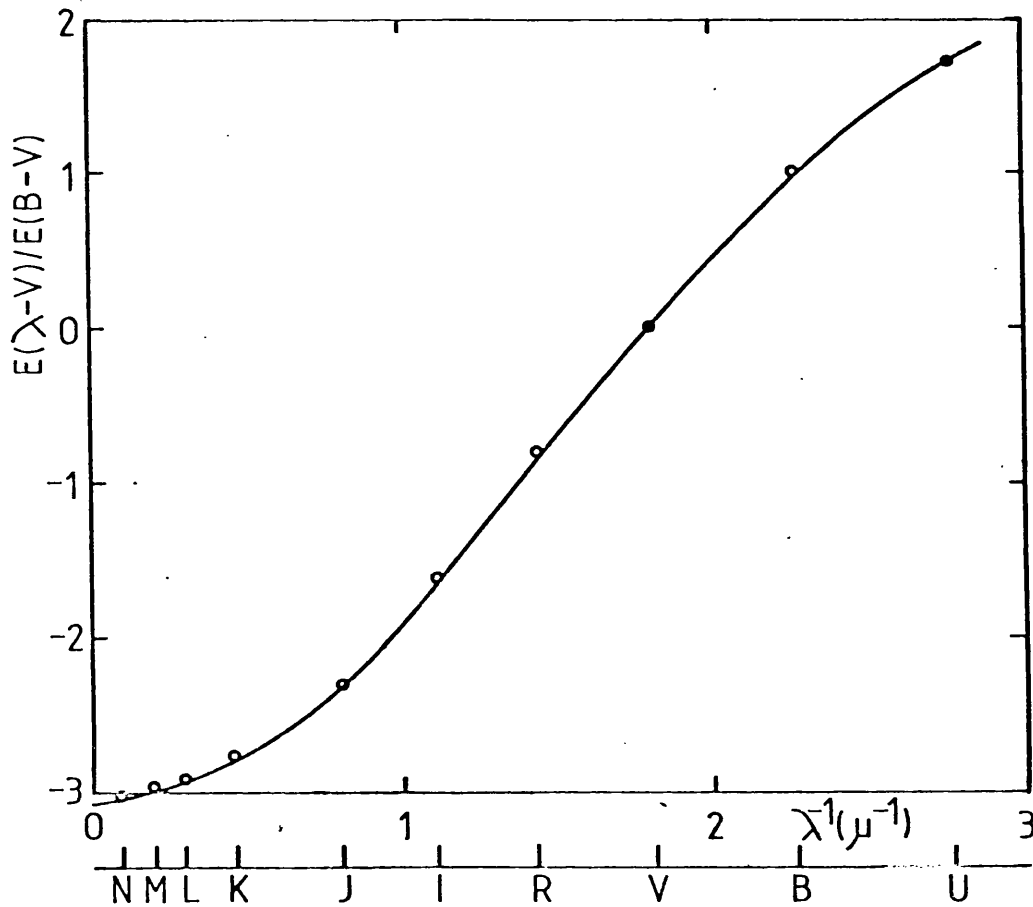


Fig. 1C van de Hulst's theoretical extinction curve No. 15 (ref. 32).

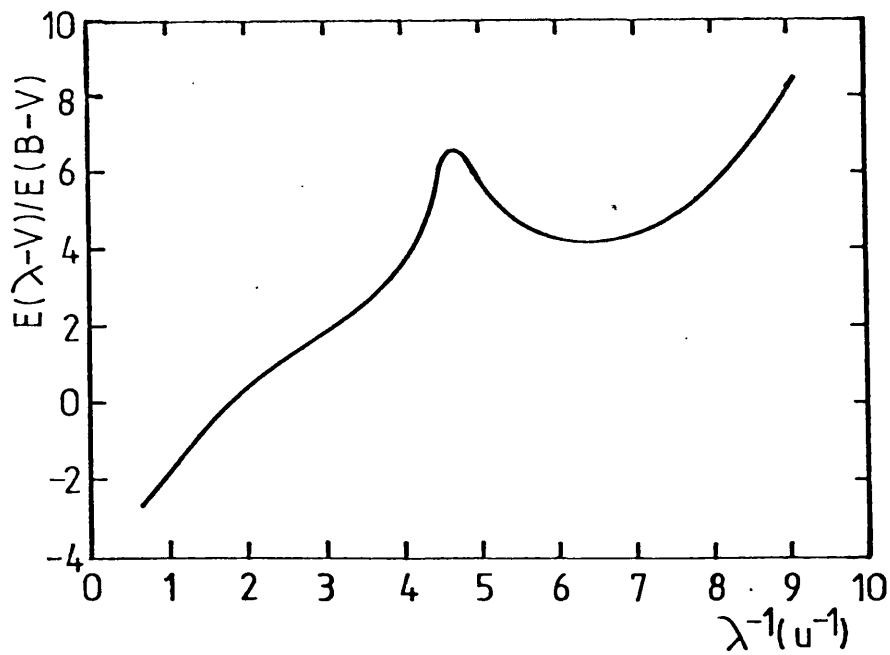


Fig. 1D Average observed wavelength dependence of extinction (2 - 0.1 microns) (ref. 38)

of 0.005 microns, about 1/20 the size of the coremantle grains. These small particles are needed to explain the hump in the colour excess diagram at 0.22 microns ($\lambda^{-1} = 4.6 \text{ microns}^{-1}$). Figure 1D shows the average observed wavelength-dependence of extinction down to 0.1 microns.³⁸

POLARISATION OF STARLIGHT

The interstellar polarisation of starlight was simultaneously discovered in 1949 by Hall and Hiltner.^{39,40} At the time this result was surprising since it was felt unlikely that interstellar grains would have a degree of ordering, over large distances, sufficient to produce a measurable polarisation.

It is now seen that polarisation affects all distant stars in the plane of the Galaxy, irrespective of spectral type or absolute magnitude. Strong polarisations are observed only for stars that are highly reddened by intervening cosmic dust, although strong reddening is not necessarily accompanied by high percentage polarisation. This partnership of polarisation and extinction strongly suggests that polarisation is due to cosmic dust.

To produce the observed degrees of polarisation requires elongated grains aligned in a common direction, over large regions of space. The only realistic alignment mechanism is the galactic magnetic field, which tends to be 'frozen' into the gas of the spiral density waves. The distribution of polarisation shows an alignment with the galactic plane over large ranges of galactic longitude when observed perpendicular to a spiral arm (e.g. $l = 90^\circ$ to $l = 150^\circ$). When observed along a spiral arm the orientation of polarisation is more random (e.g. $l = 80^\circ$ to $l = 90^\circ$). See for example the figures of the largescale polarisations of the Milky Way reproduced by Greenberg³⁸

(p.203) or Bok and Bok⁴¹ (p.202).

Not only is the amount of extinction wavelength dependent, the degree of polarisation is also. For the majority of stars there is a maximum percentage of linear polarisation at about 0.5 microns. Circular polarisation of the starlight shows a wavelength dependence, with a reversal of direction at about the same wavelength as the maximum of linear polarisation. These polarisations help to constrain any grain models. For example, if the polarisations were caused by dielectric grains the implied size would be 0.1 to 0.2 microns, whereas a metallic particle would have dimensions of about $\frac{1}{4}$ of these.³⁸

INTERSTELLAR ABSORPTION LINES^{42,43}

Interstellar absorption lines were first observed in 1904 when the H and K Calcium lines were seen to be stationary in the changing spectrum of a spectroscopic binary. By 1930 it was generally agreed that these lines, and others seen in spectroscopic binaries, were interstellar in origin. Munch⁴³ lists some of the known absorption lines, which are due to atoms of Sodium, Potassium, Calcium, Titanium and Iron and to molecules of CH and CN.

An advantage of using interstellar absorption lines to study the interstellar medium, is that it provides very high angular resolutions, in comparison, say, with 21 cm line studies which refers to all the matter in the acceptance cone of the radio aerial. Unfortunately, the observations of interstellar lines is time-consuming since high dispersion Coude spectra are needed for every object.

A very important discovery was found in some spectra where the absorption lines were split into two or more components. Since it can be assumed that the interstellar dust rotates as the rest of the Galaxy, then these multiple lines arise from separated clouds of extinction

along the line of sight, each with a different radial velocity relative to the Sun. This is definite evidence for the lumpy structure of the interstellar medium; the dust accumulating in small clouds rather than spread evenly through space.

This very useful field of study is, however, restricted to a few kiloparsecs around the Sun. To obtain quality Coude spectra requires stars with magnitudes $10^m .5$ or brighter, and the combined effects of distance and extinction drastically reduce the number of observable distant stars.

ASSOCIATION OF GAS AND DUST^{44,45}

It has long been thought that there should be a co-existence of gas and dust in the interstellar medium; the dust grains being hounded along by the gas particles during their motions. The ratio of gas to dust, though, is probably not constant: in regions of high gas density formation of new grains and molecules may occur, thereby modifying the ratio of gas to dust in such regions.

In 1955 Lilley⁴⁶ indicated for the first time a general correlation between the distribution of gas and dust. By comparing photographic absorptions from galaxy counts and the peak brightness temperature of the 21 cm line he showed this relationship over a range of 30 degrees of latitude, in the direction of the galactic anti-centre. On the other hand, at about the same time several other investigators failed to find any significant gas to dust correlations in the directions of dark clouds.

In general there is evidence that the ratio of hydrogen atoms and extinction are regionally correlated.

The theory of grain growth predicts that dust will predominately form in low temperature, high density, regions. Observations of the

21 cm line in emission, however, include a fair amount of hot gas as well. Braunsfurth and Rohlfs⁴⁵ have separated the 21 cm line profiles at intermediate latitudes into Gaussian components, one with a velocity dispersion $\sim 12 \text{ kms}^{-1}$ and another with a dispersion $\sim 4 \text{ kms}^{-1}$. They show there is a good correlation between dust and the narrow component, and a poor correlation with the wide component.

Cold gas can also be observed from absorption profiles of the 21 cm line. Extragalactic sources are observed to ensure that all the neutral hydrogen gas in the line of sight is in front of the source. The extinction can be obtained by observations of distant OB stars in the same direction.

From these sort of investigations Braunsfurth and Rohlfs⁴⁵ deduce a density ratio of neutral hydrogen to dust of $\rho_{\text{H}}/\rho_{\text{D}} \approx 50$, which is equivalent to a ratio of the total number of gas atoms to the grains of $N_{\text{H}}/N_{\text{G}} \approx 3 \times 10^{12}$.⁴⁴

In the spiral galaxy M51 Mathewson et al.²⁰ have shown that the peaks of the 21 cm continuum radiation are extremely well correlated to the visible dust lanes.

DARK NEBULAE IN EXTERNAL GALAXIES

The Hubble Atlas by Sandage⁴⁷ gives detailed descriptions and illustrations of the distribution of interstellar dust in galaxies. Although the classification of spirals into types a, b and c are made on criteria other than the dust distribution, there are marked differences between each type.

Spirals of type Sa, the first true spirals after the uniform SO's, show tightly wound patterns of obscuration. Regular spiral dust lanes are a prominent feature of the Sb type; the dust being denser and more conspicuous in Sb than in Sa systems. Spiral dust lanes are

a very important feature of the spiral pattern in Sc's, but these tend to be more irregular than in the Sb systems. The spiral pattern for Sc's first becomes apparent in the nuclei of such systems as two principal dust lanes. Further out from the nucleus, these two principal dust lanes wind out along the inside of the two most luminous outer arms.

A study of the distribution of dark nebulae in late-type spirals has been conducted by Lynds.⁴⁸ She found that the brightest HII regions were not particularly good spiral tracers, instead the primary dust lanes of an Sc galaxy define the spiral pattern better. These dust lanes are often found on the inside edge of a bright spiral arm, but may be found on the outside edge or somewhere within the luminous arm where a 'wisp' of a dark lane cuts across the arm. She also concluded that the brightest HII regions of a galaxy are always found either next to or imbedded in regions of high obscuration: the converse not being true, many dense clouds of obscuration were found without an associate HII region.

DARK NEBULAE IN OUR GALAXY⁴⁹

By 1927 Barnard had conducted a photographic survey of the Milky Way listing over three hundred non-luminous obscuring clouds. Back in the eighteenth century Herschel had discovered that these regions devoid of stars were often associated with luminous nebulae. By the time of Barnard's survey it was generally believed that the dark regions were true obscuring nebulae. Even so he admitted that some of the dark nebulae may only be vacancies among the stars caused by a random distribution of stars. The criteria for accepting a dark region as an obscuring cloud should be that the star density decreases by an amount greater than the random statistical fluctuations of the

star numbers expected at that galactic latitude. For a random distribution the statistical error is approximately given by the square root of the number of stars. Usually then, the richer the star field, the easier it is to detect a dark nebula between the star field and the observer.

From the Palomar Schmidt sky survey Lynds has compiled another catalogue of dark nebulae.⁵⁰ This list contains over eighteen hundred condensations, most of the entries being dark patches within the general obscuration of extensive dark cloud complexes. She found, for the most part, that these nebulae are confined to within 20 degrees of the plane of the Galaxy, the significant deviations being due to Gould's belt, a local irregularity in the Sun's region of the Galaxy.

Barnard noted that some of the smaller dark nebulae have relatively sharp edges. In many cases one side of a dark marking is very definite, while the other side is diffuse, as though they have been flattened against an invisible wall. Another observed property is that for any given longitude there seems to be a tendency for the structural features of dark nebulosities to align themselves with respect to each other. There are indications that in some cases the direction of parallel filaments is correlated with the plane of polarisation, and hence, may be related to the influence of the galactic magnetic field.

As well as the extended clouds of extinction, there are seen small, opaque, clouds that are usually circular or oval in shape, called globules. These globules are almost always detected when they are projected against an emission field. Small dark nebulae, of the same apparent size, would be very difficult to detect if viewed against the general stellar background. Approximately one hundred of these objects are detectable on the Palomar prints.

No direct measure of the mass of a nebula can be made purely from dynamical arguments. A lower limit to the mass can be made with the data from star counts, that is the distance to the cloud, its visible surface area, and the total extinction through the nebula.

MAPPING DARK CLOUDS

Dark clouds can easily be mapped onto the celestial sphere from the photographic surveys, as discussed in the previous section. To map the clouds in three dimensions requires an estimate of the distances to the dark nebulae, which are not so simple to come by. If a dark nebula has a luminous nebula associated with it, the distance of the bright nebula can be determined from the spectroscopic parallax of the exciting star, and this is assumed to be the distance to the entire complex.

For more extended dark nebulosities, star counts can be used to obtain an estimate of the distance to a cloud. This technique is expanded on in the next chapter. For each region for which star counts are available a complex mathematical treatment of the data has to be done, and so this method is unsuitable for mapping vast areas of sky. The resseau square star count analysis, also discussed in the next chapter, is useful for mapping cloud complexes for example, but without additional data this gives no information on the line of sight distribution of extinction.

The best technique for mapping the largescale distribution of extinction for a few kiloparsecs around the Sun, is to choose a class of object, which is evenly spread through the space, and for which the distance and extinction can be determined for each object. Neckel and Klare⁵¹ have derived extinction values and distances from optical photometry of more than 11000 O to F stars within 8 degrees of the

galactic plane. By comparing the extinction values with distance along a particular line of sight, a map of the clouds in the galactic plane can be constructed. The map produced by Neckel and Klare⁵¹ shows very little correlation between the observed dust distribution and the known spiral features, as may be expected for the Sbc classification of our Galaxy. The disadvantage with this technique is that where there is enhanced extinction, the number of suitable stars behind the cloud is fewer and so any errors of measurement are more influential on the result. Where there is expected to be high extinction values, for example, in the star formation regions of the spiral arms, the obscuration may preclude any observations of distant stars. It is for these reasons, claim Neckel and Klare, that the dust distribution obtained by this method does not correlate well with the observed spiral features.

THE FAR INFRARED

Studies of the galactic far-infrared emission relates directly to the distribution of dust in the Galaxy. Since stellar radiation is partly absorbed by interstellar grains and reradiated at far-infrared wavelengths ($\lambda > 30\mu$) where the dust is nearly transparent, studies at these long wavelengths can also indicate the distribution of star types and star formation.

Observations at these long wavelengths have to be conducted at high altitudes, because of atmospheric extinction. The use of aeroplanes, balloon platforms or satellites restricts the size of the telescopes, and the need to cool the dewars with liquid helium restricts the lifetime of the observations.

Serra et al.⁵² observed, in two wavelength bands, $\lambda = 75$ to 95μ and $\lambda = 115$ to 196μ , the galactic plane between longitudes $\ell = 26^\circ$ and

$\ell = 40^\circ$. They show that there is a broad maximum of emission near $\ell = 30^\circ$, which is probably associated with the '5 kpc ring' of dense molecular clouds. They also note that the longitude distribution suggests patching emission, ruling out previous models of a smooth emitting disc. The ratio between the short and the long wavelength channel is a good indicator of dust temperature below 50 K. They find that for standard grain models the dust temperature is ≈ 27 K except in the direction of giant HII regions where it rises to ≈ 35 K.

Nishimura et al.⁵³ present a map of emission in the 100 to 300 μ band from longitude $\ell = 352^\circ$ to 45° covering 2° either side of the galactic plane. They find that all of the far-infrared discrete sources are positionally correlated with HII regions and/or molecular clouds, and the underlying diffuse emission appears to follow the same distribution, with respect to galactic longitude, as the CO emission and the diffuse free-free continuum.

The Japanese, Maihara et al.⁵⁴ have compared the longitudinal distribution of the far-infrared emission with the 2.4 micron distribution. The 2.4 micron emission is mainly due to the stellar content, whereas the far-infrared comes from heated dust. They find that the two distributions are anti-correlated; peaks in the 2.4 micron profile tend to correspond to dips in the far-infrared profile. This should be interpreted as a fluctuation in the grain distribution rather than a structure in the stellar distribution. If grains had a smooth distribution and stars had structure, then the near and far infrared intensities would be positively correlated, because stars should contribute to the heating of the grains.

THE GALACTIC CENTRE

The last straw for the Kapteyn Universe (described in the next chapter) which places the Sun near the centre of the Galaxy, came from Shapley. He deduced from the distribution of globular clusters that the centre was very distant and in the direction of Sagittarius. The first detection of the galactic centre came in the 1930's, while Jansky was investigating the cosmic hiss with his radio equipment. He noticed that the strongest signal came from the direction of Sagittarius and it did not shift its position with the changing seasons which would imply an Earth or Solar System source. This radio source was later called Sagittarius A. Towards the end of the 1950's radio technology had advanced enough to show that Sagittarius A was a complex of sources. From spectroscopic work it was also shown that from the motions and velocity of the gas, much if not all of the radio source Sagittarius A is located at the centre of the Galaxy.

RADIO FEATURES OF THE GALACTIC NUCLEUS⁵⁵

The interstellar gas in the galactic nucleus can be investigated in several ways. Atomic hydrogen can be observed with its 21 cm line. Molecular hydrogen can be implied from observations of other molecules, such as CO, OH, H₂CO, that always occur with H₂. There are also numerous HII regions in the central area, which can be seen in the radio continuum, as well as in recombination lines. The contribution of the gas to the total mass density in the central region is negligible, but the motion of the gas as seen for example, in the 21 cm line, gives important information about this central density.

Observations of the velocity-longitude relationship for atomic hydrogen suggest that there is a rapidly rotating disc of gas, with a rotation velocity of over 200 km s^{-1} , stretching out to 4° of

longitude from the centre.

Also seen in the 21 cm velocity diagrams is an intense ridge of emission with a radial velocity at zero longitude of 53 km s^{-1} , and traced out to a longitude of -22° where it becomes 'tangential'. Since gas with a circular orbit should have zero radial velocity at zero longitude, this ridge is assumed to be an expanding 3 kpc arm. Oort⁵⁵ lists many more individual radio features seen in the nuclear region.

A major drawback in the interpretation of these results is the lack of symmetry between positive and negative longitudes for these features. If these features were axially symmetric about the centre then the velocity profiles at positive longitudes should be mirrored in those for negative longitudes. The observed data shows very little correlation between the two sides. If the interpretation for all these radio features is correct, then the nuclear region must be very turbulent and complex.

At a longitude of about $40'$ from the nucleus is the strong radio source Sagittarius B2. This source is an agglomerate of gas and dust clouds containing at least seven compact HII regions. This complex is one of the most massive objects in the Galaxy, with an estimated molecular hydrogen mass of $3 \times 10^6 M_\odot$, as seen from CO observations.⁵⁶

Maps of the thermal radiation show that $12'$ NE of the principal central source, is a spur source resolvable into several components. This was initially called Sagittarius B1,⁵⁷ but is now better known as the Arc.⁵⁵ The Arc is a string of extended clouds, looking very much as though due to an explosive phenomenon. There appear to be a considerable number of compact HII regions, lying preferentially, at the Arc's outer edge.

The principal central source, Sagittarius A, has recently been shown to consist of two sources; Sagittarius A West and Sagittarius A East, separated by about 2 minutes of arc. The eastern component has a nonthermal spectrum, and is probably a supernova remnant with a diameter of about 7 pc. Sagittarius A West has a spectrum more like a giant HII region. At the centre of Sagittarius A West is an extremely compact source, which has not been resolved for sizes of 0.001 arcseconds. Within this radius there may be an estimated mass of $4 \times 10^6 M_{\odot}$. Sagittarius A West lies in the midst of an agglomeration of infrared sources covering an area of about 20" (1 pc) diameter. This cluster contains the sharp maximum of 2.2 μ radiation which is supposedly the dynamical centre of the Galaxy.

THE INFRARED CORE

The stellar population at the centre of the Galaxy was first investigated by Becklin and Neugebauer in 1968.⁵⁸ They mapped the nuclear region at 2.2 microns with resolutions 108", 48" and 15". They found that the infrared radiation peaked at the radio position of Sagittarius A. High resolution maps at 2.2, 10 and 20 microns^{59,60} with resolutions less than 3" show that the central 30" is resolvable into many discrete sources, plus some extended regions of emission. Figures 1E and 1F reproduce the maps at 2 and 10 microns. The maps at 2.2 and 10 microns are strikingly different. The 2.2 micron map shows about 15 individual sources overlying a more or less uniform diffuse background. The 10 micron map shows 10 discrete sources overlying a ridge of emission aligned approximately along the galactic plane. Only 4 sources show up at both wavelengths. The differences in the maps is due to the fact that the emission at

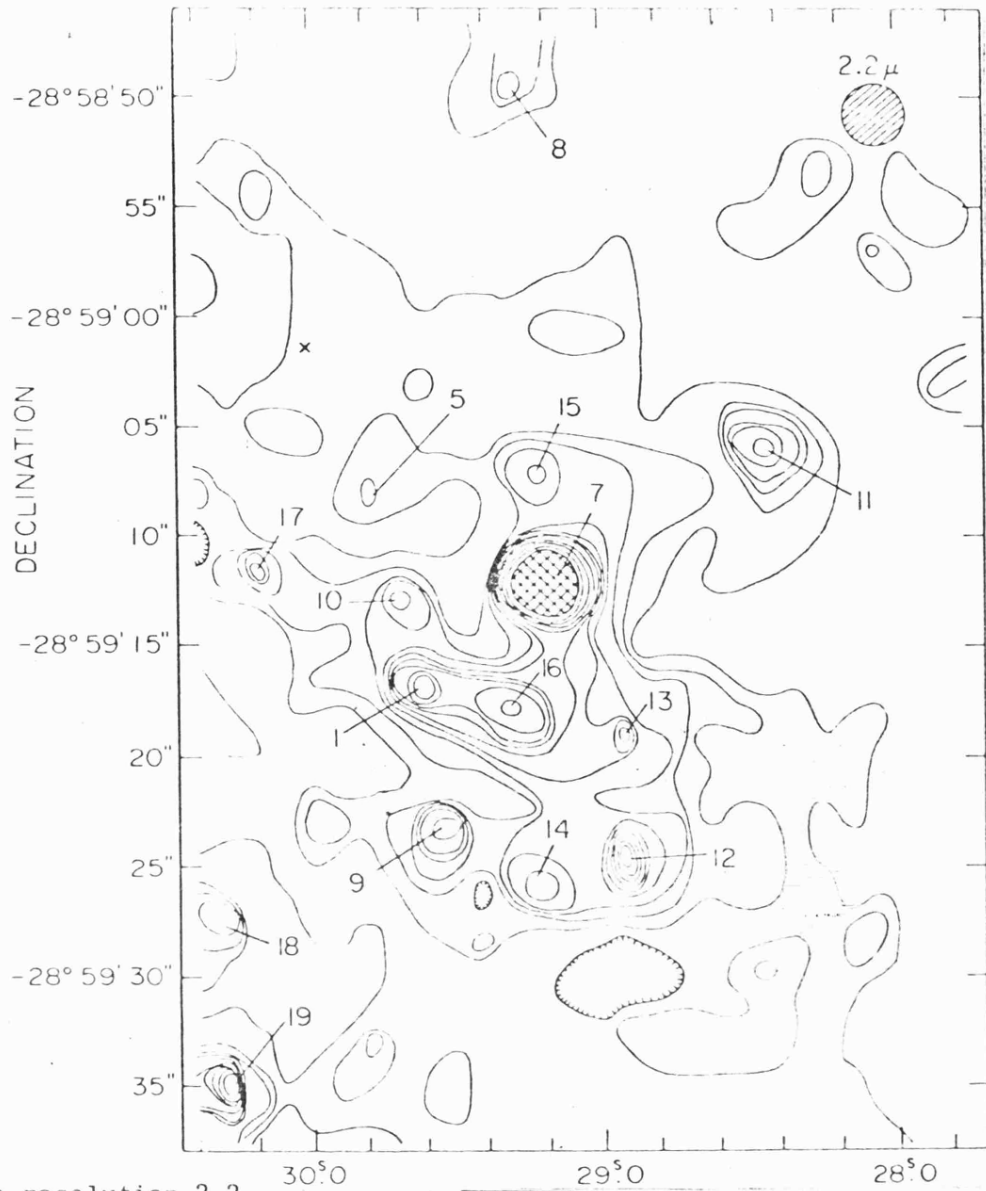


Fig. 1E High resolution 2.2 micron map of the galactic centre region (ref. 59).

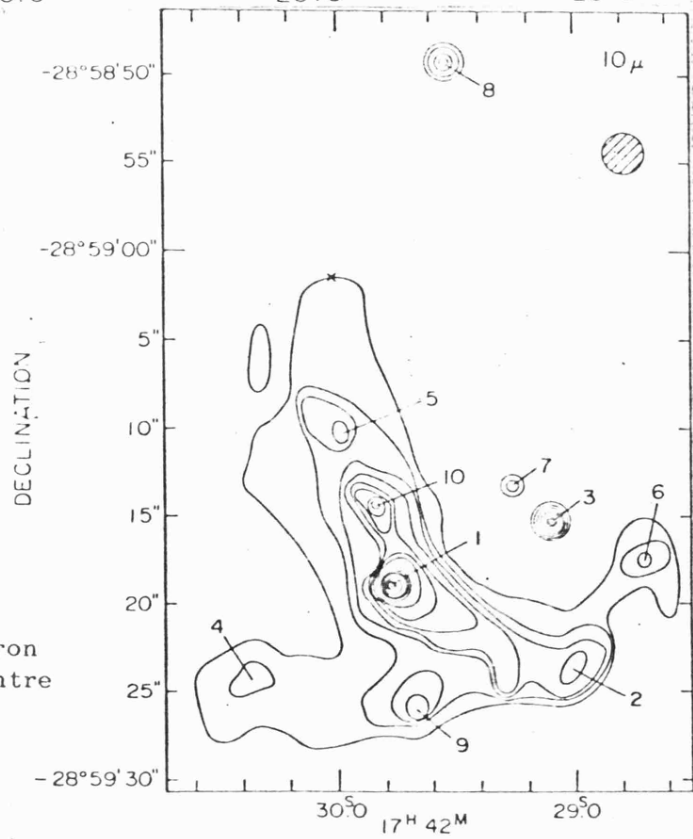


Fig. 1F High resolution 10 micron map of the galactic centre region (ref. 60).

2.2 microns is mainly direct stellar radiation, while that at 10 microns comes from solid particles, heated by stars, but radiating at a much lower temperature. This heating could come from the increase in stellar density at the very centre, or from newly formed high luminosity stars, which presumably show as the discrete sources in the 10 micron map.

Becklin and Neugebauer^{58,61} have shown that the infrared (2.2 microns) extinction to the galactic nucleus totals 2.7 magnitudes, which is equivalent to 27 magnitudes of visual extinction. From the colours of individual sources and the background they deduced that not more than 6 magnitudes of visual extinction occurred in the central 3 pc.

From far-infrared observations of the galactic centre Gatley et al.⁶² have shown that the volume density of dust is fairly uniform within about 15 pc of the centre, and is relatively small (~ 3 visual magnitudes) compared with the high gas densities. The decrease in surface brightness at these long wavelengths is then attributed to a decrease in the dust temperature, with little or no change in the dust column density.

The motions in the central regions can be studied by observing the 12.8 micron spectral line of Neon II. Lacy et al.⁶³ found there were some sources with velocities of several hundred kilometers per second. If these velocities are due to orbital motions then a mass within the central parsec of $8 \times 10^6 M_{\odot}$ is derived. They also noted that the rotation axis of this gas is inclined by $60^{\circ} - 90^{\circ}$ from that of the Galaxy. This effect is also seen in M31 where the rotation axis of the inner 5 pc is significantly different from that of the galaxy as a whole.

A major unresolved problem in the galactic centre studies is how the 27 magnitudes of visual extinction is distributed along the

line of sight. Oda et al.⁶⁴ and Maihara et al.⁵⁴ deduce from 2.4 microns and far-infrared observations that two-thirds of the extinction occurs in the galactic disc and the other third occurs in the central 300 pc of the Galaxy. Polarisation data can be used to investigate interstellar extinction. Hough et al.⁶⁵ show that the infrared polarisation of the central region agrees well with the standard interstellar law, and is aligned with optical polarisations of stars in the disc. Kobayashi et al.⁶⁶ show that over the central 7' x 7' (20 pc x 20 pc at the galactic centre) the infrared polarisations are almost uniform indicating they are generated outside the galactic core region. The high degree of polarisation cannot just be explained from the visual polarisations observed in the nearest arm. The major part of the polarisation would therefore arise in the inner regions or in the '5 kpc ring'.

Not all investigators agree, however, that the extinction across the central region is uniform. Lebofsky⁶⁷ produced a 2 micron map of the central 4' x 4' region. When compared to a radio formaldehyde map, she deduced that there are large extinction variations over the face of the nucleus.

STAR COUNTS

For a long period in the middle of this century, star counting was an unfashionable branch of astronomy. Recently there has been renewed interest because of advances in astronomical techniques. Near infrared photographic sky surveys and the advancement of infrared technology allows observations to pierce the extinction veil in the plane of the Galaxy. The forthcoming Space Telescope will use star counts to investigate the halo of our Galaxy,¹⁷ and possibly improve our knowledge of the luminosity function.

A brief review of star counting for optical and infrared wavelengths will be given at the beginning of the appropriate chapter.

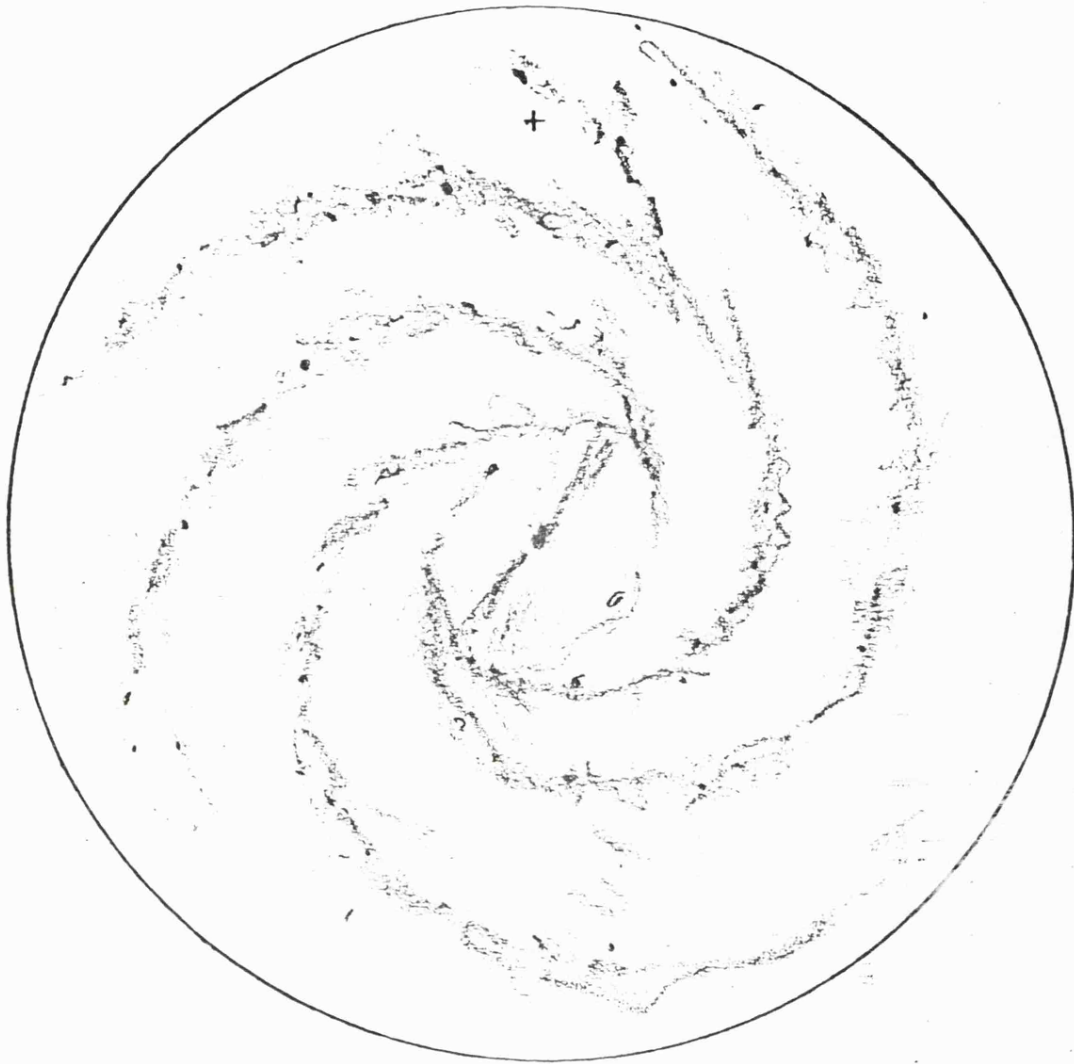


Fig. 1G A sketch of the morphology of the Galaxy implied by the SAB(rs)bc classification (ref. 8) and consistent with the spiral pattern derived from HII regions (fig. 1A).

Chapter 1

REFERENCES

1. de Vaucouleurs, G., 1959. Handbuch der Physik 53, 275,
Springer-Verlag Berlin.
2. Freeman, K.C., 1970. Astrophys. J. 160, 811.
3. Schweizer, F., 1976. Astrophys. J. Suppl. 31, 313.
4. Strom, S.E. and Strom, K.M., 1979. In IAU Symp. No. 84 'The
large scale characteristics of the Galaxy', p.9. Reidel
Dordrecht Holland.
5. Gott, J.R. and Thuan, T.X., 1976. Astrophys. J. 204, 649.
6. Larson, R.B., 1976. Mon.Not.R.astr.Soc. 176, 31.
7. Baade, W., 1944. Astrophys. J. 100, 137.
8. de Vaucouleurs, G. and Pence, W.D., 1978. Astron. J. 83, 1163.
9. Kormendy, J., 1977. Astrophys. J. 217, 406.
10. Whitford, A.E., 1978. Astrophys. J. 226, 777.
11. Nassau, J.J. and Blanco, V.M., 1958. Astrophys. J. 128, 46.
12. van den Bergh, S., 1975. Ann. Rev. Astron. Astrophys. 13, 217.
13. van den Bergh, S. and Herbst, E., 1974. Astron. J. 79, 603.
14. de Vaucouleurs, G. and Buta, R., 1978. Astron. J. 83, 1383.
15. Maihara, T., Oda, N., Sugiyama, T. and Okuda, H., 1978. Publ.
Astron. Soc. Japan 30, 1.
16. Young, P.J., 1976. Astron. J. 81, 807.
17. Bahcall, J.N. and Soneira, R.M., 1980. Astrophys. J. Suppl.
44, 73.
18. Freeman, K.C., 1978. In IAU Symp. No. 77 'Structure and
properties of nearby galaxies', p.3. Reidel, Dordrecht
Holland.
19. Lin, C.C., Yuan, C. and Shu, F.H., 1969. Astrophys. J. 155, 721.

20. Mathewson, D.S., van der Kruit, P.C. and Brown, W.N., 1972.
Astron. Astrophys. 17, 468.
21. Strömberg, B., 1948. Astrophys. J. 108, 242.
22. Morgan, W.W., Sharpless, S. and Osterbrock, D., 1952. Astron.
J. 57, 3.
23. Sharpless, S., 1965. In 'Galactic Structure', p.131, eds.
A. Blaauw and M. Schmidt, University of Chicago, Chicago.
24. Crampton, D. and Georgelin, Y.M., 1975. Astron. Astrophys. 40,
317.
25. Georgelin, Y.M. and Georgelin, Y.P., 1976. Astron. Astrophys.
49, 57.
26. Humphreys, R.M., 1979. In IAU Symp. No. 84 'The large scale
characteristics of the Galaxy', p.93. Reidel, Dordrecht
Holland.
27. Kerr, F.J., 1969. Ann. Rev. Astron. Astrophys. 7, 39.
28. Kerr, F.J. and Westerhout, G., 1965. In 'Galactic Structure',
p.167, eds. A. Blaauw and M. Schmidt, University of
Chicago, Chicago.
29. Fletcher, E.S., 1963. Astron. J. 68, 407.
30. Solomon, P.M., Sanders, D.B. and Scoville, N.Z., 1979. In IAU
Symp. No. 84 'The large scale characteristics of the
Galaxy', p.35. Reidel, Dordrecht Holland.
31. Scoville, N.Z., Solomon, P.M. and Sanders, D.B., 1979. In IAU
Symp. No. 84 'The large scale characteristics of the
Galaxy', p.277. Reidel, Dordrecht Holland.
32. Johnson, H.L., 1968. In 'Nebulae and interstellar matter', p.167,
eds. B.M. Middlehurst and L.H. Aller, University of
Chicago, Chicago.
33. Trumpler, R.J., 1933. Lick Obs. Bull. 14, 154.

34. Harris, D.H., 1973. In IAU Symp. No. 52 'Interstellar dust and related topics', p.31. Reidel, Dordrecht Holland.
35. Trumpler, R.J. and Weaver, H.F., 1953. 'Statistical Astronomy', Dover Publications New York.
36. Lynga, G., 1979. In IAU Symp. No. 84 'The large scale characteristics of the Galaxy', p.87. Reidel, Dordrecht Holland.
37. Greenberg, J.M., 1968. In 'Nebulae and interstellar matter', p.221, eds. B.M. Middlehurst and L.H. Aller, University of Chicago, Chicago.
38. Greenberg, J.M., 1978. In 'Cosmic dust', p.187, ed. J.A.M. McDonnell, Wiley-Interscience, Chichester.
39. Hall, J.S., 1949. Science 109, 166.
40. Hiltner, W.A., 1949. Science 109, 165.
41. Bok, B.J. and Bok, P.F., 1974. 'The Milky Way', Harvard Univ., Cambridge, Mass.
42. Munch, G., 1965. In 'Galactic Structure', p.203, eds. A. Blaauw and M. Schmidt, University of Chicago, Chicago.
43. Munch, G., 1968. In 'Nebulae and interstellar matter', p. 365, eds. B.M. Middlehurst and L.H. Aller, University of Chicago, Chicago.
44. Menon, T.K., 1971. In 'Dark nebulae, globules, and protostars', p.67, ed. B.T. Lynds, University of Arizona, Tucson.
45. Braunsfurth, E. and Rohlfs, K., 1973. In IAU Symp. No. 52 'Interstellar dust and related topics', p.231. Reidel, Dordrecht Holland.
46. Lilley, A.E., 1955. Astrophys. J., 121, 559.
47. Sandage, A., 1961. 'The Hubble atlas of galaxies', Carnegie Institute, Washington.

48. Lynds, B.T., 1970. In IAU Symp. No. 38 'The spiral structure of our Galaxy', p.26. Reidel, Dordrecht Holland.
49. Lynds, B.T., 1968. In 'Nebulae and interstellar matter', p.119, eds. B.M. Middlehurst and L.H. Aller, University of Chicago, Chicago.
50. Lynds, B.T., 1962. *Astrophys. J. Suppl.* 7, 1.
51. Neckel, T. and Klare, G., 1980. *Astron. Astrophys. Suppl.* 42, 251.
52. Serra, G., Boisse, P., Gispert, R., Wijnbergen, J., Ryter, C. and Puget, J.L., 1979. *Astron. Astrophys.* 76, 259.
53. Nishimura, T., Low, F.J. and Kurtz, R.F., 1980. *Astrophys. J.* 239, L101.
54. Maihara, T., Oda, N., Shibai, H. and Okuda, H., 1981. *Astron. Astrophys.* 97, 139.
55. Oort, J.H., 1977. *Ann. Rev. Astron. Astrophys.* 15, 295.
56. Scoville, N.Z., Solomon, P.M. and Penzias, A.A., 1975. *Astrophys. J.* 201, 352.
57. Burke, B.F., 1965. *Ann. Rev. Astron. Astrophys.* 3, 275.
58. Becklin, E.E. and Neugebauer, G., 1968. *Astrophys. J.* 151, 145.
59. Becklin, E.E. and Neugebauer, G., 1975. *Astrophys. J.* 200, L71.
60. Becklin, E.E., Mathews, K., Neugebauer, G. and Willner, S.P., 1978. *Astrophys. J.* 219, 121.
61. Becklin, E.E., Mathews, K., Neugebauer, G. and Willner, S.P., 1978. *Astrophys. J.*, 220, 831.
62. Gatley, I., Becklin, E.E., Werner, M.W. and Wynn;Williams, C.G., 1977. *Astrophys. J.* 216, 277.
63. Lacy, J.H., Baas, F. and Townes, C.H., 1979. *Astrophys. J.* 227, L17.

64. Oda, N., Maihara, T., Sugiyama, T. and Okuda, H., 1979.
Astron. Astrophys. 72, 309.
65. Hough, J.H., McCall, A., Adams, D.J. and Jameson, R.F., 1978.
Astron. Astrophys. 69, 431.
66. Kobayashi, Y., Kawara, K., Kozasa, T., Sato, S. and Okuda, H.,
1980. Publ. Astron. Soc. Japan 32, 291.
67. Lebofsky, M.J., 1979. Astron. J. 84, 324.

2

CHAPTER 2

METHODS OF STAR COUNTING AND ANALYSIS

THE PIONEERS¹

Before any quantitative star counts were undertaken, men like Thomas Wright and William Herschel in the 18th Century, deduced, from the concentration of stars towards the Milky Way, that the stars form a limited system of highly flattened shape. A simple approximation of this, is a system symmetrical with respect to the galactic plane, and with rotational symmetry about an axis perpendicular to this plane.

To an observer at the centre of this system the star counts will be independent of galactic longitude and the two galactic hemispheres will have the same star distribution. An observer in a non-central position will, however, see asymmetries in the stellar distribution. If the observer is situated out of the plane, for example, the star density in northern galactic latitudes will differ from that in the corresponding southern galactic latitudes. From a position in the galactic plane but away from the centre, the star density will vary with galactic longitude, but this variation will be symmetrical above and below the plane.

As can be seen from this simple model, star counts can be used to describe the position of the Sun in the Galaxy. To do this star counts for the whole sky, or for regularly spaced areas are needed. A catalogue of the positions and magnitudes of all stars, down to a limiting magnitude, for the whole sky or a defined area is called a "Durchmusterung", or survey catalogue. The data for the early Durchmusterung catalogues were determined by time-consuming visual observing methods. More recently photographic techniques have been used in such work. For stars brighter than 10th magnitude complete catalogues for the whole sky have been made. For fainter stars it is necessary to limit the catalogue to selected areas.

In 1906 J.C. Kapteyn proposed a plan of 206 selected areas spaced at 15 degree intervals over the whole sky. The Harvard-Groningen Durchmusterung covered all of the 206 areas down to a magnitude limit of 16.5. From these catalogues it has been found that toward the galactic poles the greatest contribution to the integrated light comes from stars with magnitudes of about 8.5. At the galactic equator, on the other hand, the greatest contribution is received from stars of magnitude 13. The surface brightness of the Milky Way comes primarily from stars in the magnitude range 10 to 16.

From these early studies it was found, by van Rhijn at Groningen and Seares at Mount Wilson, that the position of the galactic pole and the longitude of the galactic centre vary with the magnitude of the stars studied. This is due to 'Gould's belt of bright stars' which alters the plane of symmetry of the brightest stars from that of the fainter stars by nearly 20° . This is probably due to a local irregularity in the Sun's part of the Galaxy.

Early investigators attempted to find simple functions to describe the variation of stellar density from star counts. From the Bonner Durchmusterung Catalogue, Seeliger deduced that for stars brighter than 9th magnitude neglecting extinction, the density of stars dropped with distance from the Sun, under the description of a simple power law. When fainter magnitudes were considered it was found that this simple law did not hold and so investigators such as Schwarzschild proposed more complex functions.

By 1920, Kapteyn and van Rhijn using Schwarzschild's density formula and star counts from Kapteyn's Selected Areas had deduced a galactic model based on the assumption of no interstellar extinction. They found the stellar system to be ellipsoidal in shape with the Sun not far from its centre; this model being called the "Kapteyn

Universe". Shortly after this proposal, evidence was found to show this model was false. Shapley found, from the distribution of globular clusters, that the stellar system is much larger than the Kapteyn Universe, and that the centre is very distant in the direction of Sagittarius. The Oort and Lindblad theory of galactic rotation also predicted an eccentric position for the Sun. Finally Trumpler showed that interstellar extinction is important in the Galaxy.

THE EQUATION OF STAR COUNTS

The basic equation of star counts is

$$A(m) = \int_0^{\infty} r^2 \Delta(r) \phi(M) dr \quad (2.1)$$

where $A(m)$ is the number of stars per steradian counted in the apparent magnitude interval $m-dm/2 < m < m+dm/2$. $\Delta(r)$ is the relative (to the solar neighbourhood) space density of stars at distance r , from the Sun. ($\Delta = 1$ at $r = 0$, r in parsecs). $\phi(M)$ is the luminosity function. It specifies the number of stars per cubic parsec per unit interval of absolute magnitude M in the solar neighbourhood.

The equation relating the apparent and absolute magnitude (m, M) is

$$m = M + 5 \log r/10 \quad (2.2)$$

where no extinction is present and

$$m = M + 5 \log r/10 + \alpha(r) \quad (2.3)$$

where there is α magnitudes of extinction to distance r .

A useful quantity is the distance modulus y , defined as the difference between the apparent and absolute magnitudes

$$y = m - M \quad (2.4)$$

From equations (2.2) and (2.3) it can be seen that in the presence of extinction the distance modulus is not a simple function of the distance.

SPECIAL SOLUTION

To simplify the solution of the star count equation (2.1), early investigators proposed plausible assumptions that made it possible to draw some conclusions from the limited observational data. An important test case is one under the following three assumptions:

- 1 - the stellar system is of unlimited extent
- 2 - the stars are uniformly distributed
- 3 - space is perfectly transparent.

From assumption 2

$$\Delta(r) = 1 \quad (2.5)$$

from assumption 3 and equation (2.2)

$$m = M + 5 \log r/10$$

$$\therefore r = 10 \times 10^{0.2(m-M)} \quad (2.6)$$

$$\text{and } dr = 10 \beta 10^{0.2(m-M)} dM \quad (2.7)$$

for each value of m . $\beta = 1/5 \log e$.

Putting equations 2.5, 2.6 and 2.7 in equation 2.1 gives

$$A(m) = 10^3 \beta 10^{0.6m} \int_{-\infty}^{+\infty} 10^{-0.6M} \phi(M) dM \quad (2.8)$$

since the integral is a function of M alone its numerical value is constant and hence

$$A(m) = C 10^{0.6m} \quad (2.9)$$

where C is a constant.

The ratio of the number of stars in successive apparent magnitude intervals is

$$\frac{A(m+1)}{A(m)} = \frac{C 10^{0.6(m+1)}}{C 10^{0.6m}} = 10^{0.6} = 3.981 \quad (2.10)$$

A similar relationship to equation (2.10) holds for the total number of stars $N(m)$ brighter than apparent magnitude m . (The cumulative count)

$$\frac{N(m+1)}{N(m)} = 10^{0.6} = 3.981 \quad (2.11)$$

If the stars were uniformly distributed throughout infinite space and if space were perfectly transparent, the number of stars brighter than apparent magnitude m would increase by a factor 3.981 for each unit increase in m , irrespective of the form of the luminosity function.

If $I(m) dm$ denotes the amount of light from stars in the apparent magnitude range $m - dm < m < m + dm$ then

$$I(m) dm = I_0 10^{-0.4m} A(m) dm \quad (2.12)$$

where I_0 is the amount of light from a zero magnitude star.

The total intensity of starlight per steradian from stars brighter than apparent magnitude m is

$$T(m) = \int_{-\infty}^m I(m) dm = I_0 \int_{-\infty}^m 10^{-0.4m} A(m) dm \quad (2.13)$$

Under the three assumptions of above $A(m) = C 10^{0.6m}$

$$\therefore T(m) = C_0 \int_{-\infty}^m 10^{0.2m} dm = C_1 10^{0.2m} \quad (2.14)$$

From equation (2.14) it can be seen that as the magnitude limit m increases the amount of starlight increases to infinity. This is Olber's paradox.

The discrepancy between this conclusion and what is observed, as well as the increase of areal star density toward the Milky Way led to the early abandonment of the first assumption of an unlimited system.

THE LUMINOSITY FUNCTION

The luminosity function, or luminosity law, is a simplified form of the bivariate M, S distribution

$$\phi(M) = \int_{-\infty}^{+\infty} \phi(M,S) dS$$

where S is the spectral type of the stars and $\phi(M,S)$ is the number of stars per cubic parsec in the solar neighbourhood distributed into absolute magnitude and spectral type.

When determining the luminosity law, the volume of space representing "in the solar neighbourhood" must be small enough to be homogeneous, yet large enough to yield a significant sample of stars. A reasonable volume is a sphere centred on the Sun, with a radius of 50 pc. Within this sphere stars have parallaxes sufficiently large to be measured with reasonable accuracy. Out to a distance of 50 pc interstellar extinction can generally be neglected. Finally a sphere of radius 50 pc is small enough for the population to be considered homogeneous. A sphere twice the size, for example, would be affected by the decrease in extreme disc population stars perpendicular to the plane.

Within a sphere of 50 pc one can expect to find in the order of 50,000 stars. This is rather too many to find parallaxes for all

the stars, and so the luminosity law is statistical in nature.

In most star count analysis this luminosity law for the solar neighbourhood is assumed to be universally constant. This assumption is almost certainly incorrect, if only because of the two population types, I and II in the Galaxy. The difficulty of determining the luminosity law for anywhere but the solar neighbourhood normally prompts investigators to assume its universal constancy.

The luminosity function for visual wavelengths is shown in figure 2A.

This general luminosity function $\phi(M)$ is very broad, and it is sometimes of interest to know which part contributes most to the star count.

Taking equation (2.1)

$$A(m) = \int r^2 \Delta(r) \phi(M) dr$$

then equal contributions to the star count from all values of r occurs if

$$r^2 \Delta(r) \phi(M) = \text{constant} .$$

Assuming a uniform density distribution then $\Delta(r) = 1$ and under the assumption of no extinction then from equation (2.6)

$$r \propto 10^{-0.2M}$$

$$1/r^2 \propto 10^{0.4M}$$

$$\text{and } \phi(M) \propto 10^{0.4M}$$

If $\log \phi(M)$ is steeper than 0.4 then the lower luminosity stars dominate the star count. If $\log \phi(M)$ is shallower than 0.4 then the high luminosity stars dominate.

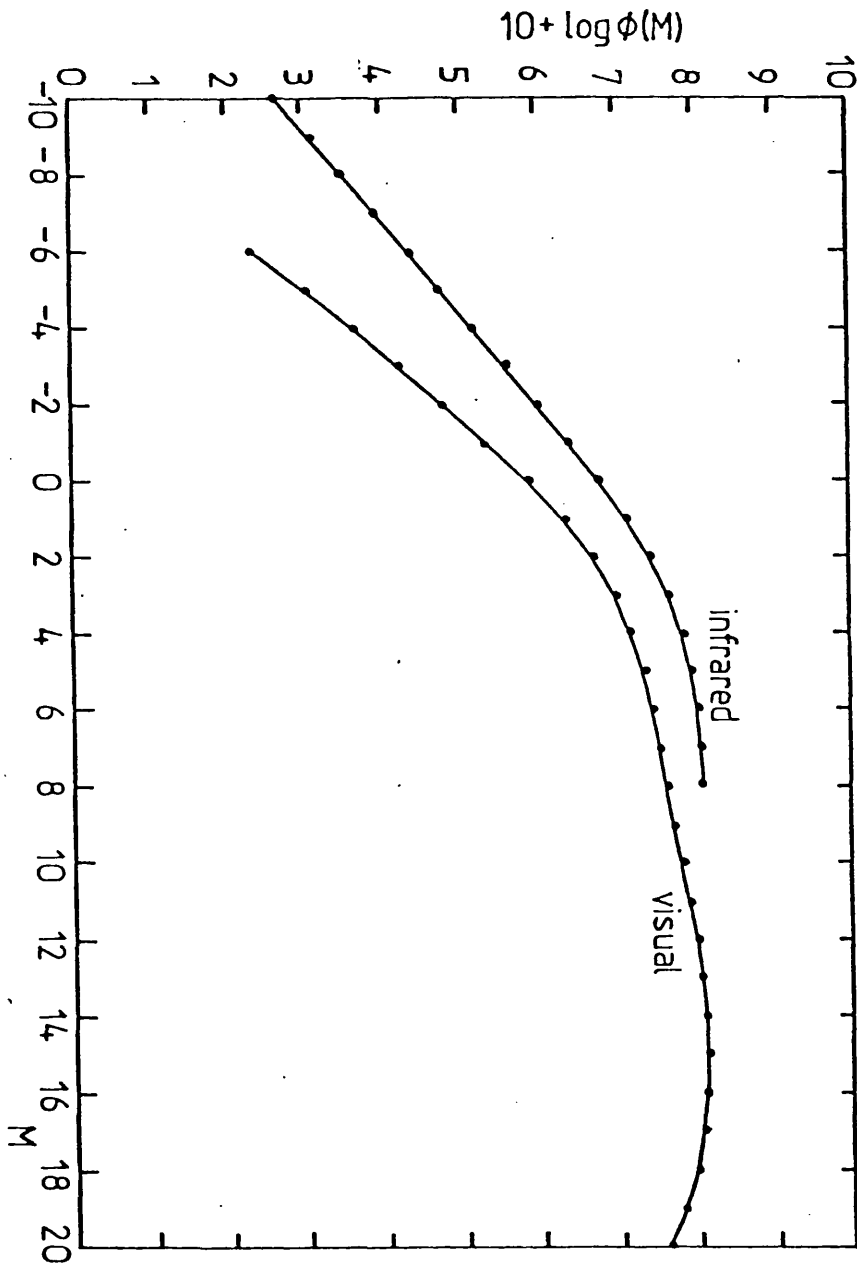


Fig. 2A Visual and infrared (2.2 micron) luminosity functions showing the number of stars per cubic parsec in the solar neighbourhood with absolute magnitude M (see pages 3.14 and 4.19).

If as for the visual luminosity function (figure 2A) the luminosity function passes from steeper than 0.4 to shallower than 0.4 then the stars around this inflexion will dominate the star count. For the visual luminosity function this occurs at approximately $M = +1$. The presence of extinction naturally favours brighter stars, and density changes can theoretically promote any part of the luminosity function into significance in the star count.

THE EFFECT OF INTERSTELLAR EXTINCTION

The star count equation (2.1) still holds when interstellar extinction is present, but the relationship between the apparent and absolute magnitudes changes to

$$m = M + 5 \log r/10 + \alpha(r) \quad (2.3)$$

The distance modulus is $y = m - M$ (2.4)

$$y = 5 \log r/10 + \alpha(r) \quad (2.15)$$

Now r cannot be explicitly expressed in terms of y .

Equation (2.1) can be written in terms of the distance modulus y

$$A(m) = \int_{-\infty}^{+\infty} \Delta(y) \phi(M) dV \quad (2.16)$$

where dV measures the volume element between the distance limits corresponding to $y \pm dy/2$, and $\Delta(y)$ is the relative density of stars at a distance corresponding to distance modulus y .

The relative density of stars $\Delta(y)$ can be replaced by the relative distribution of distance moduli $\Omega(y)$ which specifies the number of stars that should be found in unit solid angle and between distance moduli limits $y \pm dy/2$. The relationship relating these two functions is

$$\Omega(y) dy = \Delta(y) dV \quad (2.17)$$

so that

$$A(m) = \int_{-\infty}^{+\infty} \Omega(y) \phi(m-y) dy \quad (2.18)$$

In terms of r the elementary volume dV is given by

$$dV = r^2 dr = 1/3 d(r^3) \quad (2.19)$$

In the presence of interstellar extinction, from equation (2.15)

$$r = 10 \times 10^{0.2(y-\alpha(y))} \quad (2.20)$$

expressing the extinction α as a function of y , $\alpha(y)$, which specifies the extinction in magnitudes of a star with distance modulus y .

Putting equation (2.20) into (2.19) gives

$$\begin{aligned} dV &= \frac{1}{3} 10^3 \frac{d}{dy} (10^{0.6(y-\alpha(y))}) dy \\ &= \beta 10^3 10^{0.6(y-\alpha(y))} (1 - d\alpha(y)/dy) dy \end{aligned} \quad (2.21)$$

where $\beta = 1/5 \log e$.

The relationship between $\Omega(y)$ and $\Delta(y)$ is thus

$$\Omega(y) = \beta 10^3 \Delta(y) 10^{0.6(y-\alpha(y))} (1 - d\alpha(y)/dy) \quad (2.22)$$

$\Omega(y)$ depends on the density Δ and the extinction α .

Usually star counts are quoted in numbers per square degree rather than per steradian, and so to convert to square degrees any of the above expressions has to be multiplied by the factor

$$w = 1/3283 \text{ sq. degrees per steradian} \quad (2.23)$$

When trying to solve the star count equation (2.18) it is convenient to reduce the range of variation of $A(m)$ by multiplying both sides of equation (2.18) by a factor $10^{s_0-s_1 m}$ and introducing the 'reduced'

functions

$$\begin{aligned}
 a(m) &= A(m) 10^{s_0 - s_1 m} \\
 \omega(y) &= \Omega(y) K 10^{s_0 - s_1 y} \\
 \lambda(M) &= 1/K 10^{-s_1 M} \phi(M)
 \end{aligned}
 \tag{2.24}$$

where K is a normalising factor

$$K = \int_{-\infty}^{+\infty} 10^{-s_1 M} \phi(M) dM$$

Equation (2.18) then becomes

$$a(m) = \int_{-\infty}^{+\infty} \omega(y) \lambda(m-y) dy
 \tag{2.25}$$

This is the form of the star count equation which will be used in the next chapter to solve the star counts $a(m)$ for the relative distribution of distance moduli $\omega(y)$ by numerical integration.

Contrary to popular belief the effect of extinction on the star counts is not as clear cut as may be thought. Figure 2B is an excerpt from Bok's book "The distribution of the stars in space"² which shows the theoretical effect of a single infinitely thin obscuring cloud. There is no sudden horizontal shift in the count, before a sharp upturn, after the cloud has been passed, as is depicted in some books. This smoothing of the curve is due to the broad influence of the general luminosity function. Density variations are similarly smoothed by a broad luminosity function. The detection of extinction or density variations can be enhanced by counting only stars within specified spectral type limits, which reduces the width of the luminosity function. With the general luminosity function as kernel, however, the integral equation has a "poor resolving power" for study of details in the function $\omega(y)$ or $\Omega(y)$.

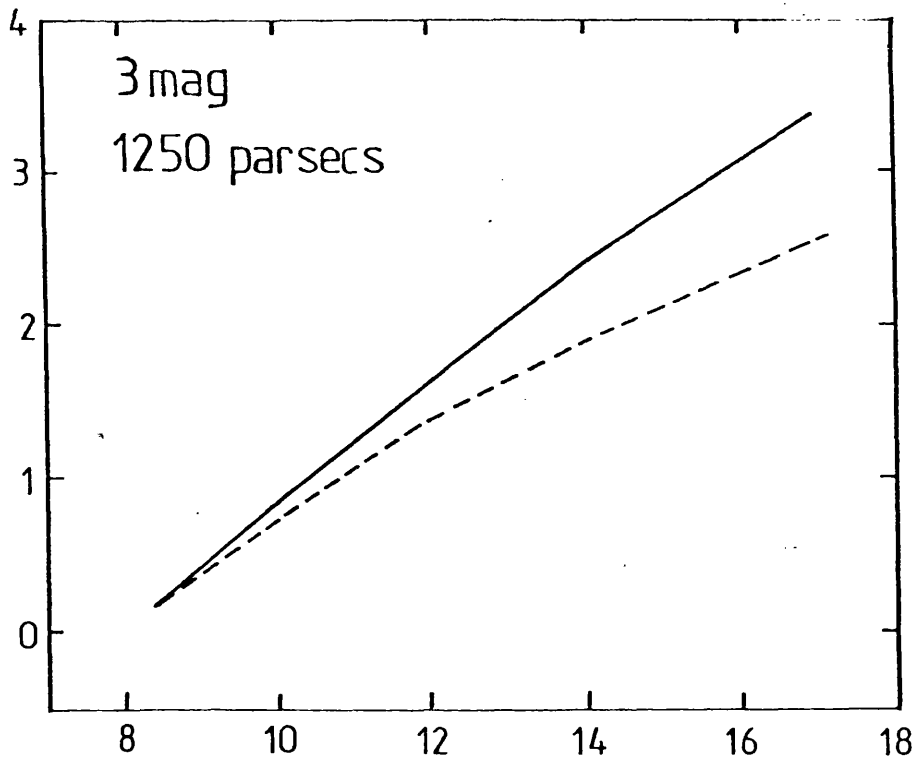
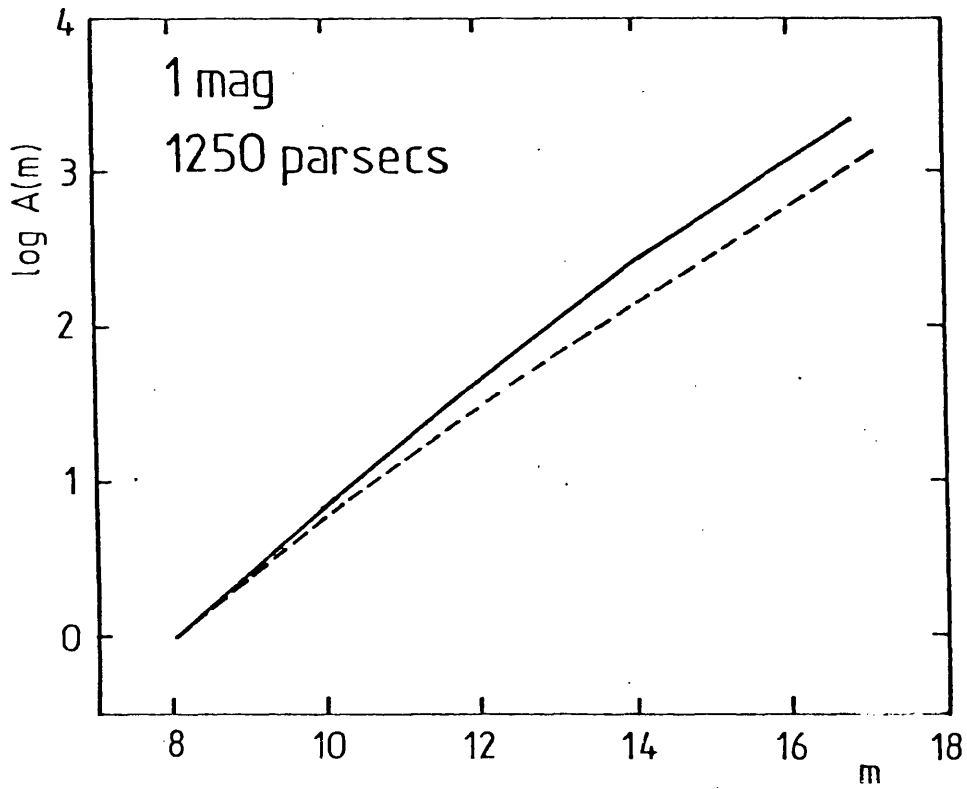


Fig. 2B The effect of an infinitely thin obscuring cloud of 1 and 3 magnitudes at 1250 parsecs on the star counts. The solid line shows the unaffected star counts, and the broken line the same after obscuration (ref. 2).

ACCURACY OF THE STAR COUNTS¹

If the actual number of stars counted in an area for a specified magnitude interval is n , the mean statistical percentage error σ/n can be approximated by

$$\frac{\sigma}{n} = \frac{1}{\sqrt{n}} \quad \text{or} \quad \sigma = \sqrt{n} \quad (2.26)$$

provided n is not a small number

Errors in the magnitude scale on which the star counts are based should also be taken into account.

INSTABILITIES OF THE INTEGRAL EQUATION^{3,4}

The basic star count equation (2.1) or the reduced equation (2.25) are a special form of an integral equation of the first kind

$$g(x) = \int_a^b K(x,y) f(y) dy \quad (a < x < b) \quad (2.27)$$

where $g(x)$ is the measured distribution of the true distribution $f(y)$ acted on by an 'apparatus function' $K(x,y)$ (the kernel).

There are several techniques which can theoretically solve for the true distribution function to any desired accuracy. This is however only theoretical. When one attempts to solve the equation accurately, irregular steep peaks and troughs appear in the solved function. These are not real but result from random errors in the measured distribution function g or to the inaccuracy of the 'apparatus function' K used.

This can be seen as follows. Let $f(y)$ be the solution to equation (2.27) and add to it the function $f_m = \sin my$. For any integrable kernel it follows that

$$g_m = \int_a^b K(x,y) \sin my \, dy \rightarrow 0 \quad \text{as } m \rightarrow \infty$$

Hence only an infinitesimal change g_m in g creates a finite change f_m in f , i.e. the equation is unstable in K . To prevent oscillations in the solution some sort of smoothing requirement is needed. This can be a mathematical or manual smoothing.

In stellar statistics the accuracy of $g(x)$ (i.e. $A(m)$) is defined approximately by the $\sigma \sim \sqrt{n}$ relationship. To decrease the percentage error more stars, i.e. a larger area has to be counted.

The kernel $K(x,y)$, is the luminosity function $\phi(M)$ which is known for the solar neighbourhood from parallax measurements, but has to be inferred for the rest of the Galaxy. In the infrared, however, the luminosity function is not so well known, and so interpretations of infrared star counts should be more restrained.

METHODS OF STAR COUNTING

Almost all optical star counts nowadays are obtained from photographs of the sky. The old technique of observing individual stars with a telescope is much too time consuming and compared to photographic techniques is inferior. A wealth of star counting material is now available from the all-sky photographic surveys of Schmidt telescopes. Specially prepared photographic plates can now 'see' into the near infrared (~ 0.9 microns) where extinction is less than half that at visible wavelengths, which is useful for studying regions close to the galactic plane, where extinction is large.

Various techniques can be used to extract star counts from photographic plates. The fastest method is by computer controlled densitometers which measure the integrated intensities of negative star images from a plate. The brighter the star the blacker the image.

The COSMOS machine at the Royal Observatory Edinburgh is an example of one of these machines, and its operation will be described in the next chapter. Another measure of a star's brightness on a plate is the size of the stellar image, which gets larger for brighter stars. Calibrations using the size of the image rather than integrated intensities are less accurate because there is a non-linear relationship between size and magnitude for bright stars.

With all the photographic techniques for reducing star counts some sort of magnitude calibration has to be obtained. This is usually done by measuring with a telescope, the photoelectric magnitudes of a sequence of bright to faint stars within the area covered by the plate. The integrated intensities or sizes of these sources are then plotted against the observed magnitude to get a calibration curve.

RESEAU SQUARE ANALYSIS

There is an application of star counts when investigating localised clouds of extinction, which can be done by hand and which does not require the magnitude of every star to be evaluated. This is the reseau square analysis. Simply it consists of dividing up the region of interest into small areas and counting the total number of stars in each area down to the plate limit. For regions of enhanced extinction fewer stars are counted, and a map of the obscuring cloud can be built up. The only magnitude calibration required is to know the plate limit, that is the magnitude of the faintest stars seen on the plate. For each reseau square the total star count is compared with the total count in unobscured space at the same magnitude limit. The unobscured count are usually taken from the mean values for the appropriate galactic latitude given in publications (e.g. *Astrophysical*

Quantities).⁵

Rossano^{6,7} used this technique to investigate the distribution of extinction in the Corona Australis dark cloud complex and for regions in Scorpio and Ophiuchus. To obtain quantitative values of the extinction, he derived for each of his reseau squares an effective apparent magnitude of the faintest stars counted, corresponding to the same count in unobscured space. The total amount of extinction due to the cloud is then given by the difference between this effective magnitude and the plate limit magnitude. It is very important in this quantitative analysis to be sure that the limiting magnitude is several magnitudes fainter than that corresponding to the back of the cloud. If this condition is not met then the extinctions obtained will be underestimates due to the smearing effect of the general luminosity function, and the influence of foreground stars. Rossano⁸ discusses the accuracy of extinctions obtained by this reseau square technique. Dickman⁹ also used this method to determine visual extinctions in dark nebulae.

This reseau square analysis is good for mapping clouds of extinction on the sky but cannot really give information on the distribution of extinction along a line of sight. To do this requires star counts binned into magnitude intervals so that the integral equation (2.1, 2.25) can be solved.

ANALYSIS OF STAR COUNTS

From the star counts of an area $A(m)$, the relative distribution of distance moduli $\Omega(y)$ can be found by solving equation (2.18). The methods of solution are discussed later in this chapter. From this function the density distribution or extinction relation can be found.

To determine the density distribution it is necessary to know

the functional form of the extinction with distance modulus α_y , or with distance α_r . If the extinction law is not known then an approximate or average law based on a simplified model of the interstellar medium may be adopted. As a first approximation the assumption of uniform extinction is often used. This law is useful over small distances, or in low galactic latitudes when local irregularities in the interstellar medium are neglected.

The extinction law can be calculated from the relative distribution of distance moduli $\Omega(y)$ if the true space density of stars is known or can be assumed. It is rare that the space density function in a given direction is actually known. In low galactic latitudes where interstellar extinction is large, however, it can be of interest to study the distribution of interstellar matter on the assumption that the space density of stars does not change much with moderate distances from the Sun (i.e. $\Delta(r) = 1$).

The mathematical approach for calculating these quantities is discussed in the chapter on visual star counts.

STUDIES OF LOCALISED CLOUDS OF EXTINCTION (Trumpler and Weaver¹ p.486)

In the Milky Way there are numerous localised condensations of dark interstellar material that obscure the light of the stars behind them. The distance depth and total extinction of such a cloud can be calculated by making star counts $A_d(m)$ in the dark area and similar counts $A_c(m)$ in a 'clear' comparison field. This comparison field must be chosen so that there is every reason to believe that the space distribution of stars is the same in both directions. In the study of a small dark cloud, the region immediately surrounding the dark area is a suitable comparison field.

In any area the relation between distance modulus and distance

depends upon the extinction law, and so for the two regions under study these must be distinguished.

$$y_c = 5 \log r/10 + \alpha_c(r) \quad \text{comparison field}$$

$$y_d = 5 \log r/10 + \alpha_c(r) + \alpha_d(r) \quad \text{dark area}$$

The function $\alpha_c(r)$ represents the extinction law in the comparison area while $\alpha_d(r)$ represents the excess extinction in the dark area over and above the comparison area. The function $\alpha_d(r)$ which describes the extinction in the cloud can be found from the above relations.

$$\alpha_d(r) = y_d(r) - y_c(r) .$$

Since, y_c is a monotonic function of the distance, α_d can also be written as a function of y_c

$$\alpha_d(y_c) = y_d(y_c) - y_c .$$

The solution of the problem is found by solving the integral equation (2.18) for the distribution of distance moduli $\Omega_c(y_c)$ and $\Omega_d(y_d)$ in the two fields which are assumed to have identical space distributions of stars. From these two distributions Ω_c, Ω_d , the functional relationship $y_d(y_c)$ is found from the values of y_d and y_c which correspond to the same distance.

STAR COUNTS AT TWO WAVELENGTHS (Trumpler and Weaver¹ p.493)

At low galactic latitudes where the interstellar extinction is irregular and large, it is very difficult to derive the space density law from star counts unless the extinction law is known accurately. A simultaneous solution for the extinction and space density laws is theoretically possible if, for the given region, star counts are made

in two distinct wavelength bands. The method of solution is similar to that for the study of localised clouds where star counts are obtained for the obscured and clear areas. The two functions $\Omega_p(y_p)$, $\Omega_Q(y_Q)$ are determined from the star counts $A_p(y_p)$, $A_Q(y_Q)$ for the two wavebands P and Q. To solve the integral equation it is necessary to know the separate luminosity functions for the two wavelengths. The functional relationship $y_p(y_Q)$ is then determined from the frequency functions $\Omega_p(y_p)$, $\Omega_Q(y_Q)$. The difference between this and the distance modulus y_Q gives the colour extinction $\gamma(y_Q)$.

$$\gamma(y_Q) = y_p(y_Q) - y_Q$$

$$\gamma(r) = \alpha_p(r) - \alpha_Q(r)$$

where α_p and α_Q are the extinction laws at each wavelength. It is assumed that the two extinction laws have a linear relationship, so that the γ function will directly give one of the extinction laws. With this extinction law the space density law can be determined from the appropriate Ω function.

In theory this method appears ideal for obtaining the density and extinction laws. In practice, however, large inaccuracies can arise if the errors in determining the Ω 's are of the order of the relatively small colour extinction by which they are separated.

METHODS OF SOLVING THE INTEGRAL EQUATION

There are many examples in the literature of methods used to solve the integral equation of star counts (equations 2.1, 2.25, 2.27). Unfortunately, almost all of these methods assume a Gaussian distribution for the luminosity function, to aid the solution. The luminosity law only approximates to a Gaussian distribution if a

limited spectral range of stars is considered. That means to reap the advantage of these methods, the star counts have to be limited to one or two spectral types. Some of these methods of solution, which include expansion in a power series, and various matrix methods are given in references 3, 4, 10, 11, 12. When there is no spectral selection in the star counts the general luminosity law (figure 2A) has to be used, and this function cannot even be approximated by a broad Gaussian distribution.

The solution of the integral equation of star counts, when the general luminosity is considered, is best achieved by numerical integration. This is the method expanded on by Trumpler and Weaver (p.460 onwards) and will be used in the analysis of visual star counts described in this thesis. The technique is a trial and error process where successive estimates of the distribution of distance moduli $\omega(y)$ are made. These estimates for $\omega(y)$ are put into equation (2.25) where they are multiplied by the elements of the reduced luminosity function $\lambda(m-y)$ to give a predicted star count $a(m)$. This prediction is compared with the observed values and if the agreement is not within the statistical errors of the count, the values of $\omega(y)$ are changed to improve the agreement. It is unlikely that the best solution will fit all the observed star counts within the individual errors whilst retaining a form for $\omega(y)$ which is physically reasonable. By "physically reasonable" it is meant that the values of $\omega(y)$ are always positive and should have a certain degree of continuity. Trumpler and Weaver quote a satisfactory solution as when at least two thirds of the residuals between the observed $a(m)$ and those computed are smaller than the individual errors, and when there are no long sequences of residuals with the same sign.

The solution by trial and error is much eased if a good first

approximation of $\omega(y)$ is found that only needs a few adjustments to give a satisfactory representation of the observed $a(m)$. Trumpler and Weaver use the first two terms of Eddington's solution

$$\omega(m - M_0) = a(m) - \frac{\sigma^2}{2} a''(m)$$

where M_0 is the mean of the reduced luminosity function λ and σ_M is the dispersion of this function. The second differential of the reduced star counts $a(m)$ is obtained by drawing a smooth curve through the $a(m)$ points.

When a satisfactory solution for $\omega(y)$ has been found the relative distribution of distance moduli $\Omega(y)$ can be calculated from equation (2.24). From the $\Omega(y)$ distribution the density distribution of the extinction law can be determined.

MODEL FITTING

Another trial and error approach to describing the shape of the star counts is to make a prediction for the density function and extinction law and put these directly into equation (2.1). In a lot of cases, related work may have given a hint as to some reasonable assumptions that could be made. For example in the galactic plane where there is a large cloud of extinction close by, the density can be assumed uniform. Then the fit to the count would be achieved by adjusting the extinction law. In all this work it is assumed that the luminosity function is constant. If the luminosity law is allowed to vary then by the nature of the integral equation an infinite number of solutions is possible. This method is used in both star counting chapters, visual and infrared, to confirm the model parameters.

Chapter 2

REFERENCES

1. Trumpler, R.J. and Weaver, H.F., 1953. *Statistical Astronomy*,
Dover Publications New York.
2. Bok, B.J., 1937. *The distribution of the stars in space*.
University of Chicago Press, Chicago.
3. van de Hulst, H.C., 1946. *Bull. Astr. Inst. Netherlands* 10, 75.
4. Philips, D.L., 1962. *J. assc. comput. mach.* 9, 84.
5. Allen, C.W., 1973. *Astrophysical Quantities*, Athlone Press,
London.
6. Rossano, G.S., 1978. *Astron. J.* 83, 234.
7. Rossano, G.S., 1978. *Astron. J.* 83, 241.
8. Rossano, G.S., 1980. *Astron. J.* 85, 1218.
9. Dickman, R.L., 1978. *Astron. J.* 83, 363.
10. Crowder, H.K., 1959. *Astron. J.* 64, 22.
11. Dolan, J.F., 1974. *Astron. Astrophys.* 35, 105.
12. Ochsenbein, F., 1980. *Astron. Astrophys.* 86, 321.

3

CHAPTER 3

OPTICAL STAR COUNTS

INTRODUCTION

Optical star counts have long been used to investigate galactic structure. At high galactic latitudes star counts can describe the disc and spheroid components of the Galaxy. Knowledge of star numbers at high galactic latitudes is also important for quasar studies. Towards the galactic plane star counts are used to map dark clouds and to determine local star density anomalies.

Perhaps the best text describing the uses and analysis of star counts is Trumpler and Weavers'¹ book 'Statistical Astronomy'. Observations of star counts at high galactic latitudes are discussed by Bahcall and Soneira.^{2,3} Rossano^{4,5} uses the reseau square analysis to determine extinctions due to nearby clouds in selected areas of the galactic plane. A clever use of dark clouds to determine the local stellar density variations has been described by Herbst and Sawyer.⁶ They obtained star counts in front of opaque molecular clouds for which the distances were known. This confirmed the existence of a local density enhancement over a region of about 500 pc, which has also been seen by McCuskey.⁷

Our interest in optical star counts concerns the investigation of star numbers towards the galactic nucleus. Becklin and Neugebauer⁸ estimated that there are 27 magnitudes of visual extinction to the centre of the Galaxy. From a study of M supergiants in Scorpius, Warner and Wing⁹ deduced that the dark clouds which produce the rift in the nuclear bulge lie predominantly at a distance of about 1.5 kpc, in the Sagittarius arm and are responsible for about 8 magnitudes of extinction. If the extinction is this severe then it should produce a noticeable effect in the star counts. The information from this investigation can be used in the construction of a model Galaxy, for the interpretation of the more penetrating infrared star counts towards

the galactic centre.

PROPOSAL OF PROJECT

A preliminary study of optical star counts towards the galactic centre was conducted using plates specially requested by D.J. Adams from the UK Schmidt telescope in Australia. Three plates (numbers J3543, R2303 and I3531) with filters IIIaJ (green), R and I were obtained. These plates are stored at the Royal Observatory Edinburgh (ROE). Star counts were obtained by projecting film copies of small areas of the plates onto a screen and measuring the sizes of the stellar images. Calibrations were taken from Antalova's¹⁰ list of OB stars in the Milky Way. Although this projection method is crude, the results for the IIIaJ plate did indicate a flattening of the curve around 13th magnitude, which could be caused by clouds of extinction in the Sagittarius arm.

This work indicated that a higher quality reduction could yield interesting results. To this end a request was made to the COSMOS plate measuring machine at ROE to analyse the three plates. Unfortunately, these plates could not be sensibly measured by the machine owing to the density of faint stars; the reduction software could not properly assign a background level from which to measure the intensities of the resolved stellar images. The only way round this problem was to re-photograph the field with shorter exposures to reduce the limiting magnitude. In 1979 the UK Schmidt unit produced three short exposure plates (numbers B5262, V5263 and R5269) with B, V and R filters. The exposure time of these plates was about 10 minutes to give a nominal limiting magnitude of 18. These plates are also stored at ROE. Measurements of these plates were made by the COSMOS machine.

THE OPERATION OF COSMOS

COSMOS is a rapid photographic plate scanning machine, sited at the Royal Observatory Edinburgh. It consists of a plate carriage with motions in both horizontal axes, a Microspot cathode ray tube and associated optics which projects a focussed light spot onto the photographic plate, and a photomultiplier to collect the transmitted light. There is also a feed-back system to allow for continuous monitoring and correction of the spot brightness.¹¹ The control of the machine is by computer and the output data is dumped directly onto magnetic tape for subsequent analysis.

The plate is measured by a raster scan technique. The plate is moved uniformly in one direction and a linear scan is set up on the face of the cathode ray tube in a perpendicular direction. The timing is so arranged that the individual scans are separated by intervals equal to the spot size. Spot sizes of 8, 16 or 32 microns can be chosen by the user.

Since the description of COSMOS by Pratt¹¹ the original concept of three modes of use has been reduced to two. The simplest mode is the mapping mode where the transmission of every pixel is measured. This mode is used for mapping extended objects such as galaxies and HII regions. The limitation of the mapping mode is that the data from a small area, 25 x 25 mm mapped at 8 micron resolution fills one magnetic tape.

The other available mode of operation is the threshold mapping (TM) mode. This mode was introduced in 1979 to replace the coarse and fine measurement modes of the original design. (COSMOS newsletter No. 4). In this mode COSMOS measures an area of the plate in a raster fashion as in mapping mode. In addition to measuring the transmission of each pixel the machine calculates a smoothed local background and applies a

threshold cutoff (specified by the user) such that only pixels above this local threshold are output to the magnetic tape. This reduces the amount of data to be stored, so that a whole Schmidt plate with 8 micron resolution can be stored on about 4 magnetic tapes. This raw data is passed through an off line image analysis program which determines which pixels are associated to form a coherent image. Various image parameters are calculated from the pixel distribution.

THE OUTPUT PRODUCE OF COSMOS

After the analysis of the plate has been completed by the Royal Observatory Edinburgh team, the user is sent a magnetic tape(s) containing the output products. The tape is 9-track, phase encoded, 1600 BPI, odd parity, in a FORTRAN readable format. The tape is divided into 1024, single length, 32 bit integer, words containing the data and measurement information. This makes the tapes simple to read since every condition and measurement is described by an integer number; no decimal points or alphabetic characters are used.

For each image recognised by the analysis program, twenty parameters are given in the output products. These are listed in table 3I. The unweighted parameters are calculated from the pixel distribution, where each pixel has equal weight. The intensity weighted parameters are calculated by weighting the pixels in proportion to the number of photons arriving at the pixel from the source. The COSMOS unit have estimated that the accuracies from the intensity weighted parameters are perhaps twice as good as the unweighted ones. (COSMOS newsletter No. 4). Word 9 of the data block $(-250 * \log (\sum_i (I_i - I_{sky})))$ gives the total intensity of the image above the background level. This gives a more accurate measure of the magnitude of the source than does the total connected area (word 7).

TABLE 3I

LIST OF PARAMETERS FOR EACH COSMOS IMAGE (TM)

<u>Word</u>	<u>Contents</u>	<u>Units</u>
1	X centroid)) unweighted	0.1 microns
2	Y centroid)	0.1 microns
3	X minimum	0.1 microns
4	X maximum	0.1 microns
5	Y minimum	0.1 microns
6	Y maximum	0.1 microns
7	Area	increments
8	Minimum transmission	0 - 255
9	- 250 x log ($\sum_i (I_i - I_{sky})$)	
10	I_{sky} at centroid	
11	X centroid)) intensity weighted	0.1 microns
12	Y centroid)	0.1 microns
13	semi-major axis)) unweighted	0.1 microns
14	semi-minor axis)	0.1 microns
15	orientation	degrees
16	semi-major axis)) intensity weighted	0.1 microns
17	semi-minor axis)	0.1 microns
18	orientation	degrees
19	blank	
20	Error word	

A full 1024 word block contains 51 images, the last 4 words being padded out with zeroes.

One difficulty in reading the output tapes at the Leicester University Computer Laboratory was that the tapes were written in 32 bit words whereas the CDC Cyber 73 computer at Leicester uses a 60 bit word length. To overcome this two subroutines from the UTILIB library were used. This library is available at the Leicester University Computer Laboratory. The two routines used were READBL which reads a block from a 'magnetic tape' file and UBYTE which separates the block into the 32 bit words.

COSMOS ANALYSIS OF FIELD 455

For our project COSMOS mapped in threshold mode a strip across the dark rift of the galactic plane, on the Schmidt plate field-number 455. Figure 3A shows a sketch of the field 455 with the position of this strip. Figure 3N is a reproduction of the I-plate of this field. The strip is 4 degrees by $\frac{1}{2}$ degree, with its long axis lying approximately parallel to the right ascension axis. It straddles the major part of the rift and includes the region in the line of sight to the galactic centre. The limits of the strip are $17^{\text{h}}29^{\text{m}}38^{\text{s}}$ - $17^{\text{h}}47^{\text{m}}51^{\text{s}}$, $-28^{\circ}41'$ - $-29^{\circ}12'$. For convenience of reference the strip is split into 8 sections each $\frac{1}{2} \times \frac{1}{2}$ degree. Region 1 is the most easterly and region 8 the most westerly, as depicted in figure 3A. The three plates in B, V and R were measured.

The tapes from ROE were transferred to the Cyber 73 computer at Leicester. The tapes were read and translated into the 60-bit words of the Cyber and the data was compressed by selecting only 8 of the 20 image parameters. These 8 words contained the relevant information for the star counting project. They were words, 11, 12, 7, 9, 16, 17, 18, 10 containing the intensity weighted X and Y centroids, the connected area, the integrated intensity, the semi-major and minor axes and the

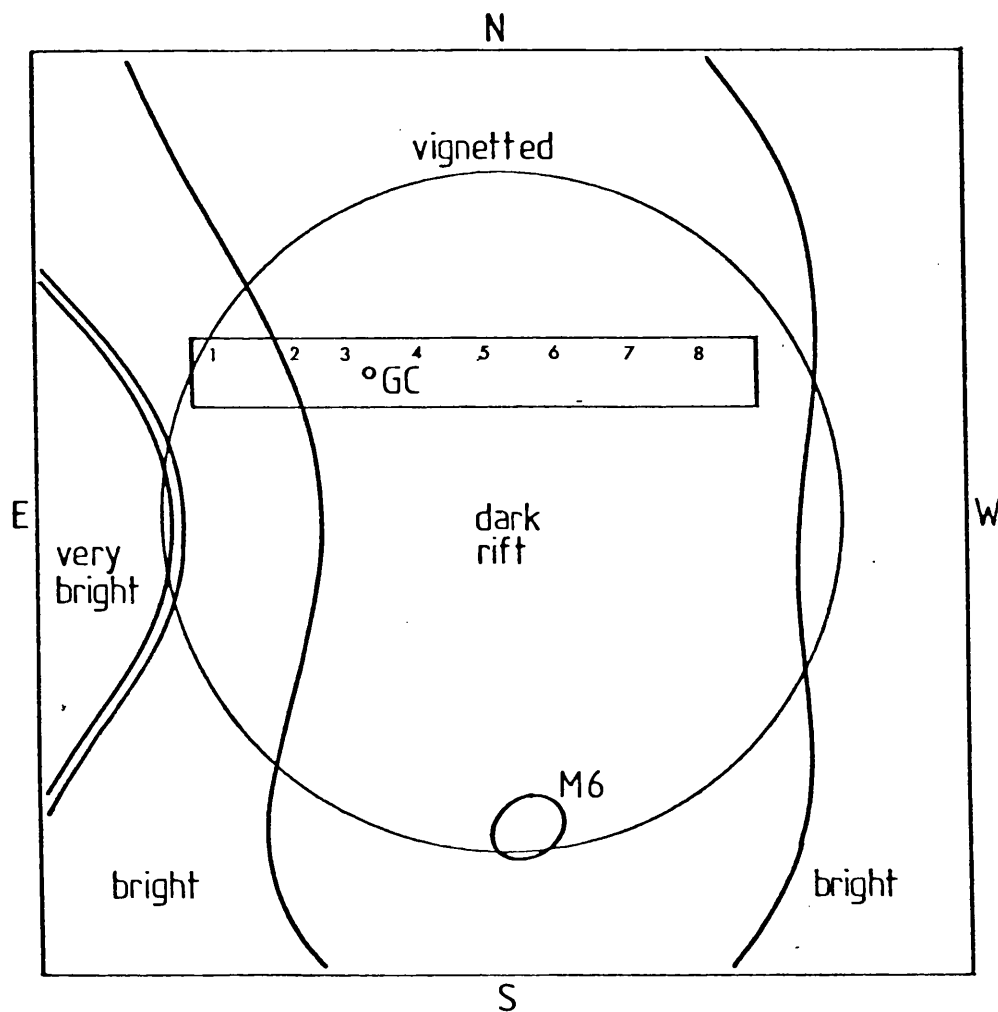


Fig. 3A A sketch of the Schmidt field 455 showing the position of the COSMOS strip. The limits of the strip are

$$\begin{aligned}
 &17^{\text{h}} 29^{\text{m}} 38^{\text{s}} - 17^{\text{h}} 47^{\text{m}} 51^{\text{s}} \\
 &- 28^{\circ} 41' - - 29^{\circ} 12'
 \end{aligned}$$

GC denotes the position of the galactic centre
 M6 is the open cluster Messier 6

The circle shows the limit of vignetting on the UK Schmidt.

orientation of the image plus the sky intensity at the image.

Computer programs were written to plot out the sources as crosses or ellipses using the image parameters, so that source identification from the photographic plates could be made.

CALIBRATION OF COSMOS SOURCES

The most accurate way of calibrating the source strengths determined by COSMOS for their magnitude, is to compare the integrated intensity (word 9) with the photoelectric magnitude for known sources. By making this comparison for a range of magnitudes between the brightest and faintest on the plate, a calibration curve is established against which any other source can be measured. For the strip analysed by COSMOS only one published source of calibration stars could be found. This was Antalova's list of OB stars in the Milky Way, around Sagittarius and Scorpio. Unfortunately this list only contains 4 stars which overlap the COSMOS strip.

To improve the accuracy of the calibration curve photoelectric measurements of selected stars in the COSMOS region were obtained from the South African Astronomical Observatory (SAAO) in April 1981.

UBV PHOTOMETRY OF COSMOS SOURCES

For this observing run the University of Cape Town UBV photometer was installed on the 0.75 m telescope. It had been hoped that a photometer with B, V and R filters, to match the photographic plates would be available, but circumstances dictated otherwise.

The University of Cape Town (UCT) photometer has an uncooled photomultiplier tube mounted beneath an offset guide box. A flip-in mirror directs the centre of the field to the offset eyepiece or the photomultiplier tube. A filter wheel and aperture wheel are provided.

A second push-in eyepiece behind the aperture wheel allows a check to be made on the position of the star in the aperture, and aids the selection of the best aperture size for the seeing conditions. A Nova mini-computer controls the selection of integration time and the output of the data to paper copy and paper tape. A cathode ray tube monitor is used to display the data and to plot out the intensities in real time. By making a number of integrations a visual check of the signal to noise can be made.

The observing technique was to make a number of integrations (usually 5s each) at the three wavelengths, on the star until a satisfactory accuracy had been reached. The faintest star measured, $m_V \sim 15$, $m_B \sim 16$ required 10 minutes at each wavelength to attain accuracies of $0^m.02$ at V and $0^m.03$ at B. After measuring the star a nearby background region was carefully chosen, devoid of stars, which was measured at each wavelength for a comparable time, to check the brightness and noise of the sky signal.

So that air-mass corrections could be applied during the later analysis, a single comparison star was measured with the three filters at intervals during the night. The time at the start of each measurement of every source was noted so that the zenith angles, which are needed for the air-mass correction, could be subsequently calculated. To determine the air-mass correction the logarithm of the photomultiplier count ($\log C$) for the comparison star was plotted against the secant of its zenith angle ($\sec z$). The slope of the resulting line could then be used to determine the count at $\sec z = 0$, knowing $\log C$ and $\sec z$, for any other source. The intercept of the correction line at $\sec z = 0$ gives the theoretical value of the count which would be obtained in the absence of the Earth's atmosphere ($\log C_0$). The slope of the correction line is different for each wavelength, shorter wavelengths being dimmed

more by the atmosphere, and it can vary from night to night. The corrections were calculated for each wavelength each night. The slopes of the correction lines were approximately

$$\begin{aligned} \log C/\sec z &\sim -0.048 \quad V \\ &\sim -0.095 \quad B \\ &\sim -0.220 \quad U \end{aligned}$$

Another calibration which had to be performed was to determine the colour equations of the photometer. These colour equations are the relationships between the magnitudes and colours of stars as measured by the photometer, and those as published for the calibration stars.

To determine the colour equations about 20 to 30 standard stars have to be measured, with a wide range of B - V colours. After correcting each measurement for the air-mass extinction, an instrumental magnitude defined as $-2.5 \log C_0$ was calculated. From now on the instrumental magnitudes will be represented by the lower case letters u, b, v, and the standard magnitudes by the upper case U, B, V. For each star the instrumental colours u - b and b - v were determined. To transform these into the real colours U - B, B - V, graphs of u - b versus U - B, and b - v versus B - V, were plotted for the standard stars. These relationships were found to be linear and did not change from night to night. For the UCT photometer the least squares fit to these relationships were

$$B-V = (1.0320 \pm .0042)(b-v) + (1.3416 \pm .0040) \quad (3.1)$$

$$U-B = (0.9895 \pm .0062)(u-b) + (-0.8731 \pm .0079) \quad (3.2)$$

The transformation of the v instrumental magnitude to the standard system is more complicated since photometers can have non-linear responses for stars of different colour due to variations in tube and filter characteristics. To check this relationship the difference between the magnitudes v - V was plotted against the B - V

colour of the standard stars. A horizontal line of gradient zero implies there is no colour factor in the transformation from v to V .

For the UCT photometer the V transformation was found to have a slight dependence on the colour. The relationship between $v - V$ and $B - V$ was

$$v - V = (0.0465 \pm .0061)(B - V) + V_0 \quad (3.3)$$

where V_0 is the zero point correction to the V magnitude. This zero point correction changed from night to night, and so had to be updated accordingly. As can be seen from equation (3.3) the colour dependence of this photometer is quite small. Even with a large $B - V$ of 2 the correction is only 0.09 magnitudes. Even so, the correction was applied to all the stars on our sequence.

The UCT photometer has a linear response between the number of incident photons and the number of resultant pulses, up to a counting rate of about 1 million events per second. This is equivalent to about 7th magnitude at B with no tube protection, and so all the calibration stars were chosen to be fainter than this.

The calibration stars came only from AWJ Cousins list of E region standards (catalogue from the SAAO, also see Vogt et al.²⁰) to ensure consistency in evaluating the colour corrections.

For the calibration of the COSMOS sources, 30 stars were measured in the B and V wavelengths of the Schmidt plates. For all but the faintest source the U magnitude was also obtained during the observations. For each star the photon count was corrected for the air-mass extinction by application of the appropriate equation, given the star's zenith angle. The instrumental magnitudes v , b , u were transformed into the magnitude and colours V , $B - V$, $U - B$ by application of equations 3.1, 3.2 and 3.3.

Of the 30 sequence stars 13 were SAO stars within the limits of

the COSMOS area, 3 were repeat observations of stars from Antalova's¹⁰ list, and 14 were newly observed stars.

The newly observed stars were picked from regions 3 and 6 of the strip. Finding charts for these stars are given in figures 3B and 3C. The stars are numbered from 1 to 14 by increasing right ascension. The stars were picked from plots of the COSMOS sources as having a wide range of magnitudes, and being well separated from other sources to avoid contamination, either of the photoelectric measurement, or of the COSMOS measurement, by other stars.

Table 3II lists all 30 stars with their V magnitudes and B - V and U - B colours. The quoted errors are combined from the errors in the measurement of star and background, transformation equations, and the largest error from the air-mass correction. Also listed are the positions of the stars for the 1950 epoch. The positions of the SAO stars are from the SAO catalogue,¹² the positions of the other stars are calculated from the COSMOS measured position transformed into celestial coordinates by comparison with the measured positions of SAO stars. These latter positions are probably accurate to about 10 arcseconds.

From the B and V magnitudes of the sequence stars the calibration curves were obtained by plotting magnitude against COSMOS intensity (word 9) for the sources. Figure 3D shows these graphs for the two wavelengths. Three sources have been omitted from these plots. Two SAO stars, numbers 185542 and 185521 were badly measured by COSMOS; very close stars being included in the image. Antalova's star number 242 had an observed magnitude much brighter than that implied by its COSMOS intensity, and this is probably due to a misidentification at the telescope. Antalova quoted $m_v = 14.13$ for star 242.

Neglecting the three badly measured sources the least squares

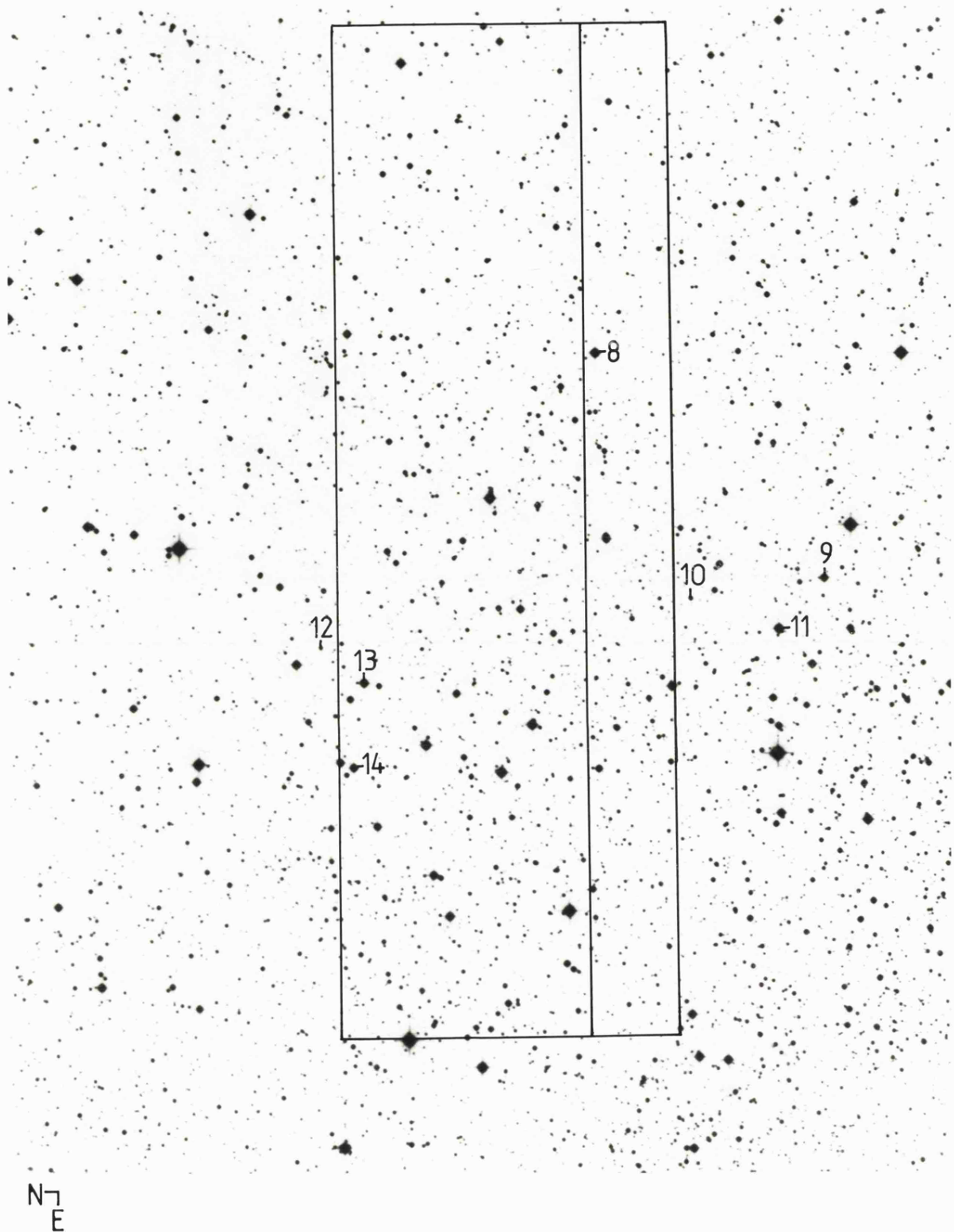


Fig. 3B Finding chart for COSMOS calibration stars in region 3 (see table 3II). The box indicates the limits of the infrared star count scans for the 0° region. Scans in the smaller box, which includes the direction to the galactic centre, were badly affected by weather (see page 4.6).

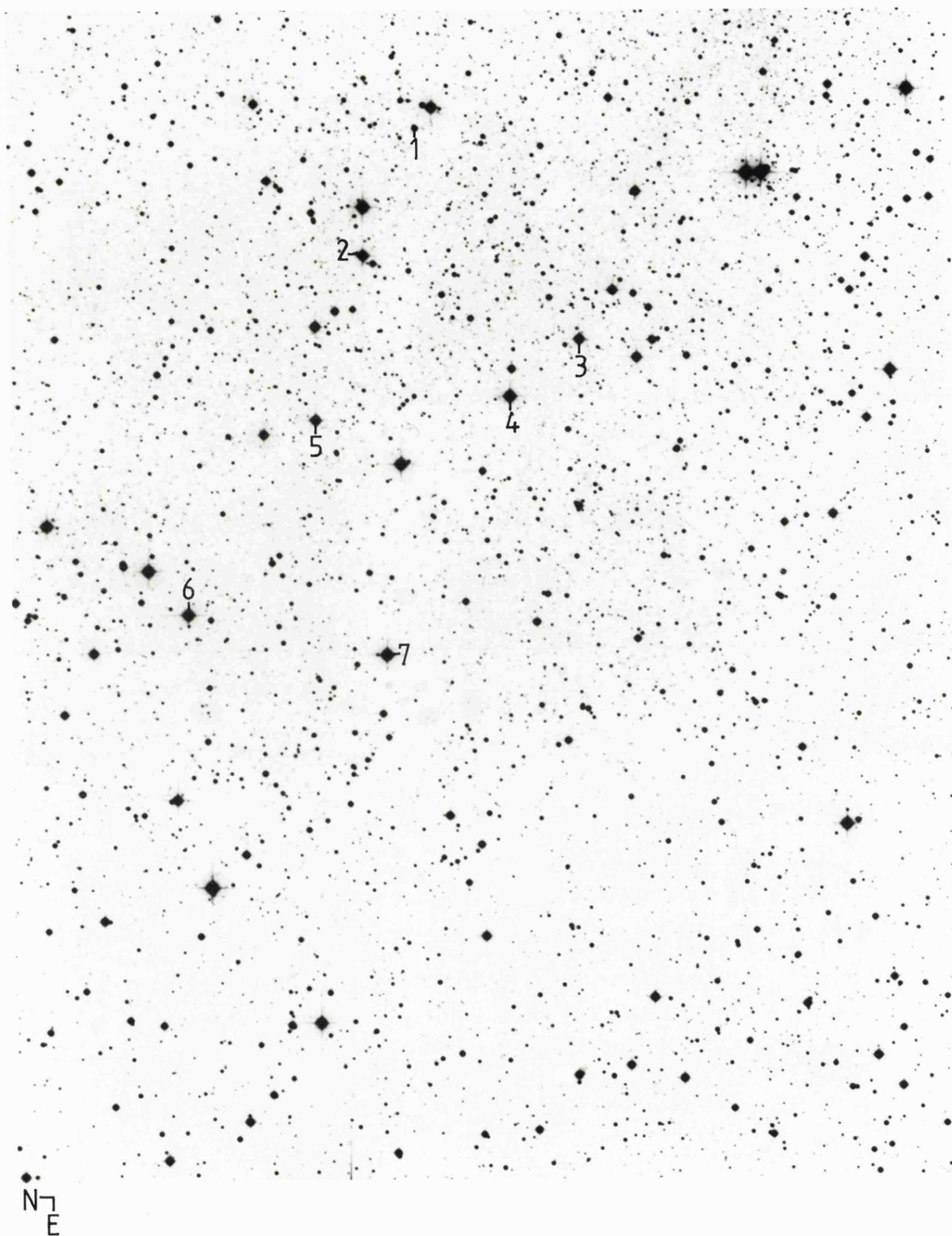


Fig. 3C Finding chart for COSMOS calibration stars in region 6 (see table 3II).

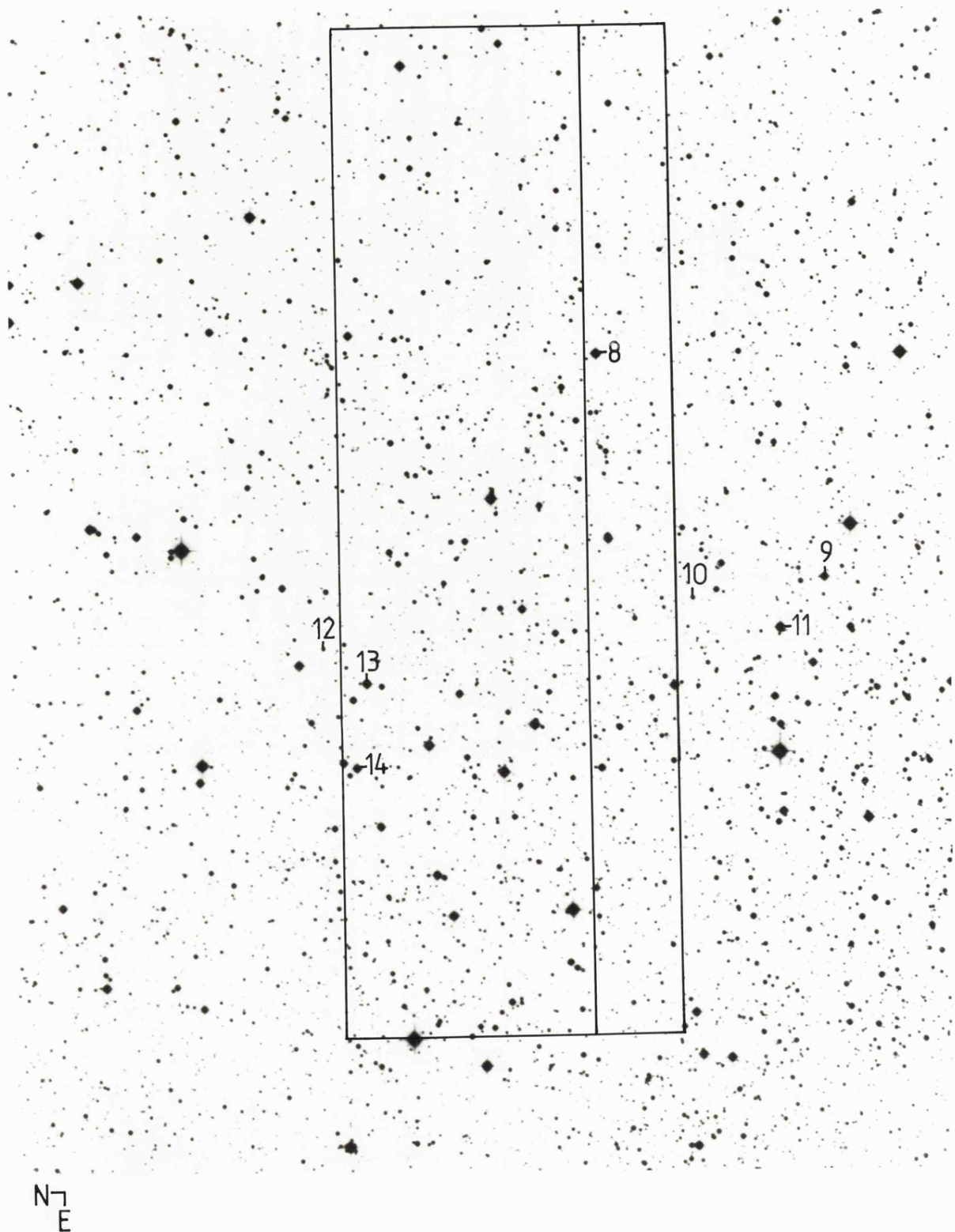


Fig. 3B Finding chart for COSMOS calibration stars in region 3 (see table 3II). The box indicates the limits of the infrared star count scans for the 0° region. Scans in the smaller box, which includes the direction to the galactic centre, were badly affected by weather (see page 4.6).

TABLE 311

UBV PHOTOMETRY OF COSMOS SEQUENCE STARS

STAR	RA	DEC	V	B-V	U-B
SAO 185508	17 ^h 30 ^m 43 ^s	-29°11'24"	8.43 [±] .01	1.69 [±] .02	2.10 [±] .05
185521	31 44	-29 6 55	9.20 .01	0.52 .02	-0.07 .05
185534	32 39	-28 54 43	9.43 .01	2.03 .02	2.23 .06
185542	33 18	-29 8 41	10.10 .01	1.05 .02	0.67 .02
185570	34 53	-29 4 57	9.51 .01	0.76 .02	-0.33 .03
185597	36 20	-29 8 18	9.83 .01	1.31 .02	0.97 .02
185604	37 14	-28 53 50	7.21 .01	0.23 .02	-0.32 .02
185626	38 47	-29 4 6	9.16 .02	0.45 .03	-0.01 .02
185689	41 56	-29 7 25	9.56 .01	1.69 .02	1.93 .04
185702	42 19	-29 5 53	10.03 .02	0.55 .03	0.45 .02
185704	42 22	-28 46 4	9.24 .02	1.05 .03	0.73 .02
185715	42 50	-29 3 43	9.02 .02	1.23 .03	0.97 .02
185730	43 28	-28 52 47	9.57 .03	0.41 .04	0.14 .02
ANT 160	34 31	-29 4 30	12.00 .01	0.65 .02	-0.21 .04
ANT 177	35 12	-29 8 10	14.92 .04	0.95 .07	0.29 .12
ANT 242	40 28	-29 2 50	13.33 .02	0.80 .03	0.22 .06
STAR 1	34 48	-28 54 40	12.68 .01	2.01 .02	2.19 .12
2	35 5	-28 53 20	11.16 .01	0.60 .02	0.07 .02
3	35 16	-28 59 30	11.13 .01	0.83 .02	0.34 .02
4	35 23	-28 57 30	10.53 .01	0.61 .02	0.15 .02
5	35 27	-28 51 50	10.54 .01	1.79 .02	1.99 .03
6	35 53	-28 48 10	10.74 .01	0.33 .02	0.24 .02
7	35 58	-28 53 50	9.87 .01	1.41 .02	1.17 .02
8	41 56	-28 57 20	10.89 .01	1.47 .02	1.55 .04
9	42 26	-29 4 50	11.56 .01	1.26 .02	0.88 .04
10	42 28	-29 0 20	13.80 .01	2.22 .03	1.82 .29
11	42 33	-29 3 30	11.29 .01	0.72 .02	0.16 .04
12	42 35	-28 50 10	15.06 .02	1.01 .03	
13	42 40	-28 51 30	11.35 .01	1.29 .02	0.81 .05
14	42 51	-28 51 30	12.04 .01	0.57 .02	0.24 .05

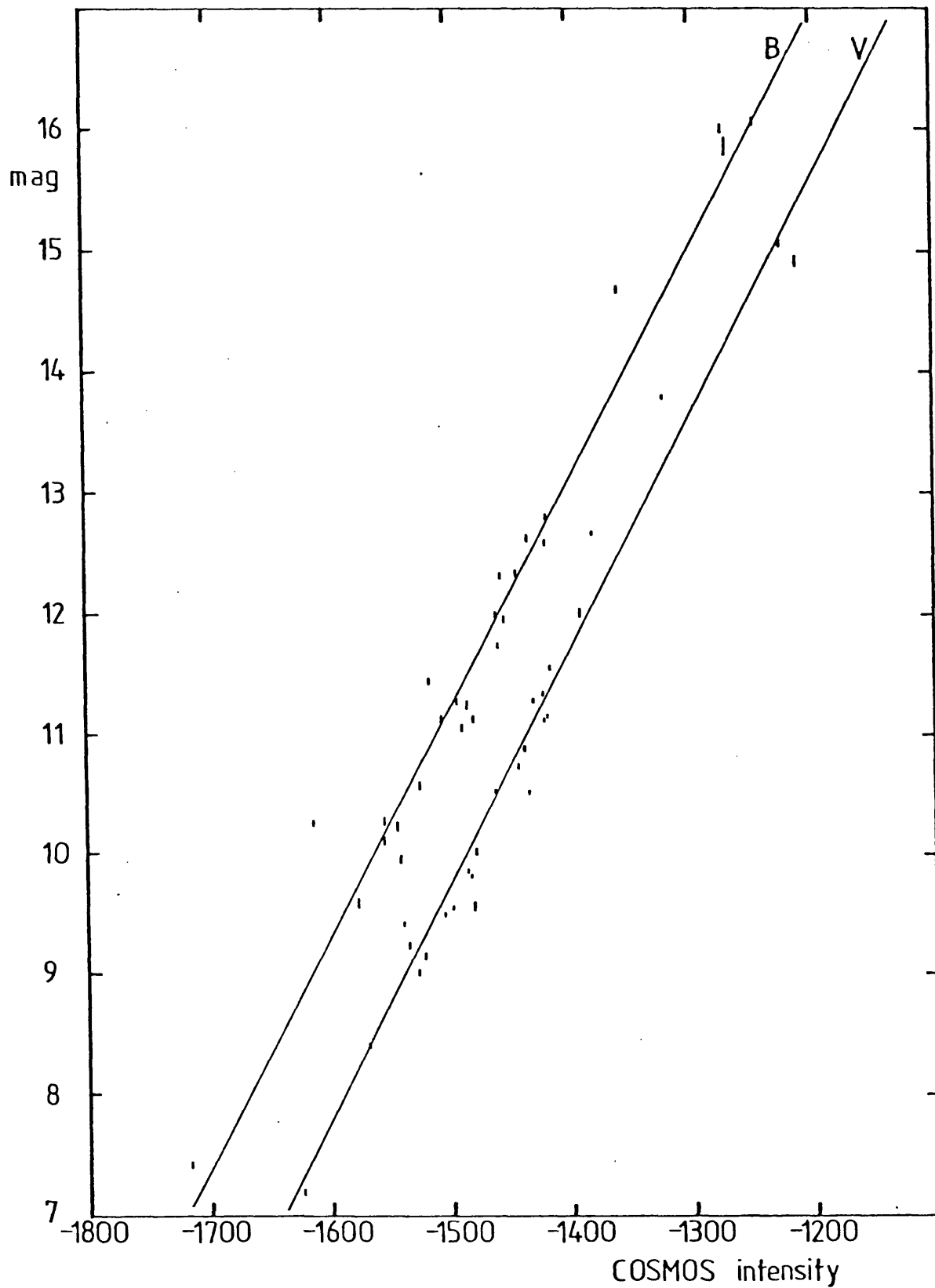


Fig. 3D Calibration curves for the COSMOS data. The COSMOS integrated intensity (word 9) of a star image is plotted against the photometric magnitude. The straight lines show the least squares fit to these points.

fit lines to the points are

$$m_v = 0.0198 \times \text{word } 9 + 39.44 \quad (3.4)$$

$$m_B = 0.0193 \times \text{word } 9 + 40.19 \quad (3.5)$$

The statistical errors in the magnitude scale derived from the deviation of the points from these lines, including observational errors, and assuming the COSMOS intensity is accurate are

$$\pm 0^m.30 \text{ in } V \quad \text{and} \quad \pm 0^m.31 \text{ in } B \quad (3.6)$$

Hawkins¹³ has shown that the COSMOS measurement of a star's magnitude is linear in the magnitude range 14 - 22 for a B plate, using the connected area of the star as the magnitude indicator. He also showed that the gradient of this line varies with the background threshold used. Although for our calibrations we used the COSMOS integrated intensity and not the connected area there is no indication from fig. 3D that there is any significant deviation from linearity in the magnitude range 7 - 16. COSMOS personnel have shown that the integrated intensity is a more accurate magnitude measure than is the connected area. (COSMOS newsletter No. 4). It is important for the purposes of the star count investigation to include stars to a magnitude limit of $18^m.5$, so the calibration lines have to be extrapolated to this limit. In view of Hawkins' finding of linearity down to 22 magnitude, this seems a justifiable procedure. As a check the areas of the calibration stars were plotted against the photoelectric magnitudes as done by Hawkins. In the magnitude range 10 to 16 the connected areas gave a linear relationship, although for stars brighter than 10th magnitude there is evidence that the photographic plate is non-linear in this mode, which is not apparent when the COSMOS integrated intensity is used. This is a further indication that for the COSMOS machine the integrated

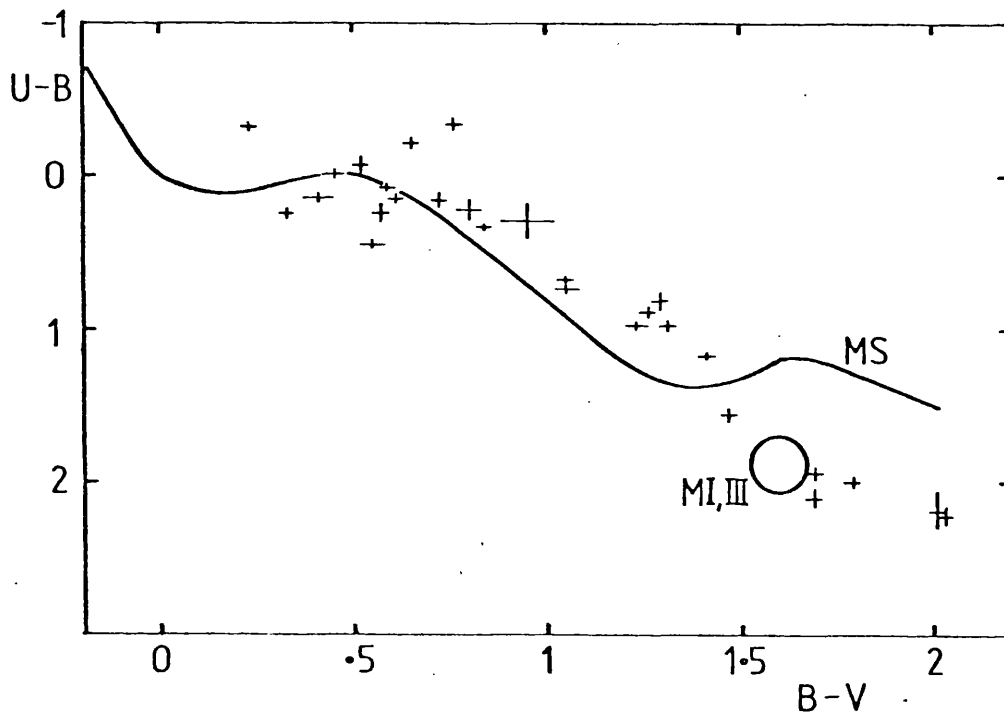


Fig. 3E U-B, B-V two colour plot of the COSMOS calibration stars. The error bars reflect the uncertainties of the photometry (see page 3.12). The curve labelled MS indicates the position on the two colour plot of unreddened main sequence stars, and the area labelled MI, III the position of M giants and supergiants (ref. 14).

intensity gives a better measurement of magnitude than does the area.

From the UBV colours of the measured sequence stars a U - B, B - V plot can be drawn. This is shown in figure 3E, along with the observed colours for unreddened main-sequence stars and M giants and supergiants from Johnson.¹⁴ It appears from figure 3E that most of the calibration stars are reddened main sequence stars. Assuming a reddening line of gradient $U - B/B - V = 0.72$,¹⁵ an average reddening can be calculated for the stars by retracing along a reddening line to the unreddened main sequence. Assuming $A_V/E_{B-V} = 3.1$ this gives an average reddening of $A_V = 0.8 \pm 0.6$.

THE STAR COUNTS

From the calibration equations (3.4) and (3.5) the magnitude of any COSMOS source can be found. To obtain the star counts $A(m)$ the number of stars between magnitude limits $m - \frac{1}{2}$ and $m + \frac{1}{2}$ has to be determined. The Cyber 73 computer at Leicester was used for this task because of the large number of images recorded by COSMOS; over 46000 at V and over 36000 at B. Table 3III lists the star counts for the eight regions in the strip between 7 and 18th magnitude for the B and V plates. Although COSMOS measured many sources fainter than $18^m.5$, the star counts are not continued beyond this, because the plates had an ascribed limiting magnitude of 18, and also the errors from extrapolating the calibration sequence beyond this limit could be significant.

Table 3III also contains the average count for the eight regions as well as those for the photographic ($\sim B$) and visual ($\sim V$) wavelengths for zero galactic latitude from Astrophysical Quantities.¹⁵ For magnitude intervals 10 - 14 the star counts in regions 1 and 2 are considerably larger than those in Astrophysical Quantities. The star numbers in

TABLE 3111

DIFFERENTIAL STAR COUNTS A(m) PER SQUARE DEGREE

V	A.Q.	REGION								
mag	count	1	2	3	4	5	6	7	8	ALL
7		0	0	0	0	4	0	0	0	1
8	2	8	0	0	0	0	0	0	4	2
9	6	24	4	8	4	8	4	12	4	9
10	18	84	52	16	16	4	28	12	16	29
11	54	284	92	64	68	52	76	48	52	92
12	150	828	252	160	108	104	104	176	124	232
13	400	1720	728	444	296	224	264	348	296	540
14	1050	2772	1300	744	552	384	380	468	544	893
15	2630	3380	1984	1092	804	540	624	728	788	1243
16	6030	4368	2388	1444	964	880	852	1032	844	1587
17	13500	5016	3060	1760	1244	1032	1336	1380	1240	2009
18	31600	5940	3344	2044	1432	1072	1684	1672	1540	2341

B	A.Q.	REGION								
mag	count	1	2	3	4	5	6	7	8	ALL
7		0	0	0	0	4	0	0	0	1
8	1	0	0	0	0	4	0	0	0	1
9	4	4	0	0	0	0	4	8	0	2
10	11	24	12	8	4	8	4	0	12	9
11	32	72	56	28	32	16	32	24	16	35
12	87	256	104	72	56	24	56	56	72	87
13	224	612	228	168	148	132	128	168	148	217
14	560	1172	572	324	224	244	232	268	296	417
15	1410	2044	1100	720	516	332	304	400	444	733
16	2880	2812	1536	988	656	436	452	588	704	1022
17	6920	3624	1884	1208	876	672	612	700	728	1288
18	15850	4452	2336	1456	1016	868	852	984	896	1608

Astrophysical Quantities were obtained from averages of stars in the Mount Wilson selected areas for latitude zero,¹⁶ so the enhancement for regions 1 and 2 can be explained by looking towards some of the densest regions of the galactic plane.

For the V waveband the fewest stars are seen in region 5 and for the B waveband regions 5 and 6 have almost equally few stars. The reduction of star counts in these regions is indicative of the increased extinction in the dark rift. Figure 3P and 3Q show the visible star counts for regions 1, 3, 5 and 7.

THE SOLUTION FOR THE RELATIVE DISTRIBUTION OF DISTANCE MODULI

The solution of the star count equation (2.1) by numerical means was introduced in the last chapter. The technique will now be applied to some of the star counts from the strip in the galactic plane. The following example is for the visible star counts of region 5 (5V).

Firstly the star counts per magnitude interval $A(m)$ from Table 3III, are translated to the 'reduced' star counts $a(m)$ by multiplication with the factor $10^{s_0 - s_1 m}$. The values of s_0 and s_1 are fixed so that the range of variation of $a(m)$ is reduced to a minimum. This is done by approximating the star counts ($\log A(m)$ versus m) by a straight line having the equation

$$\log A'(m) = s_0 + s_1 m \quad (3.7)$$

which is minimised by least squares. Clearly none of the regions studied (see figures 3P and 3Q) can be properly represented by a straight line; the purpose of the exercise is to reduce the range of $a(m)$ to a minimum.

The reduced star counts $a(m)$ are then calculated from equation (2.24)

$$a(m) = A(m) 10^{s_0 - s_1 m} \quad (2.24)$$

Table 3IV lists the original and reduced star counts for region 5V.

The error in $a(m)$ is calculated from the percentage statistical error in the star counts $A(m)$ (eqn. 2.26) for the $\frac{1}{4}$ square degree area.

Figure 3F shows the reduced star counts $a(m)$ plotted with these errors.

The next step is to calculate the reduced luminosity function $\lambda(M)$

$$\lambda(M) = \frac{1}{K} 10^{s_1 M} \phi(M) \quad K = \int_{-\infty}^{+\infty} 10^{-s_1 M} \phi(M) dM \quad (2.24)$$

The visual luminosity function $\phi(M_V)$ is taken from Astrophysical Quantities¹⁵ (p.248). Table 3V lists the original and 'reduced'

luminosity functions for $s_1 = 0.192$. Also listed in table 3V are the values of K the normalising constant, M_0 the mean value of $\lambda(M)$ and σ_M^2 the dispersion of the $\lambda(M)$ distribution.

As Trumpler and Weaver¹ comment, the work of solving the integral equation

$$a(m) = \int_{-\infty}^{+\infty} \omega(y) \lambda(m-y) dy \quad (2.25)$$

is greatly eased if a reasonable first approximation for $\omega(y)$ can be made. As mentioned in the previous chapter the first two terms of Eddington's solution can be used for this purpose

$$\omega(m - M_0) = a(m) - \frac{\sigma_M^2}{2} a''(m) \quad (3.8)$$

$$(y = m - M = 5 \log r/10 + \alpha(r) \quad (2.3))$$

where M_0 and σ_M^2 are calculated from the reduced luminosity function $\lambda(M)$. For this first iteration the second derivatives $a''(m)$ of the reduced star counts are obtained from a smooth continuous curve, fitting the observed $a(m)$ approximately. For the region 5V under study, a hand drawn smooth curve joins the points, this is shown in figure 3F.

TABLE 3IV

ORIGINAL AND REDUCED STAR COUNTS FOR REGION 5V

m	A(m)	log A(m)	a(m)	error in a(m)
11	52	1.716	0.736	0.204
12	104	2.017	0.946	0.185
13	224	2.350	1.309	0.175
14	384	2.584	1.442	0.147
15	540	2.732	1.303	0.112
16	880	2.945	1.368	0.092
17	1032	3.014	1.030	0.064
18	1072	3.030	0.687	0.042
	$S_0 = 0.263$		$S_1 = 0.192$	

TABLE 3VIFIRST ESTIMATE FOR THE DISTRIBUTION OF DISTANCE MODULI $\omega(y)$

m	a(m)	a''(m)	m-M ₀	$\omega(m-M_0)$
11	0.736	0.048	6.0	0.44
12	0.946	0.460	7.0	-1.86
13	1.309	-0.240	8.0	2.77
14	1.442	-0.162	9.0	2.43
15	1.303	-0.125	10.0	2.07
16	1.368	-0.097	11.0	1.96
17	1.030	-0.066	12.0	1.43
18	0.687	0.0	13.0	0.69

TABLE 3V

THE ORIGINAL, $\phi(M)$, AND 'REDUCED', $\lambda(M)$, LUMINOSITY FUNCTIONS
FOR THE STAR COUNT ANALYSIS

M_V	$\log \phi(M) + 10$ (ref 16)	λ_M $S_1 = .192$
-6	2.1	
-5	2.8	
-4	3.46	.001
-3	4.10	.002
-2	4.72	.005
-1	5.40	.015
0	6.05	.042
1	6.54	.084
2	6.80	.098
3	7.06	.115
4	7.28	.122
5	7.53	.140
6	7.63	.113
7	7.55	.061
8	7.62	.046
9	7.73	.038
10	7.89	.035
11	7.99	.028
12	8.03	.020
13	8.07	.014
14	8.11	.010
15	8.10	.006
16	8.08	.004
17	8.03	.002
$\log K + 10 = 7.425$	$M'_O = 5.00$	$\sigma_M^2 = 12.19$

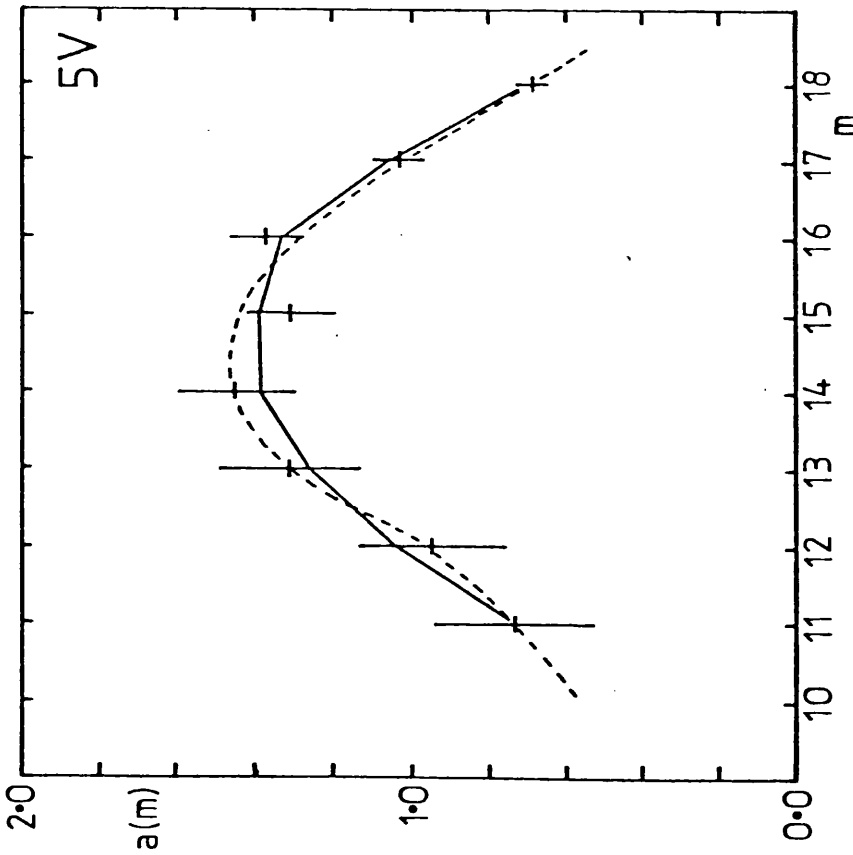


Fig. 3F The reduced star counts $a(m)$ with statistical errors. The broken line shows the hand drawn smooth curve joining these points, and the solid line shows the best fit curve of the calculated star counts.

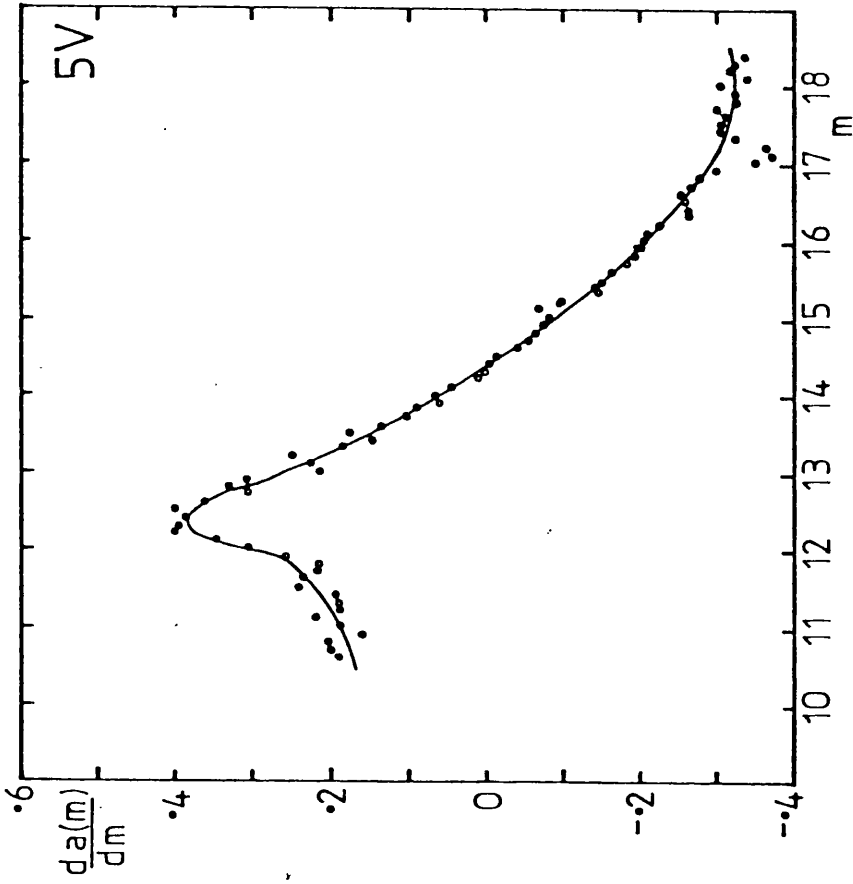


Fig. 3G The gradients of the hand drawn smooth curve of Fig. 3F at 0.1 mag intervals. The solid line is the best, by eye, fit.

The gradients of this curve at $0^m .1$ intervals are plotted in figure 3G, and the second derivative, at unit intervals, is calculated from the gradients of this new curve. The values of $a(m)$ and $a''(m)$ are listed in table 3VI. With these the first estimate of $\omega(y)$ can be calculated from equation (3.8). These are listed in table 3VI. Since $\omega(y)$ must be at all times positive, the negative value in this example at $y = m - M_0 = 7$ must be adjusted; a sensible value being obtained from a smooth fit between $\omega(6)$ and $\omega(8)$.

IMPROVEMENT BY TRIAL AND ERROR

Using the approximate values of $\omega(y)$ from above, the resultant reduced star counts $a(m)$ can be calculated from equation (2.25) by numerical integration

$$a(m)_c = \sum \omega(y) \lambda(m - y) \quad (3.9)$$

Since this calculation may be repeated many times during the improving procedure it is best done by a computer program. On the Leicester computer a program (NIC1STA) calls upon files containing the reduced luminosity function $\lambda(M)$ and the observed star counts $a(m)$ (NIC2STA), and the estimates for $\omega(y)$ (NIC3STA). The output of the program was designed to be similar to Trumpler and Weaver's table 5.9 (p.468) where an array is constructed with apparent magnitude m describing the columns and distance modulus y and its distribution $\omega(y)$ describing the rows. Tables 3VII and 3VIII show this design with the initial and final values of $\omega(y)$. The elements of the array, each a unit of the summation (3.9), are added in columns to give the calculated star counts $a(m)_c$. The difference between the observed (O) and calculated (C) star counts, $O - C$, gives an indication of the quality of the fit. If the fit is unsatisfactory the values of $\omega(y)$ are updated

and the process repeated. Trumpler and Weaver (p.467) describe in detail the construction of the array and the best technique for improving the $\omega(y)$ values. A satisfactory fit is obtained, according to Trumpler and Weaver (p.464), when at least two-thirds of the residuals (O - C) are smaller than the observed errors, and when there are no long sequences of residuals with the same sign. If the residuals from the final fit (table 3VIII) are compared with the errors of $a(m)_o$ from table 3IV it can be seen that this fit is excellent. In figure 3F the curve of these $a(m)_c$ points are plotted for comparison with the observed data.

As can be seen from table 3VIII, the final estimate of $\omega(y)$ the relative distribution of distance moduli, is significant for only a few values of y . This suggests that the shape of the star counts is derived from a region of little radial dimension. The fact that $\omega(y)$ goes to zero at $y = 7$ and $y = 13$ does not necessarily mean that these are its true values, but rather that the original star counts do not cover a sufficient range of magnitude to predict the values of $\omega(y)$ for these distance moduli.

When a satisfactory estimate of $\omega(y)$ has been found the relative distribution of distance moduli $\Omega(y)$ can be calculated from equation

(2.24)

$$\Omega(y) = \frac{\omega(y)}{K 10^{s_o - s_1 y}} \quad (3.10)$$

where K is the normalising factor for the reduced luminosity function $\lambda(M)$ (eqn. 2.24).

TABLE 3VIICALCULATION OF $a(m)$ FROM THE $\omega(y)$ VALUES FOR REGION 5VINITIAL VALUES OF $\omega(y)$

	m	11	12	13	14	15	16	17	18
y	$\omega(y)$								
6	.44	.062	.050	.027	.020	.017	.015	.012	.009
7	1.60	.195	.224	.181	.098	.074	.061	.056	.045
8	2.77	.319	.338	.388	.313	.169	.127	.105	.097
9	2.43	.238	.279	.296	.340	.275	.148	.112	.092
10	2.07	.174	.203	.238	.253	.290	.234	.126	.095
11	1.96	.082	.165	.192	.225	.239	.274	.221	.120
12	1.43	.021	.060	.120	.140	.164	.174	.200	.162
13	.69	.003	.010	.029	.058	.068	.079	.084	.097
	$a(m)_c$	1.095	1.329	1.471	1.447	1.295	1.114	0.917	0.716
	O-C	-.359	-.383	-.162	-.005	.008	.254	.113	-.029

TABLE 3VIIIFINAL VALUES OF $\omega(y)$

	m	11	12	13	14	15	16	17	18
y	$\omega(y)$								
6	0								
7	0								
8	1.30	.149	.159	.182	.147	.079	.060	.049	.045
9	1.44	.141	.166	.176	.202	.163	.088	.066	.055
10	2.40	.202	.235	.276	.293	.336	.271	.146	.110
11	4.90	.206	.412	.480	.564	.598	.686	.554	.299
12	1.80	.027	.076	.151	.176	.207	.220	.252	.203
13	0								
	$a(m)_c$.725	1.047	1.265	1.381	1.383	1.324	1.068	.713
	O-C	+.011	-.101	+.044	+.061	-.080	+.044	-.038	-.026

THE SOLUTION FOR EXTINCTION

Knowing the relative distribution of distance moduli $\Omega(y)$, the extinction or the density variations can be determined if the other function is known. Equation (2.21) describes the relationship between these three functions

$$\frac{d}{dy} (10^{0.6(y-\alpha(y))}) = \frac{3}{w10^3} \frac{\Omega(y)}{\Delta(y)} \quad (3.11)$$

Integrating over y gives

$$10^{0.6(y-\alpha(y))} = \frac{3}{w10^3} \int_{-\infty}^y \frac{\Omega(y)}{\Delta(y)} dy \quad (3.12)$$

The extinction law is then

$$\alpha(y) = y - 5/3 \log \int_{-\infty}^y \frac{\Omega(y)}{\Delta(y)} dy - 5/3 \log \frac{3}{w10^3} \quad (3.13)$$

where $5/3 \log 3/w10^3 = 1.656$ for star counts per square degree.

The values of the extinction $\alpha(y)$ are calculated numerically from the integral (3.13). Values of the distance r corresponding to these $\alpha(y)$ can be determined from equation (2.3)

$$\log r/10 = 0.2 (y - \alpha(y)) \quad (3.14)$$

When solving equation (3.13) for the extinction it is unlikely that the relative density distribution of stars $\Delta(y)$ will be known. At low galactic latitudes, where the interstellar extinction is large, it is of interest to study the distribution of extinction with the assumption that the space density of stars is constant. Under this assumption $\Delta(y) = 1$ and the extinction is found from the function $\Omega(y)$

$$\text{for } \Delta(y) = 1 \quad \alpha(y) = y - 5/3 \log \int_{-\infty}^y \Omega(y) dy - 1.656 \quad (3.15)$$

Table 3IX lists the stages in evaluating the extinction from

equation (3.15) for region 5V. The variation of extinction with radius, as calculated, is plotted in figure 3H. Of course the value $\alpha(y) = -0.26$ is a physical impossibility, and is due to the high value of $\omega(y)$ at $y = 8$. Having negative extinctions in the final result does not necessarily mean that the $\Omega(y)$ function is incorrect; a negative extinction is equivalent to an increase in relative density, but in this case it is probably due to trying to fit the data points at bright magnitudes, where the statistical errors are largest, too well. An important point is that the process of summing the Ω function to derive the extinction, improves the accuracy with increasing y .

The negative extinction is not particularly significant for this study, as the region of interest is around $y = 11$ and 12 where the extinction increases markedly.

This analysis was also repeated for region 5 in the B waveband, using the photographic luminosity function ($\sim B$) from Astrophysical Quantities (p.248). The fit of the calculated to the observed star counts for 5B was reasonable except at the bright magnitude end. The results are listed in table 3X and the resulting extinction plotted in figure 3H.

Two more regions 3V and 7V were also analysed by this technique. The fits of the calculated to the observed star counts were not particularly good, but the resulting extinctions are of interest for the regions covered by $y = 11$ and $y = 12$. The results are listed in table 3X.

The negative extinctions for small distance moduli y , derived for all three regions in V, and the high extinction at $y = 9$ in B, are caused by the poor statistics, and therefore large uncertainties in the star counts at the bright magnitude end.

It is difficult to estimate the errors of the derived values of

TABLE 3IXEVALUATION OF THE EXTINCTION FROM THE $\Omega(y)$ FUNCTION FOR REGION 5V

y	$\omega(y)$	$\Omega(y)$	$\int_{-\infty}^y \Omega(y)dy$	$\log \int_{-\infty}^y \Omega(y)dy$	$\alpha(y)$	r
8	1.3	9161	9161	3.96	-0.26	450
9	1.44	15789	24950	4.40	0.01	630
10	2.4	40946	65896	4.82	0.31	870
11	4.9	130076	195972	5.29	0.53	1240
12	1.8	74349	270321	5.43	1.29	1380

TABLE 3X

THE DISTRIBUTION OF EXTINCTION FROM THE COSMOS STAR COUNTS

y	3V		5V		7V		5B	
	$\alpha(y)$	r	$\alpha(y)$	r	$\alpha(y)$	r	$\alpha(y)$	r
8			-0.26	448	-0.41	480		
9	-0.32	732	0.01	628	-0.36	743	0.79	440
10	-0.47	1243	0.31	867	0.01	995	0.58	765
11	0.18	1461	0.53	1243	0.38	1332	0.83	1080
12	0.86	1690	1.29	1384	1.09	1518	1.41	1310

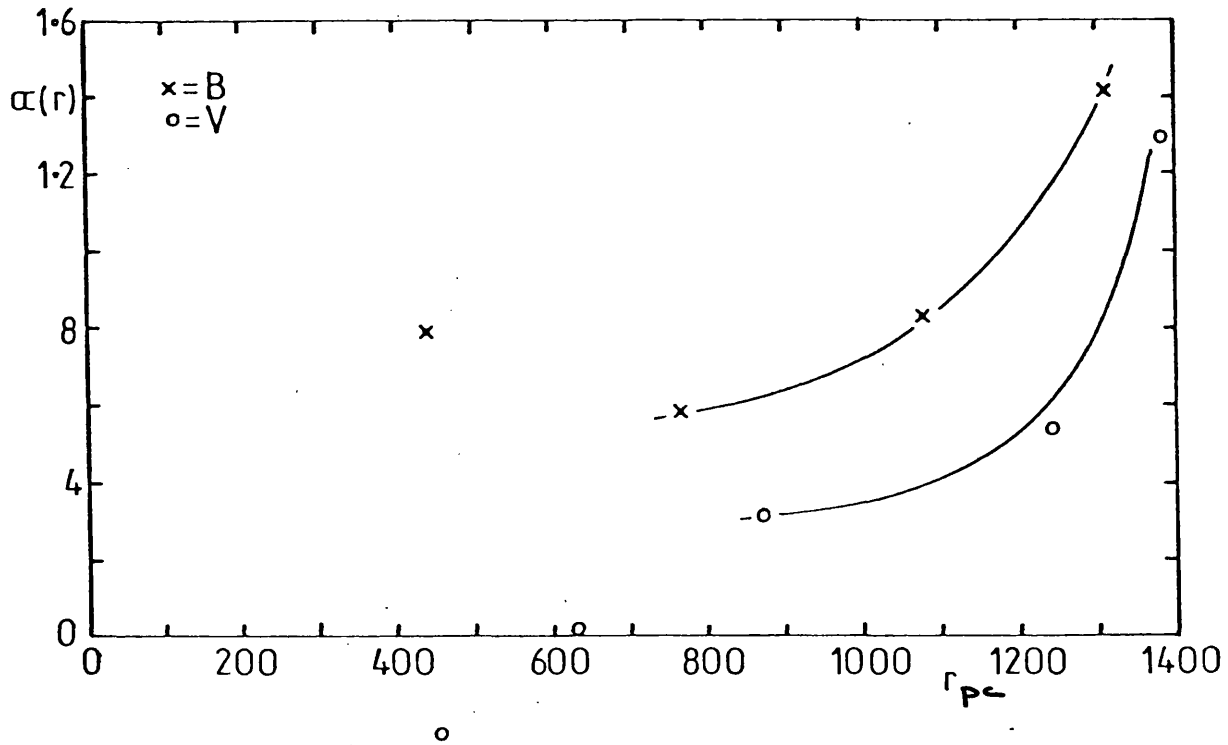


Fig. 3H The radial variation of extinction for regions 5V and 5B, from the solution of the integral star count equation (see page 3.17).

extinction and distance. As an indication of the sensitivity of the result to changes in $\omega(y)$, the best fit values of $\omega(y)$ for region 5V were systematically varied by 10%. At $y = 12$ these changes altered the extinction by 0.06 magnitudes and the distance by 40 pc; about 4%. This shows that the accuracy of the results increases with increasing y ; that is as more $\Omega(y)$ terms are summed in equation (3.15).

THE LINE OF SIGHT DISTRIBUTION OF EXTINCTION

In table 3X are listed the line of sight distributions of extinction as derived by the solution of the integral star count equation for regions 3V, 5V, 7V and 5B. The distributions for regions 5V and 5B are plotted in figure 3H. In the regions where the solution can be expected to be more accurate, $y = 10, 11, 12$, the extinctions show some interesting features. For all three visual regions the extinction rises steeply, by about $0^m.7$, in the space of about 200 pc, and the indication is that beyond this the extinction is still rising steeply. This sharp increase in the extinction indicates the front face of the cloud producing the dark rift in the galactic plane. From table 3X it can be seen that the solution indicates that, for the three visual regions 3V, 5V and 7V, the influence of this cloud is effective at different distances. The extinction for region 3V, which includes the direction to the galactic centre, becomes significant at about 1700 pc, compared to 1400 pc and 1500 pc for regions 5V and 7V respectively. (For a given distance modulus y , a smaller total extinction implies a greater distance (eqn. 3.14)). The increased distances for regions 3V and 7V over region 5V for $y = 12$, can either be caused by the extinction 'wall' curving away with distance, or a thinning of the extinction in these directions. Between $y = 11$ and $y = 12$ all three regions have increased extinction of about $0^m.7$ within

about 200 pc, which would suggest that the former argument is dominant.

Warner and Wing⁹ have shown that the dark clouds which produce the rift in the nuclear bulge lie predominantly at a distance of about 1500 pc, associated with the Sagittarius arm, and cause a visual extinction of about 8 magnitudes. This study supports their first conclusion, but can say little about their second. If there are 8 magnitudes of extinction at this distance it would require star counts as faint as 26th magnitude at V to resolve the cloud radially.

Neckel and Klare¹⁷ have produced maps of extinction in the galactic plane for latitudes less than 8° . There is little suggestion in their maps of a dramatic increase in extinction towards the galactic centre at a distance of 1500 pc. Instead they deduce that the extinction rises to $3^m.0$ within 1 kpc and then remains approximately constant to 5 kpc. However their method of using only stars for which accurate absolute magnitudes have been obtained is highly selective for regions at small distances and with moderate extinctions. Towards the galactic centre their extinctions are derived from only about sixty stars in an area covering 5° in longitude and 15° in latitude.

For region 5 the numerical analysis of the star count equation has been completed in two colours, B and V. The derived extinction relationships are shown in figure 3H. As expected the extinction at B is greater than at V. If the extinction versus wavelength curve is constant throughout the Galaxy, or at least along the line of sight, then the extinction ratio

$$\chi = \frac{\alpha_B(r)}{\alpha_B(r) - \alpha_V(r)} \quad (3.16)$$

will also be constant. Using a standard extinction curve (see fig. 1C and Chapter 1) this ratio is $\chi = 4.0$. From the derived extinctions in

the two wavelengths, figure 3H, this ratio is $\chi = 2.6$ for $r = 1310$. (The visual extinction at this distance was interpolated from adjacent values). For distances less than this, the ratio from the calculated extinctions becomes less. It seems unlikely that in this direction the extinction curve is completely different from the rest of the Galaxy, and so the errors must be caused by some inconsistency in the calculation of the distribution of distance moduli for the two wavelengths. The simultaneous solution of the star counts at two wavelengths (see page 2.15) is rendered impossible by this variation in the extinction ratio χ .

It should be remembered that for the purposes of investigating the distribution of extinction, the relative density of stars Δ is assumed constant. Various investigators have shown^{6,7} that there is an average local density enhancement of about double the galactic 'background' over a region of about 500 pc round the Sun. If this is included, as a step function in the evaluation of the extinction (eqn. 3.13) then the extinctions are reduced as the density is halved beyond 500 pc; negative extinctions are increased and some small positive extinctions turn negative. This situation increases the problem of the negative extinctions.

ANALYSIS BY RESEAU SQUARES

The reseau square analysis was introduced in the last chapter. Rossano¹⁸ discusses the limitations and accuracies of this method of star counting. His most important conclusion with respect to this project is that reasonably accurate extinctions can only be derived if the number of stars counted behind the cloud is significantly greater than the number of foreground stars, otherwise the extinction is underestimated. For the dark rift, with an assumed distance of

1500 pc and an extinction of 8 magnitudes, the distance modulus to the back of the cloud is $y = m - M = 19$. Star counts to a limiting magnitude of 18 clearly do not satisfy Rossano's condition and so accurate extinctions from these star counts cannot be derived.

Rossano points out that if this condition is not met, the reseau star counts can only be used to map out the general location of the extinction. The reseau square analysis is therefore only used here to describe the distribution of extinction.

The size of the reseau square can be decreased to improve spatial resolution, or increased to improve counting statistics. Rossano¹⁸ suggests that the minimum resolution should be that in the absence of obscuration the number of stars counted per sampling element is at least 50. For the region under study it is found that with a resolution of 1/20 degree, 60 to 80 stars are counted at the edge of region 1 where the extinction is least. This angular resolution gives a spatial resolution of 1 to 2 parsecs at the distance of the cloud complex (~ 1500 pc).

To speed the analysis the counting was done by the University Cyber 73 computer. A program (NICRESO) scanned a COSMOS file of the region rejecting any source with magnitude fainter than 18, and calculated the element square to which any star belonged from the COSMOS coordinates. The final output was an array 10 x 80 (equal to $\frac{1}{2}$ x 4 degrees with 1/20 degree resolution) containing the number of stars in each element. A picture of the extinction distribution was produced from a grey-scale routine which shaded each element of the map by an amount proportional to the inverse of the logarithm of the star number. The inverse was used so that the areas with fewest stars had the highest density of lines, i.e. the blackest, and the logarithm was used to enhance the contrast in the regions with few stars.

Figures 3J and 3K show these extinction maps for the B and V wavebands. In figures 3L and 3M the resolution has been reduced to 1/10 degree to increase the counting statistics and to emphasize the general pattern of extinction. For the 1/20 degree resolution the maximum and minimum number of stars in any element are 81 and 1 at V, and 51 and 0 at B. For the 1/10 degree resolution the corresponding numbers are 299 and 25 at V and 167 and 12 at B.

A casual glance at the extinction maps immediately shows that the extinction is not concentrated in the plane of the Galaxy, but about 1 degree in latitude from the plane. At a distance of 1500 pc, 1 degree corresponds to 25 pc. Since star counts to 18th magnitude may be scarcely penetrating the dark rift, it could be that only the front face of the cloud has this imbalance. The star count analysis suggested that the face of the cloud corresponding to the darkest region (region 5) is closer than that of regions 3 and 7. An inspection of a near-infrared (I) plate of the region, which penetrates further into the obscuring clouds shows that the extinction is more uniformly distributed about the galactic plane. The whole of the I plate (I3531) is shown in figure 3N.

The extinction maps also show that the distribution is patchy, with variations over regions of just a few parsecs or less (one square at 1/10 degree resolution at a distance of 1500 pc). Astrophysical Quantities¹⁵ quote a mean size for interstellar clouds of 8 pc having an absorption of $0^m.3$ and spaced at intervals of 5 kpc^{-1} along a line of sight. The variations on the maps are of this order of size but the cloud density will have to be much greater than the galactic mean to produce an increase in extinction of $0^m.7$ or more in the space of 200 pc.

Underlying the surface irregularities there appears to be a more

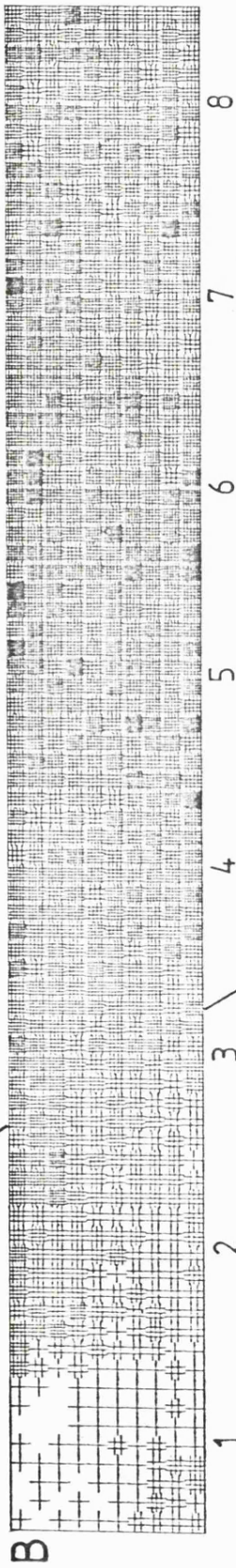


Fig. 3J Extinction map from reseau star counts in the B waveband at 1/20 degree resolution.

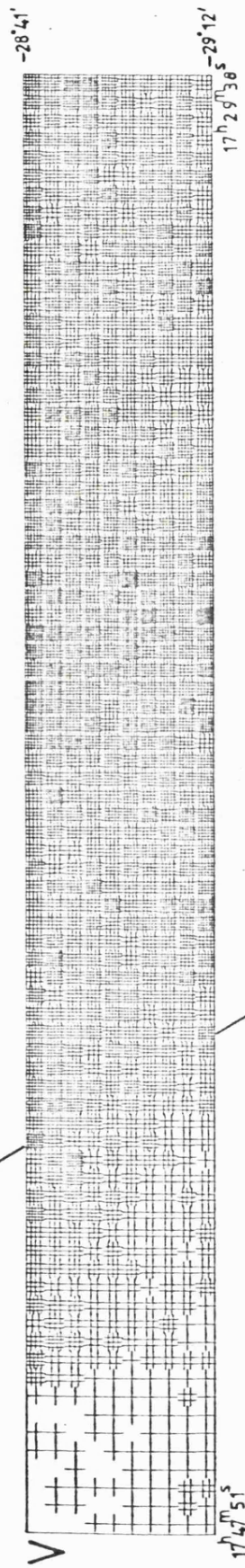


Fig. 3K Extinction map from reseau star counts in the V waveband at 1/20 degree resolution.

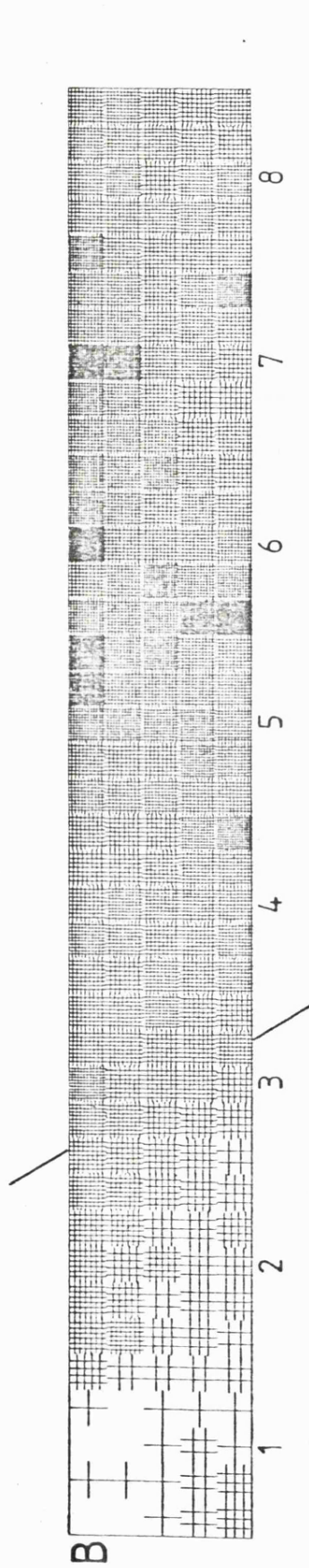


Fig. 3L Extinction map from reseau star counts in the B waveband at 1/10 degree resolution.

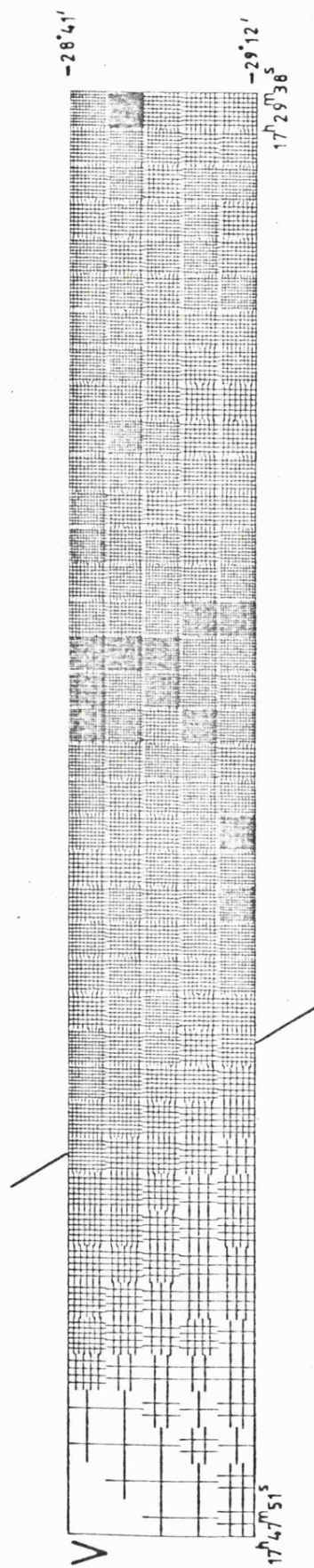


Fig. 3M Extinction map from reseau star counts in the V waveband at 1/10 degree resolution.

uniform extinction spreading from region 3 to region 8 and beyond. From region 1 to region 3 the extinction increases in layers approximately parallel to the galactic plane. Note that even region 1 is not completely free of extinction as indicated by the dense star clouds in nearby Baade's window.

A comparison of these maps with the corresponding areas on the I-plate (fig. 3N) is very revealing. As already mentioned the bulk of the dark rift is more symmetrical about the galactic plane than is seen in the visible. The width of the rift near the galactic centre is about 2.2° , corresponding to 53 pc at 1500 pc. The region with the greatest extinction for visible star counts to 18th magnitude (region 5) is on the westerly edge of this rift. Regions 7 and 8 are in directions where, at the near infrared wavelength, the dense star clouds of the galactic bulge are apparent. The extinction to the west of the dark rift, and to a lesser extent to the east, is distributed in chaotic clouds and filaments.

It seems that the star counts to 18th magnitude are not properly describing the underlying distribution of extinction in the dark rift of the galactic plane. For example fewer stars are counted in region 7 than in region 3 (see table 3III) whereas the I plate indicates that the extinction is much greater in region 3 than in region 7. Wide angle photographs of the galactic plane (for example in Bok and Bok¹⁹) show a substantial cloud complex about 4° north and west of the galactic centre, to which the chaotic clouds to the west of the rift could be associated. On figure 3N the heaviest extinction of this cloud complex is just above the right hand corner of the plate.

The extinctions in regions 1, 2 and 3 appear to reflect the distribution of extinction in the rift, the extinctions increasing parallel to the galactic plane. The extinctions in regions 6, 7 and 8

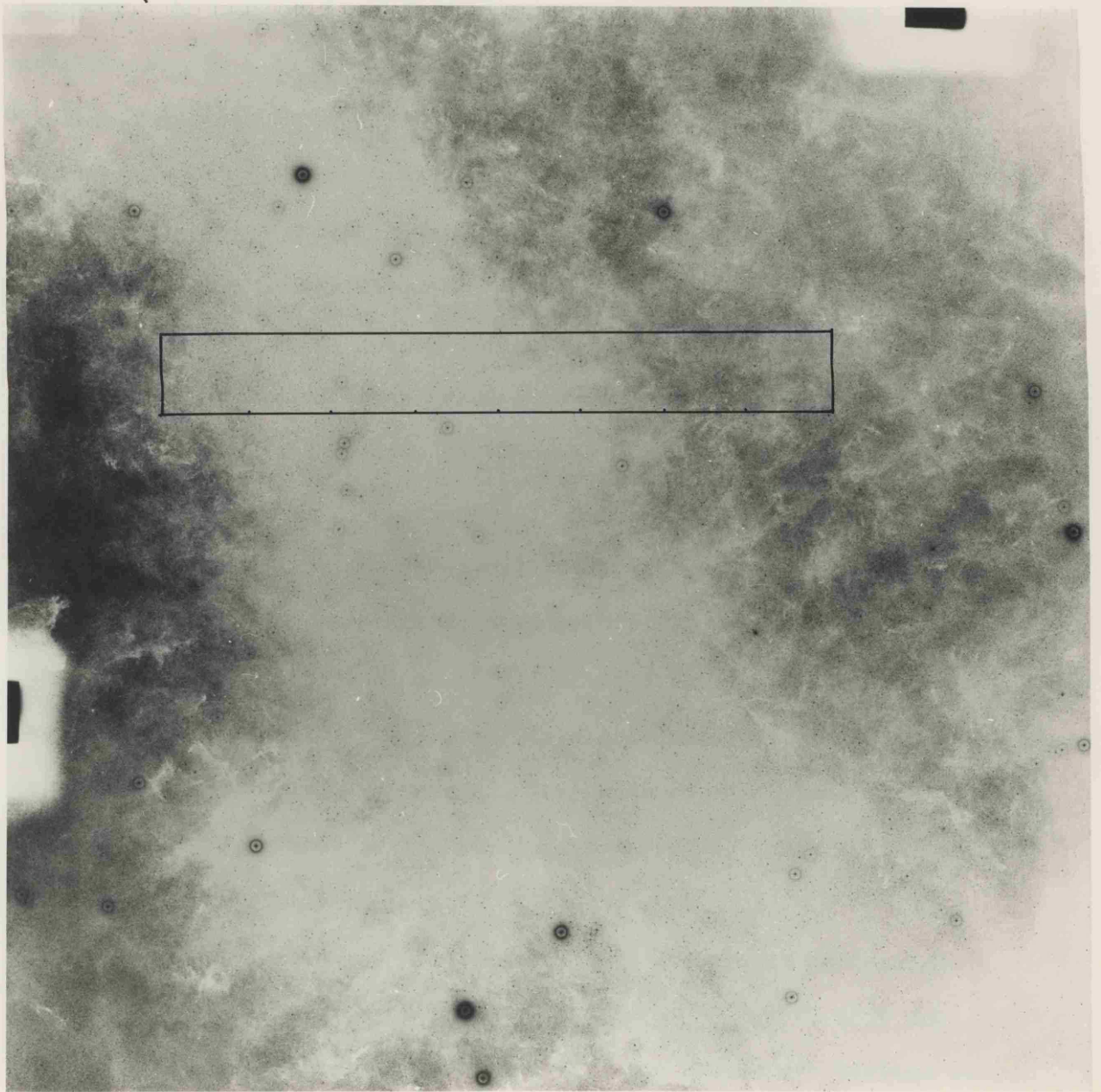


Fig. 3N A near-infrared I plate of field 455. The box indicates the position of the strip measured by COSMOS. The position of the galactic plane is also shown (see figure 3A).

are caused by the chaotic clouds to the west of the rift. The distances derived from the analysis could be explained by this dichotomy. In regions 5 and 7 the extinction rises to over one magnitude within 1500 pc whereas in region 3 the extinction is only 0.9 magnitudes at 1700 pc.

SIMPLE MODELS TO SIMULATE THE STAR COUNTS

To check the conclusions reached by the solution of the star count integral equation, the reverse procedure, of modelling the star counts was performed. Simple assumptions of the distribution of stellar density and extinction predict star counts which can be compared with the observations.

The process involves numerical integration of equation (2.1) over distance (r) and apparent magnitude (m). The extinction is introduced through the equation (2.3) relating the apparent to absolute magnitude (M). Equation (2.1) predicts star counts per steradian, and so to reduce this to square degrees, they have to be divided by 3283 (eqn. 2.23). The visual luminosity function $\phi(M)$ is taken from Astrophysical Quantities.

The relative density of stars $\Delta(r)$ was assumed to be constant ($\Delta(r) = 1$) over the region of interest. Figures 3P and 3Q show the star counts for regions 1V, 3V, 5V and 7V. The counts are plotted on two diagrams for the sake of clarity. The solid lines show the prediction of the model for various extinction patterns.

These are

a - zero extinction plus infinite uniform Galaxy

b - $0^m .5 \text{ kpc}^{-1}$

c - $0^m .5 \text{ kpc}^{-1}$ plus $8^m .0$ at 1700 pc

d - $0^m .5 \text{ kpc}^{-1}$ plus $8^m .0$ at 1500 pc

e - $0^m .5 \text{ kpc}^{-1}$ plus $8^m .0$ at 1400 pc.

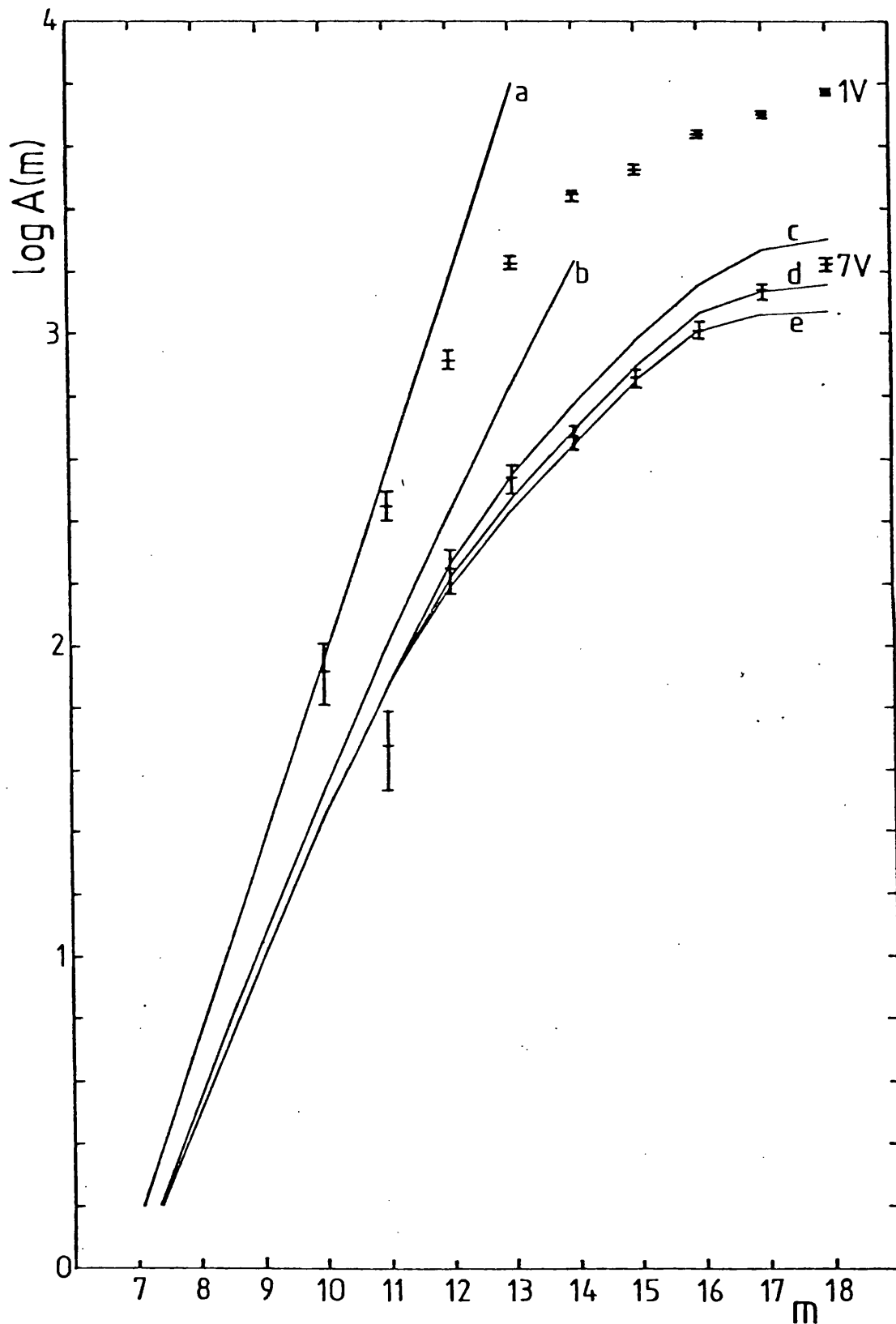


Fig. 3P The visible star counts for regions 1V and 7V. The solid lines indicate the predictions of the models as discussed in the text (page 3.25).

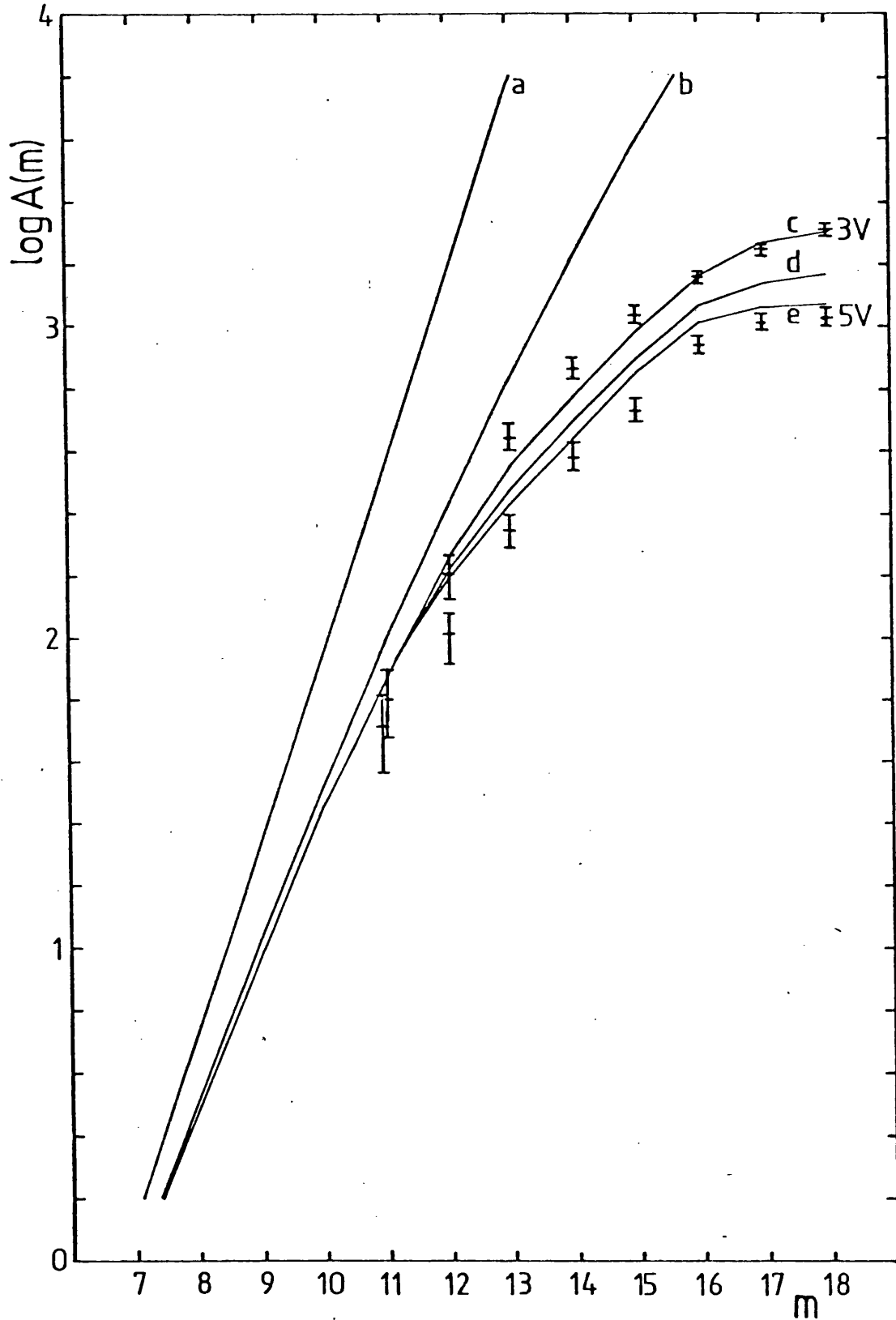


Fig. 3Q The visible star counts for regions 3V and 5V. The solid lines indicate the predictions of the models as discussed in the text (page 3.25).

Model (a) is the special solution discussed in Chapter 2 (eqn. 2.10). In models (c, d and e) the uniform extinction of $0^m.5 \text{ kpc}^{-1}$ was chosen as the best fit for the star counts for bright magnitudes. The thin 'wall' of extinction in models (c, d and e) was positioned according to the indications of the star count analysis for regions 3V, 5V and 7V, and took the value of $8^m.0$ in accordance with Warner and Wings⁹ conclusion. This very simple model fits the star counts in regions 3V, 5V and 7V surprisingly well. The star counts for region 1V approach the zero extinction solution for bright magnitudes. With the broad general luminosity function and constant density, no model of extinction can predict the shape of the star count for region 1V.

The high extinction ($8^m.0$) for the 'wall' used in the model is required to predict the low star counts for magnitudes 17 and 18 in regions 3V, 5V and 7V. An extinction in the 'wall' of say $4^m.0$ predicts too many stars in these magnitude intervals. The upper limit of the extinction cannot be deduced from these star counts since more than $8^m.0$ of extinction produces the same curve as for $8^m.0$ over the observed magnitude range.

This modelling supports the conclusions of the star count analysis with respect to the approximate positions of the sudden increase of extinction.

NOTE In none of this analysis of the visual star counts has the problem of confusion of sources been considered. This confusion is when two or more stars closely spaced are measured as one. The effect of the confusion is to flatten the star count curve at the faint end, since the more numerous faint stars are more likely to be close to another star. This flattening of the star count curve will have the effect of implying too much extinction. To see if the confusion is

significant a small area of region 5V was studied. All sources measured by COSMOS above $18^m.0$ were plotted out and directly compared with a photograph. Only about 12% of all the COSMOS sources contained multiple stars, where both stars had magnitudes approximately 18th magnitude or brighter. This error when spread amongst the magnitude intervals will be of the order, or less than the statistical errors.

CONCLUSION

Analysis of star counts in a strip across the dark rift of the Galaxy and containing the line of sight to the galactic centre has shown that the extinction in these directions starts to increase significantly at a distance of about 1500 pc, approximately at the distance of the Sagittarius arm.

Using a reseau square star counting method it is shown that the direction of the thickest extinction in the visible, for star counts to $18^m.0$, is not coincident with the plane of the Galaxy but about $+1^\circ$ (~ 25 pc at 1500 pc) in latitude away. The surface of the dark cloud appears patchy with the extinction varying over distances of a few parsecs. There are indications that some of the extinction increase is caused by a screen of extinction lying above the galactic plane, separate from the dark rift.

A simple model of the extinction is employed to test the conclusions of the star count analysis. It is found that a significant rise in extinction ($\gtrsim 8$ mag), at the distances derived for the cloud, is needed to account for the star counts.

Chapter 3

REFERENCES

1. Trumpler, R.J. and Weaver, H.F., 1953. *Statistical Astronomy*,
Dover Publications, New York.
2. Bahcall, J.N. and Soneira, R.M., 1980. *Astrophys. J. Suppl.* 44, 73.
3. Bahcall, J.N. and Soneira, R.M., 1980. Preprint.
4. Rossano, G.S., 1978. *Astron. J.* 83, 234.
5. Rossano, G.S., 1978. *Astron. J.* 83, 241.
6. Herbst, W. and Sawyer, D.L., 1981. *Astrophys. J.* 243, 935.
7. McCuskey, S.W., 1965. In 'Galactic Structure', ed. A. Blaauw
and M. Schmidt, p.1, University of Chicago Press, Chicago.
8. Becklin, E.E. and Neugebauer, G., 1968. *Astrophys. J.* 151, 145.
9. Warner, J.W. and Wing, R.F., 1977. *Astrophys. J.* 218, 105.
10. Antalova, A., 1970. *Bull. Astron. Inst. Czech.* 21, 331.
11. Pratt, N.M., 1977. *Vistas in Astronomy*, 21, 1.
12. Whipple, F.L., 1971. *Smithsonian Astronomical Observatory Star
Catalog. Vols. 1-4*, Smithsonian Institute, Washington.
13. Hawkins, M.R.S., 1979. *Mon.Not.R.astr.Soc.* 188, 691.
14. Johnson, H.L., 1966. *Ann. Rev. Astr. Astrophys.* 4, 193.
15. Allen, C.W., 1973. *Astrophysical Quantities*, Athlone Press,
London.
16. Seares, F.H. and Joyner, M.C., 1928. *Astrophys. J.* 67, 24.
17. Neckel, T. and Klare, G., 1980. *Astron. Astrophys. Suppl.* 42, 251.
18. Rossano, G.S., 1980. *Astron. J.* 85, 1218.
19. Bok, B.J. and Bok, P.F., 1974. *The Milky Way*, Harvard Univ.
Press, Cambridge, Mass.
20. Vogt, N., Geisse, H.S. and Rojas, S., 1981. *Astron. Astrophys.
Suppl.* 46, 7.

4

CHAPTER 4

INFRARED STAR COUNTS

1. OBSERVATIONS

PREAMBLE

An important field for star counts is the study of the stellar distribution in the plane of the Galaxy: however this is severely hampered for visible wavelengths by the presence of large and patchy obscuration. Neckel and Klare¹ have used star counts to derive the spatial distribution of interstellar extinction in the plane to a distance of about 3 kpc, but investigations to greater distances are only possible in the visible through absorption windows. At an infrared wavelength of 2.2 microns (K) the interstellar extinction is about ten times less than in the visible (V). On average in the galactic plane it is only possible to see to about 1 kpc at V, whereas at K the visibility can extend to 10 kpc. At K normal stars are still detectable, so infrared star counts can be used to examine the galactic structure.

To the galactic nucleus there is an estimated 27 magnitudes of visual extinction^{2,3} which reduces to 2.7 magnitudes at K. Assuming a distance (d), to the nucleus, of 8 kpc, the formula

$$m - M = 5 \log \left(\frac{r}{\text{pc}} \right) - 5 + a(r) \quad (4.1)$$

will tell what apparent magnitude m will result from a star with absolute magnitude M at the galactic centre. ($a(r)$ is the total extinction to distance r). In the visible the brightest stars have an absolute magnitude of about -7 .⁴ Seen at the galactic centre such a star would have an apparent magnitude of $m_v = 35$ which is too faint to be measured by any detection instrument. At K the brightest stars have an absolute magnitude of about -10 .⁵ At the galactic centre such a star would have an apparent magnitude of $m_k = 7$ which is easily detectable by infrared equipment.

On these grounds it was decided to obtain star counts at 2.2 microns in the direction of the galactic centre.

LITERATURE GUIDE

In 1968 Becklin and Neugebauer² first published a map of the galactic centre at 2.2 microns. With higher resolution maps⁶ they showed that most of the 2.2 micron radiation comes from discrete sources. They have also published a low resolution map covering approximately one square degree around the central region⁷ which suggests that most of the point sources on their map are bright foreground stars. Ito et al.⁸ and Okuda et al.⁹ have produced maps showing the distribution of 2.4 micron radiation from the nucleus out to a galactic longitude of 60 degrees. Since at this wavelength it is likely that most of the radiation will be stellar, these maps can predict the largescale distribution of stars.

The use of infrared star counts has, up to now, mainly been to look for young stars hidden in thick dust clouds. In 1973 Grasdalen, Strom and Strom¹⁰ produced a map of 2 micron sources in the Ophiuchus dark-cloud region. In 1976 Strom, Strom and Vrba^{11,12,13} published, back to back, the results of infrared surveys in three dark cloud complexes. Elias in 1978^{5,14,15} scanned three obscured regions looking for embedded sources. By modelling the distribution of infrared stars⁵ he concluded that most of the objects he detected were field stars i.e. stars not physically associated with the dark cloud. Jones et al.¹⁶ scanned a Bok globule in the southern Coalsack and concluded that all the observed stars were field stars.

OBSERVING TECHNIQUE

The major problem of mapping in the infrared when sky chopping is used, is that sources in the negative (reference) beam influence the positive measurement. This is especially significant in crowded fields such as towards the galactic centre. To produce their low resolution map of the galactic centre region Becklin and Neugebauer⁷ overcame this problem by using a single sky beam and chopping against a constant blackbody source. For more accurate photometry or photometric mapping in the infrared this method is unsuitable because of variations of the background sky level. For their high resolution map⁶ a widely separated sky chop was used. They then assumed that over the small area of the map any changes in the negative beam (positioned well outside the map area) are negligible compared to large changes found in the nucleus. For mapping large areas in the galactic plane it is not possible to position the negative beam far enough from the positive beam to be confident that it has little influence. Rieke and Low¹⁷ in 1973 mapped the galactic centre at four infrared wavelengths using 5 arcsecond beams separated by 10 arcseconds. For extended sources such as the nucleus this beam arrangement results in loss of signal. To retrieve the information they used a method of direct and Fourier deconvolution.

To obtain infrared star counts for large areas of sky in the galactic plane, it was decided to use a variation of Rieke and Low's mapping technique. By using a very small chopping distance, with the two beams aligned in the direction of the scan, a point source passes quickly from the positive beam to the negative beam producing a characteristic up/down profile. A slit aperture is used with its long axis perpendicular to the direction of the scan which allows the beam separation to be further reduced while still covering a wide strip

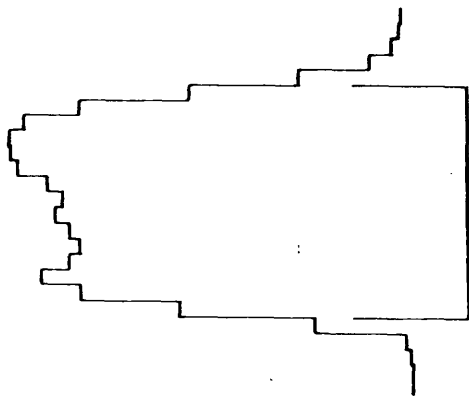


Fig. 4A

Fig. 4B

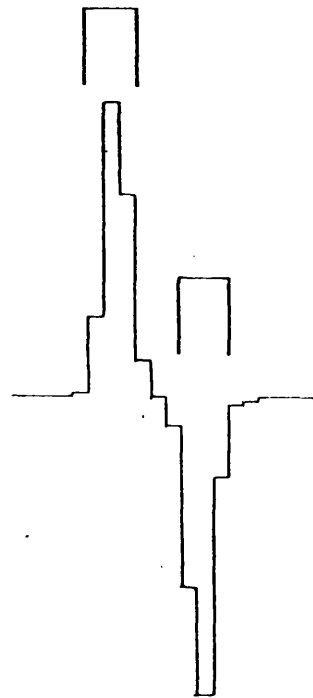
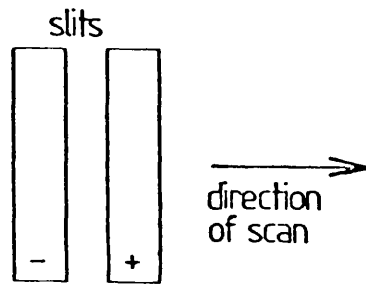


Fig. 4C

Fig. 4A The response of the detector to a star scanned along the slit length.

Fig. 4B The configuration of the beams for infrared star counting.

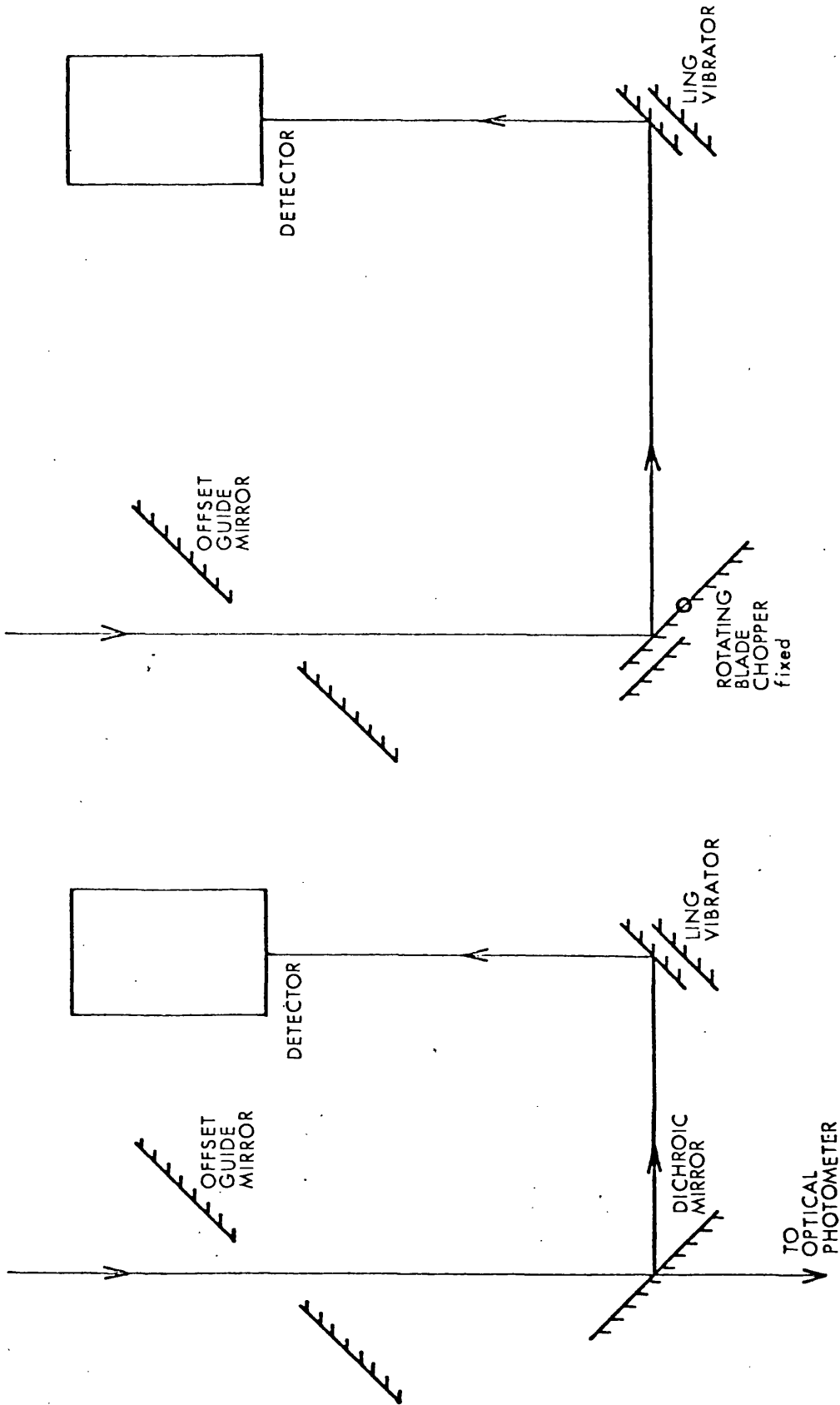
Fig. 4C The response of the detector to a star scanned across both slit beams.

of the sky. A slit aperture also covers less area than a circular one of the same length, so reducing the possibility of having more than one source in the beam. Figures 4A, 4B, 4C show this slit configuration, and the resultant profiles when a star is scanned across the slit and along its length. The non-uniform response of the slit along its length (figure 4A) is probably due to imperfections in the Fabry lens, or to a misalignment of this lens, which focusses the radiation onto the infrared detector.

The effect of the narrow beam chop in cancelling out extended regions is advantageous for star counting. The magnitude of any point source is directly proportional to the difference between the up and down measurements, irrespective of how bright the background may be.

THE OBSERVATIONS

In July of 1979 we went to the 1m telescope at the South African Astronomical Observatory (SAAO) to obtain star counts at 2.2 microns in the direction of the galactic centre. The instrumentation was freighted out from Leicester, the important constituents being : an adapted wide throw photometer, the best of the Leicester InSb detectors, a Brookdeal 9401 phase sensitive detector, a digital voltmeter and a microprocessor system for data handling. The detector's construction and performance has been described by Abolins¹⁸ in his Ph.D. thesis. The photometer, referred to by Abolins as Photometer II¹⁸ (p.2.9), is sketched in figure 4E. Two choppers were installed in this photometer; a Ling solenoid vibrator with an angled mirror was used for the star counting work, and a rotary blade, wide throw chopper used for mapping extended sources. During the star count observations the rotary chopper was held stationary and acted only as a 45° mirror. The output of the detector preamplifier was rectified in the PSD and this



PHOTOMETER 2

PHOTOMETER 1

Fig. 4E The Leicesters Photometer II, the wide throw of the rotary chopper is used for scanning extended sources.

Fig. 4D The Leicesters Photometer I, used for simultaneous infrared and optical measurements.

output voltage was digitised before being punched out onto paper tape for transfer back to Leicester. Before the observations the Santa Barbara InSb detector was cooled to 64K (pumped liquid nitrogen) and flashed (exposed to a 60W light bulb through the J filter for about 5 minutes) to decrease the intrinsic noise. The detector was kept at 64K throughout the observations. A standard 2.2 micron (K) pass-band filter was used. On this 1m telescope with the equipment used, the signal to noise was such that a star of magnitude 10.5 would produce the same size signal as the standard deviation (σ) of the noise. (1 σ in 1 sec).

The observations consisted of a number of parallel right ascension scans using SAO 185730 ($17^{\text{h}} 43^{\text{m}} 28^{\text{s}}$, $-28^{\circ} 52' 47''$ 1950) as the origin for the scans. The scans were set up using a graticule in the eyepiece, each scan starting one graticule division (= 38 arcseconds) in declination from its neighbour. Drifts in declination of the telescope over the length of a half a degree scan, and the return, were less than 20 arcseconds, and were always in the same direction.

It was decided not to overlap the scans since it was felt that as only star counts were required, the problem of unravelling coincident sources would make an added difficulty. After this visit it was realised that this advantage was more than negated by the problem of a star being improperly measured at the edges of the slit. For this reason on subsequent observing runs, it was decided to use a slight overlap to counter this problem.

For the July 1979 observations a small slit (2mm x 0.5mm equivalent to 26 x 7 arcseconds on the 1m telescope) was used to reduce the possibility of having more than one source in the beam toward the crowded regions of the galactic centre. The chop size was set at about 20 arcseconds (\sim 3 times the slit width) by adjusting

the amplitude of the Ling drive waveform. An equatorial drive rate of 0.6 arcseconds per second was utilized with each scan covering 28.8 arcminutes of the sky, and the microprocessor system integrating every second.

The first scan, going in negative right ascension from SAO 185730 was only 14.4 arcminutes long. After seeing that no problems arose over the length of the scan it was decided to double this for all subsequent scans.

A total of twelve usable scans covering 144 square arcminutes of the sky to the north of the galactic centre were made. Four more scans to the south, including the galactic centre, were rendered useless by bad weather. The position and coverage of the observed area is itemized in table 4I. The star counts obtained are listed in table 4II and shown in figure 4H. A map of the sources brighter than $10^m .0$ is shown in figure 4Q. The observed sources are listed in Appendix A. Discussion of the star count diagrams are given in a later section.

2. The interest stirred by the results of the above observations prompted a further investigation by obtaining star counts for selected regions along the plane of the Galaxy. In May of 1980 we observed three areas at approximate galactic longitude 10° , 20° and 30° with the 1.5m flux collector of the Cabezon Observatory Tenerife. (From now on all these areas will be referred to by their approximate galactic longitude. The galactic centre coverage will be referred to as the 0° region).

The equipment taken for this visit was the same as for the SAAO visit except this time the other Leicester photometer (Photometer I) was taken. Abolins¹⁸ and Sherrington¹⁹ have discussed the construction of this photometer in their theses. The basic elements of this

TABLE 4I

THE POSITIONS AND COVERAGE OF THE OBSERVED AREAS

Area Designation $l^{\circ}\sim$	Limits of Scanned Area (1950)		Total Area Scanned sq.arcmin.	Gal Coords of Centre l'' b''
0	$17^{\text{h}} 41^{\text{m}} 18^{\text{s}}$ $-28^{\circ} 50' .7$	$17^{\text{h}} 43^{\text{m}} 28^{\text{s}}$ $-28^{\circ} 58' .0$	144*	-0.01 0.01
10	$18^{\text{h}} 04^{\text{m}} 07^{\text{s}}$ $-19^{\circ} 50' .0$	$18^{\text{h}} 06^{\text{m}} 07^{\text{s}}$ $-19^{\circ} 53' .5$	99	10.42 0.13
20	$18^{\text{h}} 21^{\text{m}} 56^{\text{s}}$ $-11^{\circ} 20' .2$	$18^{\text{h}} 23^{\text{m}} 56^{\text{s}}$ $-11^{\circ} 23' .7$	103	19.93 0.46
30	$18^{\text{h}} 40^{\text{m}} 49^{\text{s}}$ $- 3^{\circ} 10' .7$	$18^{\text{h}} 42^{\text{m}} 49^{\text{s}}$ $- 3^{\circ} 23' .5$	384	29.26 0.08
40	$19^{\text{h}} 00^{\text{m}} 34^{\text{s}}$ $+ 6^{\circ} 14' .2$	$19^{\text{h}} 02^{\text{m}} 34^{\text{s}}$ $+ 6^{\circ} 10' .7$	104	39.96 0.07
50	$19^{\text{h}} 18^{\text{m}} 51^{\text{s}}$ $+14^{\circ} 52' .5$	$19^{\text{h}} 20^{\text{m}} 51^{\text{s}}$ $+14^{\circ} 48' .3$	121	49.68 0.16
60	$19^{\text{h}} 39^{\text{m}} 48^{\text{s}}$ $+23^{\circ} 35' .7$	$19^{\text{h}} 41^{\text{m}} 48^{\text{s}}$ $+23^{\circ} 31' .5$	101 ⁺⁺	59.70 0.09

* In the case of the galactic centre region the scans did not overlap, and so the total area scanned is not quite the same as the area between the limits of the scans.

⁺⁺ For the 60° region one scan (totalling 14 sq. arcminutes) between the limits was lost due to noisy data.

photometer are sketched in figure 4D. The sensitivity of the detector on this telescope was measured for 1σ in 1s at K at 11.8 magnitudes. This is a factor of 3.5 times more sensitive than was obtained at SAAO. From a comparison of telescope areas one would expect an increase by a factor of about 2.4. The reason for the extra sensitivity of the Tenerife measurements is not known for certain, but is probably due to differences in the photometers used.

On this observing run overlapping scans were used to ensure that no stars were incompletely measured at the edges of the slit. The expected lower density of stars away from the galactic nucleus allowed the use of a larger slit (4.5 x 1 mm equivalent to 50 x 11 arcseconds on the 1.5m telescope). As before, the observations were based at a convenient SAO star. With a slit width of 50 arcseconds the declination offset between scans was set to 40 arcseconds. For all the areas investigated the scan length was kept constant at 30 arcminutes of right ascension on the equator.

The chop size was again set at about 20 arcseconds, but for these observations the drive rate was speeded up to 3 arcseconds per second, with the sampling rate still at one integration per second. This is just about the optimum configuration for this kind of work: the chop size twice the slit width and the sampling rate such that there are about 6 or 7 bins between peak and trough.

For the observations in the 10° region SAO 161110 ($18^{\text{h}}06^{\text{m}}07^{\text{s}}$ - $19^\circ53'04''$ 1950) was used as the origin for the scans. Five scans going in negative right ascension, covering 99 square arcminutes were done. For the 20° region SAO 161476 ($18^{\text{h}}23^{\text{m}}56^{\text{s}}$ - $11^\circ23'14''$ 1950) was used as the origin. Again five scans in negative right ascension were done, this time covering 103 square arcminutes, due to the increase in the $\cos \delta$ factor (δ = declination). For the 30° region SAO 142588

($18^{\text{h}} 42^{\text{m}} 49^{\text{s}} - 3^{\circ} 17' 05''$ 1950) was used as the origin. Nineteen scans were completed in this region covering 384 square arcminutes. A larger area was scanned in this region since around the galactic longitude of 30 degrees there are some unusual phenomena. The later chapter on obscured sources details some of these properties.

The position and coverage of these observed areas are itemized in table 4I. The star counts obtained are listed in table 4II and shown in figures 4J, 4K, 4L. Maps of the areas for sources brighter than $10^{\text{m}}.0$ are shown in figures 4R, 4S, 4T. All the observed sources are listed in Appendix A.

3. Another opportunity arose in May of 1981 to obtain more star counts in the plane of the Galaxy. The 1.5m flux collector of the Cabezón Observatory Tenerife, was again used, and we observed three regions at approximate galactic longitudes 40° , 50° and 60° .

For this visit the Mark I photometer and the best detector were again used. The data collecting equipment, however, differed from the two previous runs. A Brookdeal 9412 A phase sensitive detector was used with an alternative digital voltmeter and microprocessor system. During the observations the sensitivity of the detector was measured for 1σ in 1s at 11.7 magnitudes, in good agreement with the previous year's result of 11.8 magnitudes.

The observing technique for this visit was almost identical with the previous Tenerife one. The chop size was slightly smaller than before, about 15 arcseconds, and the scan rate had to be slowed to 1.5 arcseconds per second because the replacement microprocessor had a dead-time of about one second while the teletype printed out the preceding number. Apart from these, the same slit size, the same length of scan, the same integration time and the same declination offset were used.

For the observations in the 40° region SAO 124243 ($19^{\text{h}}02^{\text{m}}34^{\text{s}} + 6^\circ11'06''$) was used as the origin. Five scans going in negative right ascension, covering 104 square arcminutes were done. For the observations in the 50° region SAO 104779 ($19^{\text{h}}20^{\text{m}}51^{\text{s}} + 14^\circ49'25''$) was used as the origin. Six scans in negative right ascension covering 121 square arcminutes were done. For the observations in the 60° region SAO 087637 ($19^{\text{h}}41^{\text{m}}48^{\text{s}} + 23^\circ33'17''$) was used as the origin. Five usable scans covering 101 square arcminutes were done. One scan between these five was rendered useless by the detector warming up and becoming too noisy.

The position and coverage of these observed areas are itemized in table 4I. The star counts obtained are listed in table 4II and shown in figures 4M, 4N, 4P. Maps of the areas for sources brighter than $10^{\text{m}}.0$ are shown in figures 4U, 4V, 4W. All the observed sources are listed in Appendix A.

REDUCTION

On the return to Leicester all the data were stored on the Cyber mainframe computer for subsequent analysis. Reduction of these observations to the position and strength of the stars was done by visual deconvolution. From a plot of the digitised data the up/down profiles were picked out and then the corresponding numbers of the maximum and minimum points subtracted to give the source strength.

For the Tenerife data there was the problem that some sources may have been measured on adjacent scans. To overcome this, if a source appeared on an adjacent scan within six arcseconds (two integration bins) either side of the first star's position, the weaker of the two sources was deleted. For most of the areas corrected in this way, it was found that more stars were deleted than could be

expected from the amount of sky duplicated by the scans. If the correspondence of stars was accepted only if they appeared within three arcseconds (one integration bin) of another source, then fewer stars than could be expected were deleted. The difference between the expected number of stars to be duplicated, and the actual number deleted either with one or two integration bin correspondence was about 5 per cent of the total number of sources. The quoted star counts were obtained using the six arcsecond correspondence limit. No correction for the excess of deleted sources using this limit was made.

For the SAAO data and for the edges of the Tenerife scanned areas, no corrections were made for stars being improperly measured at the edges of the slit.

Calibrations of the stars was achieved by scanning sources from the photometric lists of Johnson et al.²⁰ and Glass²¹ with the same slit, chopsize and scan speed. The total up/down count of any source picked out from the scans was compared to that of the calibration star and converted into magnitudes using the relation,

$$m_{\text{source}} = m_{\text{cal}} + 2.5 \log \left(\frac{C_{\text{cal}}}{C_{\text{source}}} \right) \quad (4.2)$$

where m is the magnitude and C the total count.

For each region the sources were binned into half magnitude intervals and then summed in increasing magnitude to obtain the cumulative count. The results for each region are listed in table 4II and plotted in figures 4H-4P. The diagrams are plotted with cumulative count per square degree below the limiting magnitude against the magnitude. The error box for each count consists of a ± 0.2 magnitude error due to the deviations from a flat topped response of the detector along the slit (see figure 4A), and the standard square root of the

TABLE 411

STAR COUNTS IN THE OBSERVED AREAS

Cumulative star counts $N(m)$ per square degree
Original (O) and after confusion correction (C)

	0	10	20	30	40	50	60
	O	C	O	C	O	C	O
	C	O	C	O	C	O	C
4.5				28		30	30
5.0				28		30	30
5.5			85	85	35	60	60
6.0	37	37	35	159	35	89	89
6.5	37	37	35	225	69	89	36
7.0	75	183	210	365	69	89	107
7.5	151	402	490	543	207	149	179
8.0	577	548	735	843	380	238	286
8.5	1908	876	1260	1199	725	507	464
9.0	5622	1533	1890	1667	932	834	678
9.5	9513	17319	2373	2285	1346	1281	1035
10.0	11697	21310	3030	2857	1932	1848	1321
10.5	11847		3395	5414	2967	2891	2321
11.0				4692	6348	4470	3784
11.5				5900	9262	5871	7604

count error (Trumpler and Weaver²² p.646). For magnitude intervals where there are two boxes (dotted lines and solid lines) the dotted box shows the original count and the solid box shows the count after having been corrected for confusion as discussed in the next section. Where there is only one box no correction to the original count for confusion was needed.

All the hand-picked sources are listed by region in Appendix A into position along a scan and magnitude. Maps of the sources in each region brighter than $10^m .0$ are shown in figures 4Q-4W.

CONFUSION

It was hinted earlier that problems arise when more than one source is measured in the beam at one time. We have called this effect confusion of the sources. The main effect of this confusion on the star counts is a flattening of the curve towards fainter magnitudes, due to faint stars being hidden within the profiles of brighter ones. This is especially significant in the galactic centre region, as can be seen in figure 4H, because of the high stellar densities. For a random distribution of stars, the probability of two stars appearing in the same bin is described by Poisson statistics. Unfortunately, the correction to our star counts cannot just be calculated from a Poisson distribution of faint sources hidden under brighter ones, since a secondary effect of the confusion can be to push the dominant star up into a brighter magnitude interval. Also to calculate the probability of confusion with the Poisson function requires the true number of stars not the observed number to be known. The mean of the Poisson distribution μ depends on the resolution of the instrument, which is difficult to accurately determine in the up/down mode.

To correct the star counts for confusion a computer simulation

technique was used. To begin with an estimate of the corrected distribution was made, and then the number in each magnitude interval were randomly scattered by the computer along a line. For each source an up/down profile with an amplitude proportional to the source strength was summed into an array. The number of resolvable individual sources in each magnitude interval was then counted, and these were compared with the observed results. If the agreement was poor then the input estimate was modified and this loop repeated. To overcome the random nature of this process, the calculation at each estimate was repeated sixteen times so that a mean and standard deviation (σ) could be calculated. For all the regions away from the galactic centre the simulations agreed with the observed results in all magnitude intervals to better than 1σ . Despite using a small beam of only 180 square arcseconds the confusion of sources towards the galactic centre severely reduced the detection of stars with magnitudes greater than 9.5. This factor made the corrections calculated from the above method, where these are large, more uncertain. In the magnitude intervals for which the simulations did not agree with the observations at the 1σ level the error bars plotted in figure 4H have been increased proportionately. In the diagrams of the star counts (figures 4H-4P) the original counts are shown by dotted boxes, and the corrected counts by solid boxes.

In all these regions the confusion, and not the detector sensitivity, has determined the faint magnitude limit for which star counts could be obtained. To give some idea of this, there is listed below the magnitude at which fewer stars were picked out in the star count interval fainter than that magnitude than in the interval brighter, due to the confusion. Also listed is the detector sensitivity quoted as the magnitude for a one sigma in one second detection.

REGION	CONFUSION LIMIT (m) fewer stars picked out in interval $m \rightarrow m + \frac{1}{2}$ than in interval $m \rightarrow m - \frac{1}{2}$	DETECTOR SENSITIVITY 1σ 1s	SLIT AREA sq. arc sec.
0	9.5	10.5	180
10	9.5	11.8	550
20	10.0	11.8	550
30	10.5	11.8	550
40	11.0	11.7	550
50	11.0	11.7	550
60	11.5	11.7	550

As can be seen from the table only in the 60° region does the confusion limit approach the detector limit. Presumably for regions even further out in the plane, detector sensitivity, with the Leicester detector at Tenerife, and not confusion would be the limiting factor.

During the course of this work Barry Giles²³ and Richard Willingale at Leicester produced a computer program which would perform a Fourier deconvolution of the scans, using the raw data and a normalised up/down star profile. Figure 4G shows the result of this deconvolution on a scan from the 40° region. On the raw data plot (figure 4F) are marked the sources which were picked out by hand, and on the deconvolved plot are marked the peaks corresponding to these hand picked stars. As can be seen more sources are resolved by the deconvolution program than can be picked out by eye from the raw data. It would appear that this Fourier deconvolution method is a much more efficient way of producing infrared star counts. Unfortunately there are drawbacks to this technique. The major problem is that from this deconvolution it is difficult to calculate the brightnesses of the sources. By comparing the strengths of the sources with hand picked

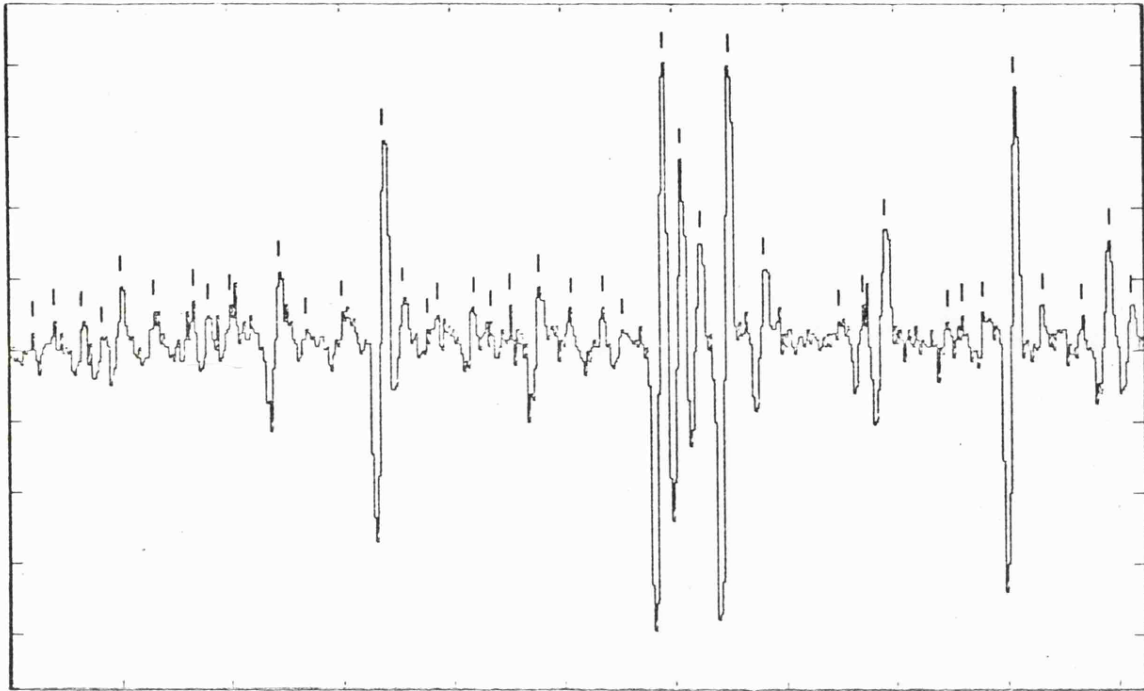


Fig. 4F Raw data scan from the 40° region. The marks indicate hand-picked stars.

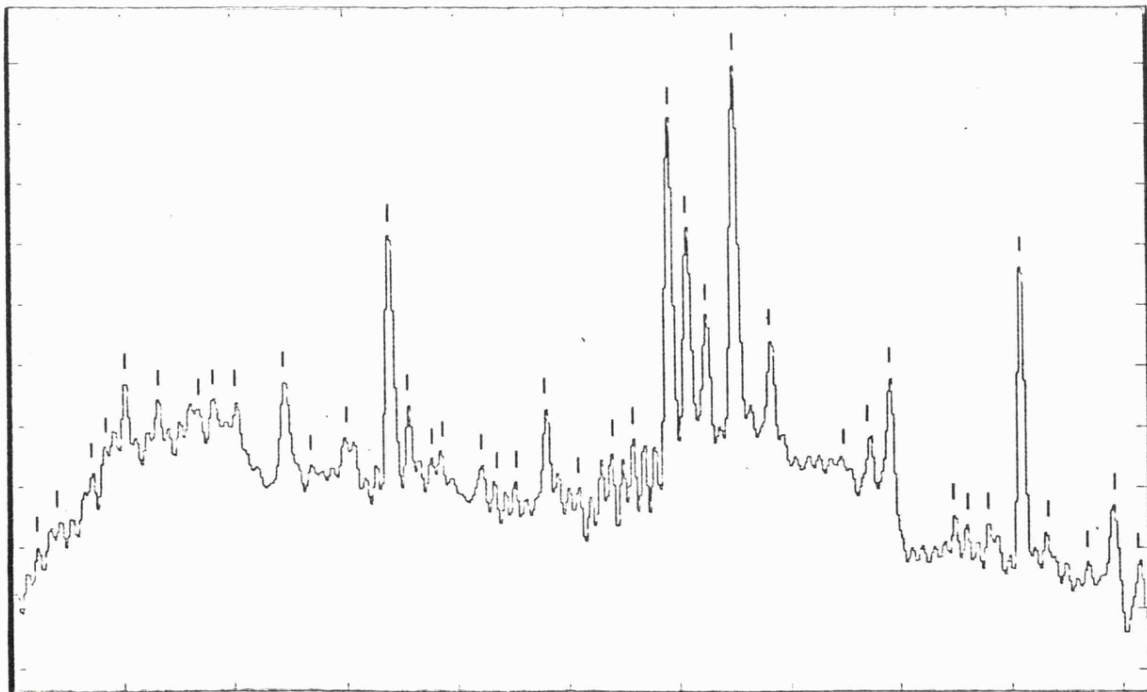


Fig. 4G Fourier deconvolution of the scan from the 40° region. The marks indicate the hand-picked sources from the raw data (see page 4.13).

counterparts, it is found that the zero level varies along the scan in a non-linear way. One reason for this is because the program joins the two ends of the scan for the deconvolution, and any discontinuity at this point affects the result. This can be seen in the diagram where the two ends drop below the average level, possibly due to the effect of the source at the extreme right hand end. This joining of the two ends can also produce spurious results within the width of an up/down profile of this point. Other irregularities occur in the 'background' level; for example about three quarters of the way along the scan the level noticeably changes either side of a brightish source. One advantage of the up/down scanning for star counting, the cancellation of any slowly varying background, is negated by the deconvolution since the program will attempt to reconstruct any extended sources.

A problem which affected early versions of the program, and is possibly present in this run, is the appearance of secondary, decaying, oscillations either side of a bright peak. For example in the diagram just before the bright star three-fifths of the way along the scan are some regularly spaced peaks, only two of which were identified in the original data. The program does have a smoothing coefficient which could rid these effects, but then the resolving power is reduced.

For these reasons this Fourier deconvolution technique was not used to produce the star counts.

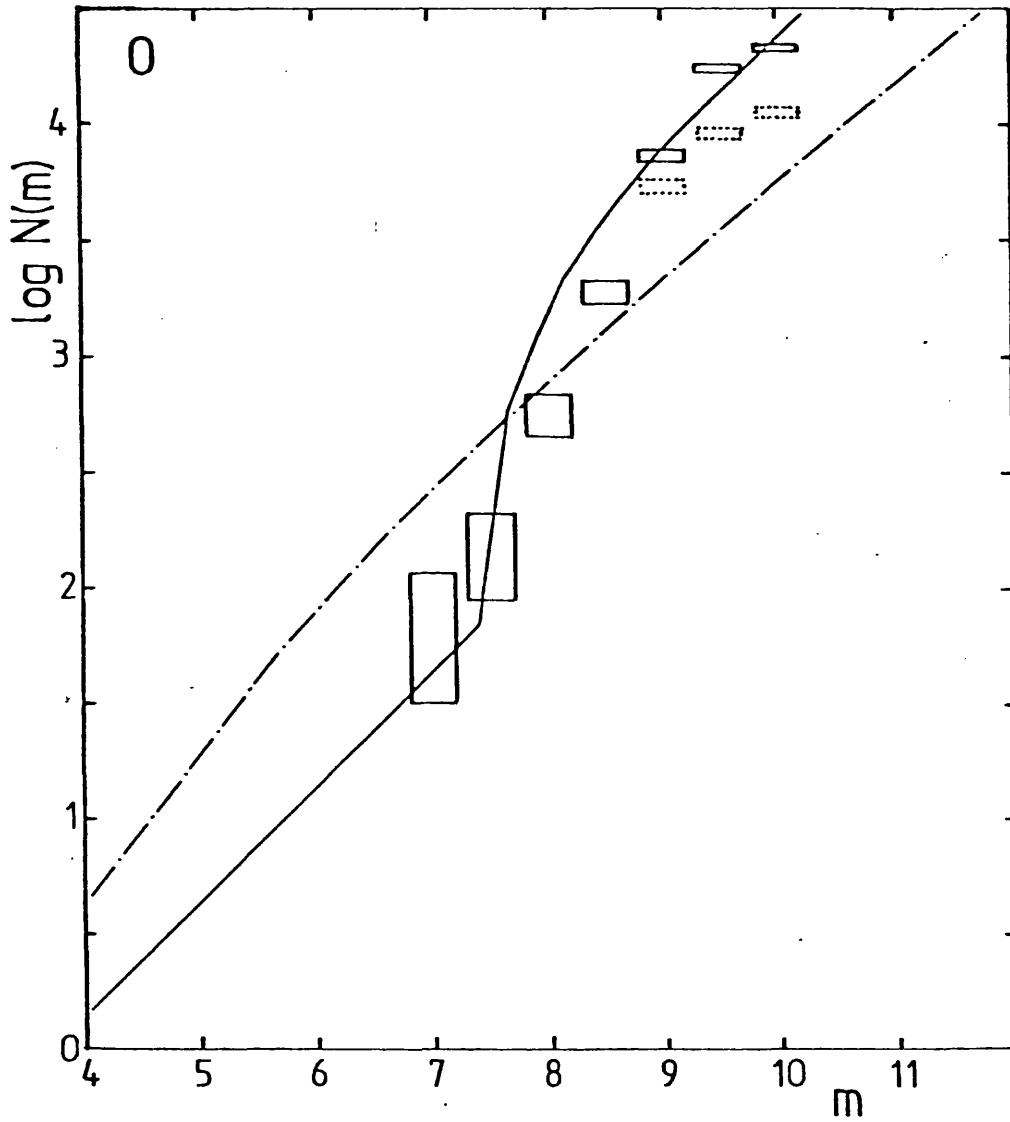


Fig. 4H The infrared star counts for the 0° region. Cumulative counts $N(m)$ are plotted against magnitude m . The model predictions are exponential disc with uniform extinction of 0.1^m kpc^{-1} (broken line) and disc plus nucleus with 0.275^m kpc^{-1} of uniform extinction and $0^m.8$ extinction wall at 1700 pc (solid line) (see page 4.23).

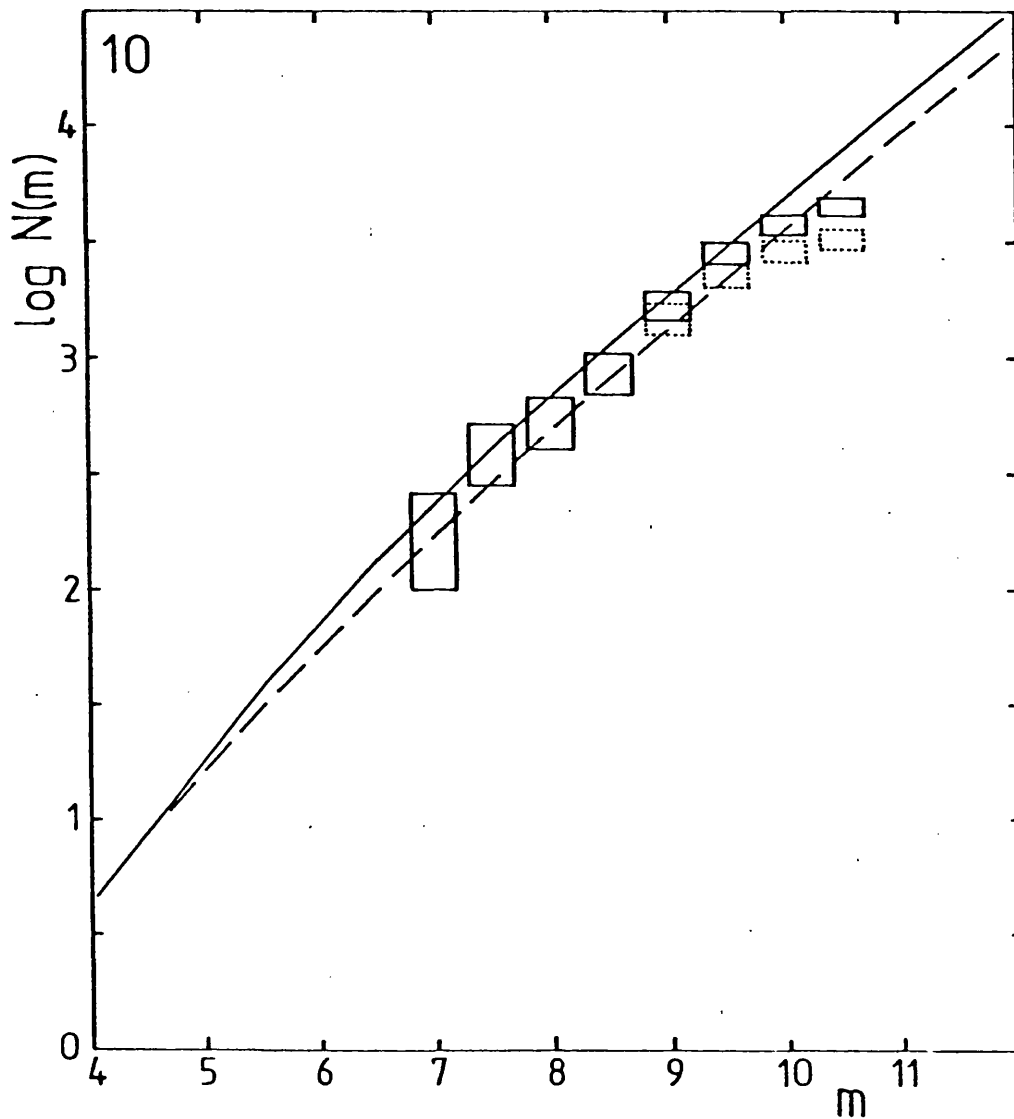


Fig. 4J The infrared star counts for the 10° region. Cumulative counts $N(m)$ are plotted against magnitude m . The model predictions are exponential disc with uniform extinction of 0.1^m kpc^{-1} (solid line) and disc with radial extinction (broken line)(see page 4.20).

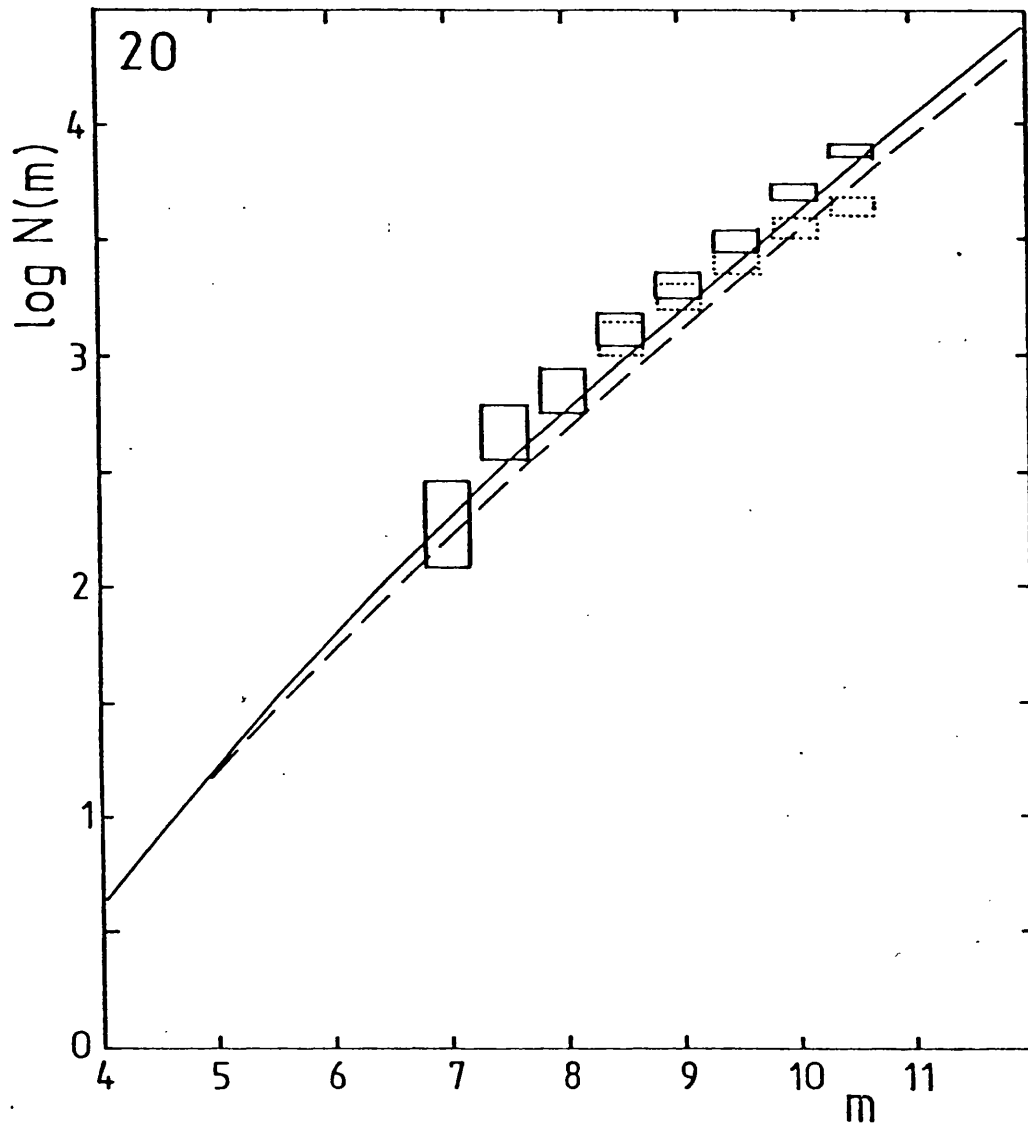


Fig. 4K The infrared star counts for the 20° region. The model predictions are described in fig. 4J and on page 4.20.

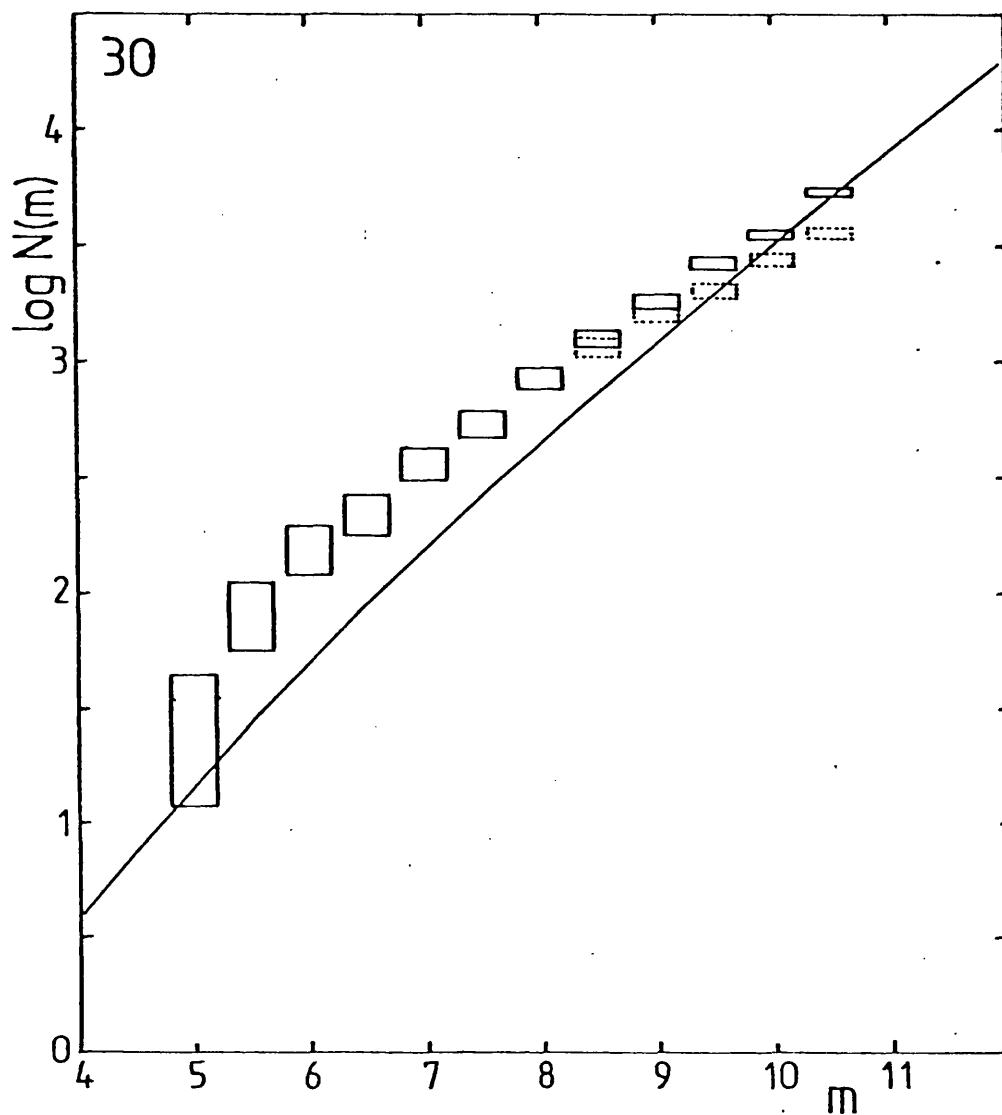


Fig. 4L The infrared star counts for the 30° region. The model predictions are described in fig. 4J and on page 4.20.

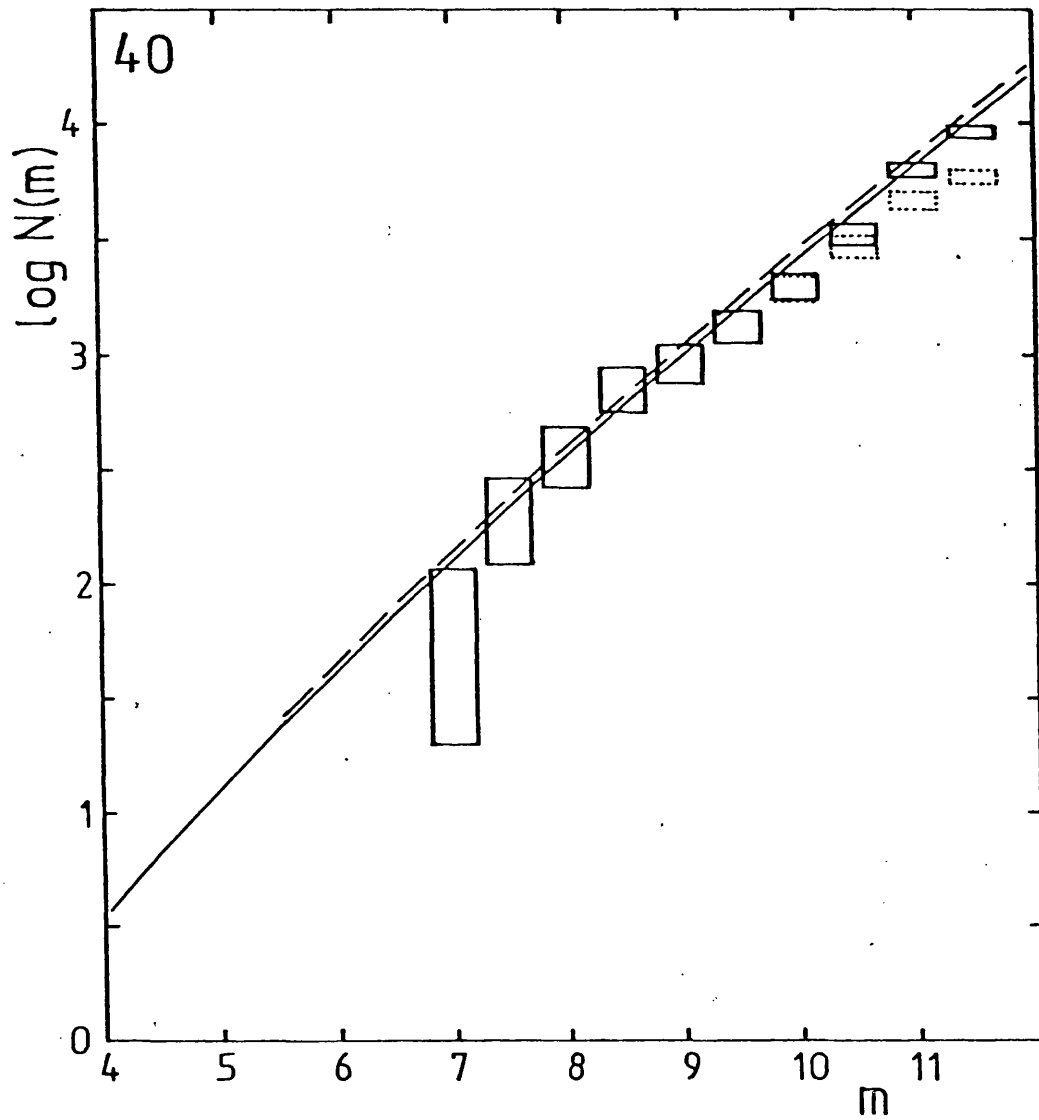


Fig. 4M The infrared star counts for the 40° region. The model predictions are described in fig. 4J and on page 4.20.

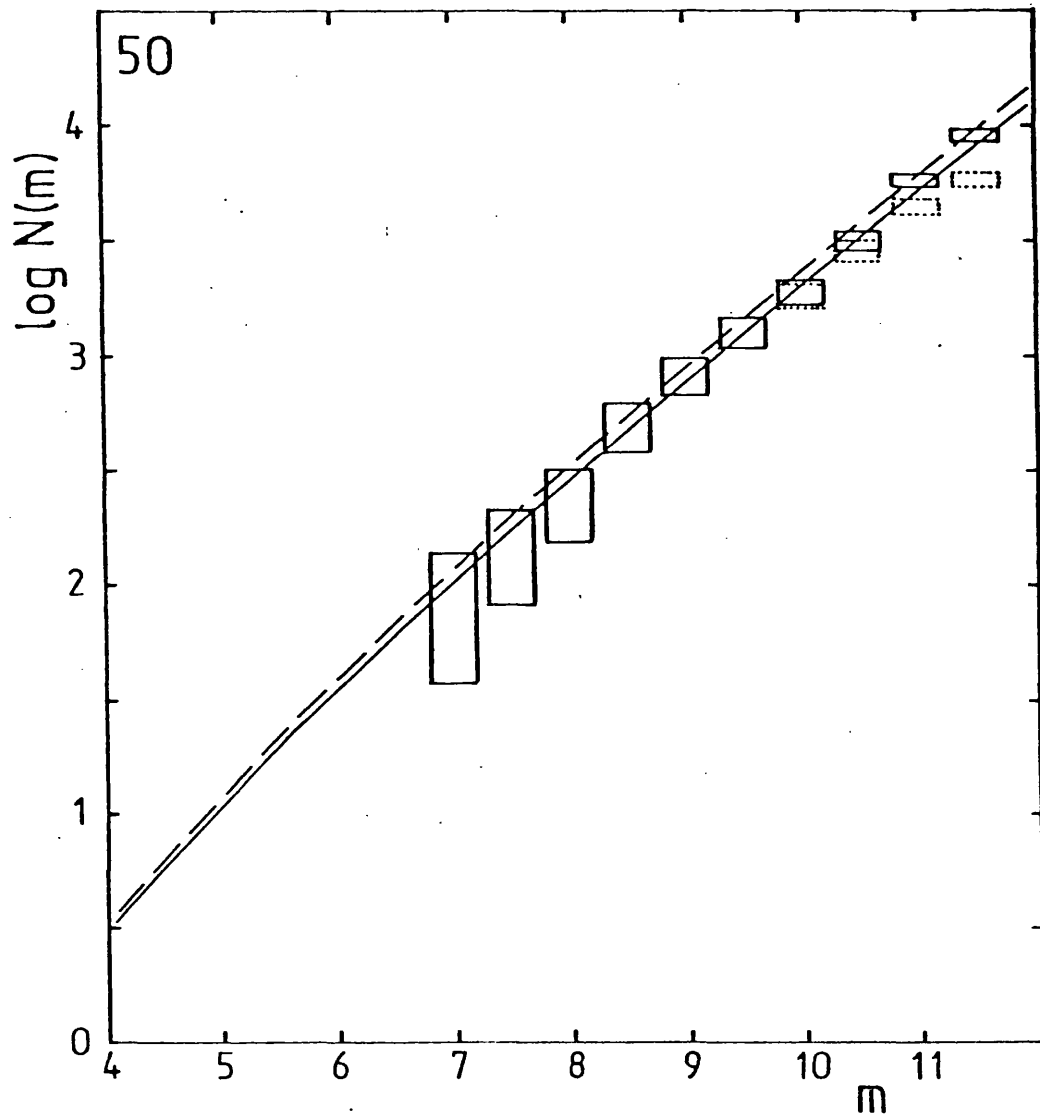


Fig. 4N The infrared star counts for the 50° region.
The model predictions are described in fig. 4J
and on page 4.20.

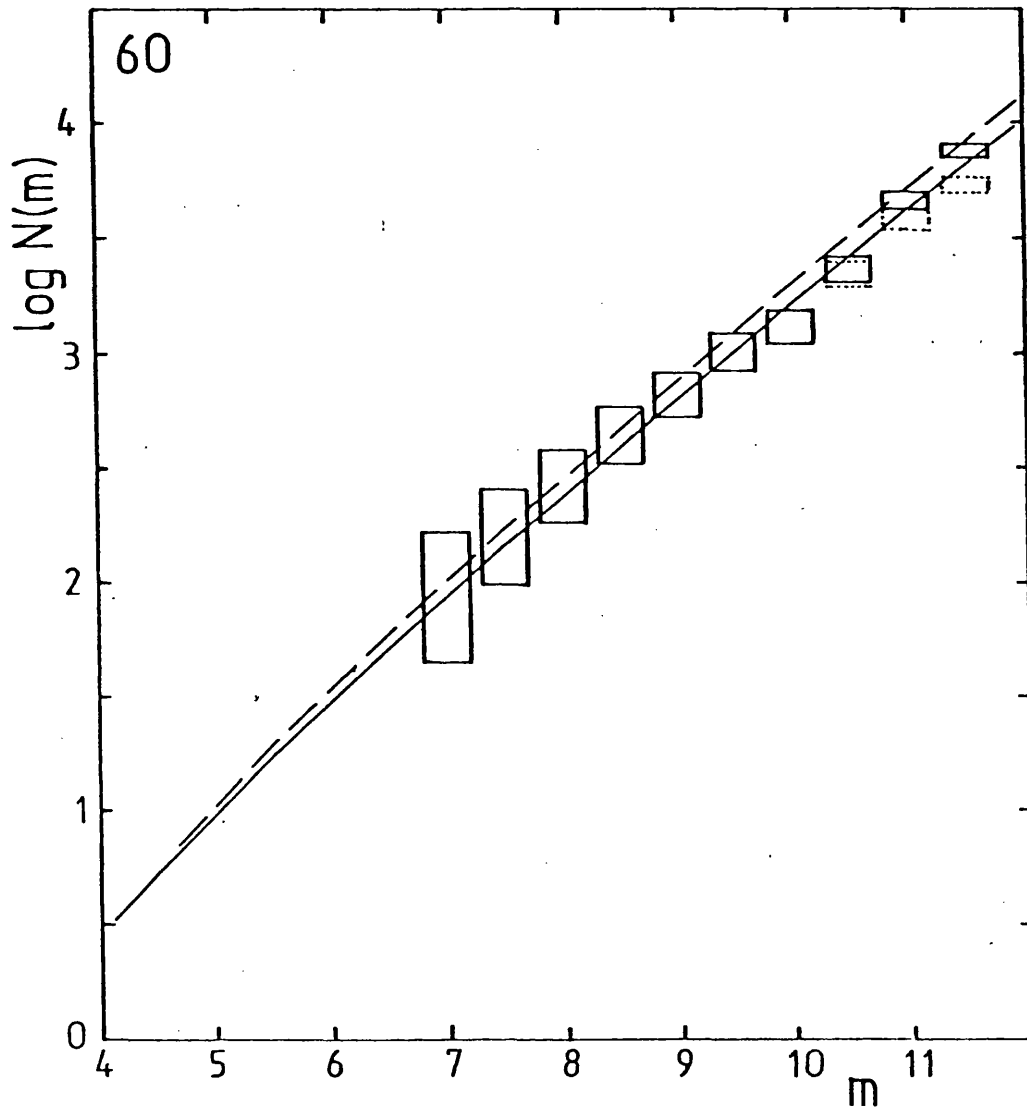


Fig. 4P The infrared star counts for the 60° region. The model predictions are described in fig. 4J and on page 4.20.

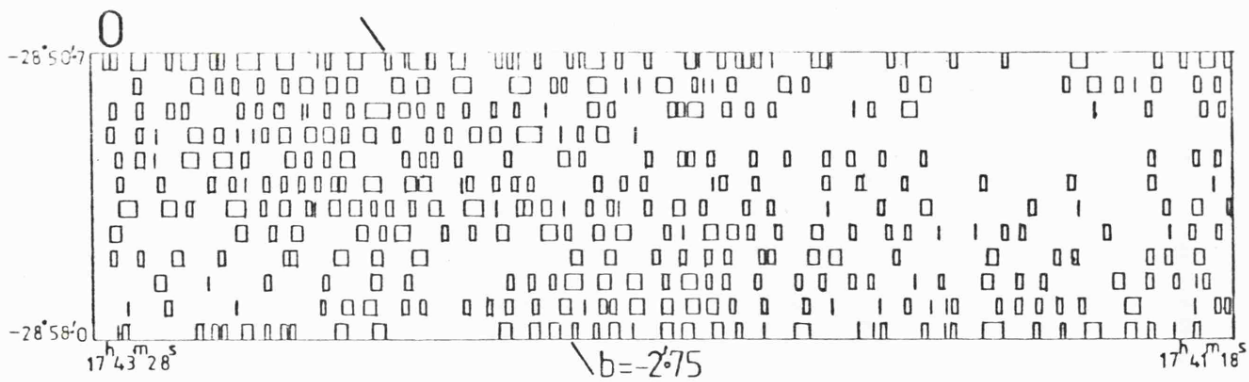


Fig. 4Q A map of the sources brighter than $10^m.0$ in the 0^o region.

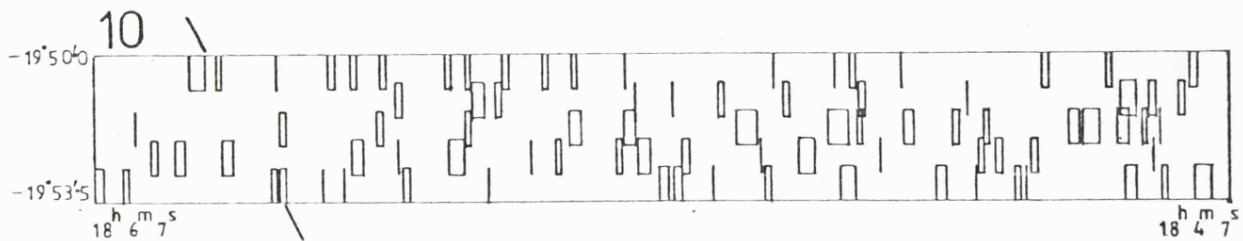


Fig. 4R A map of the sources brighter than $10^m.0$ in the 10^o region.

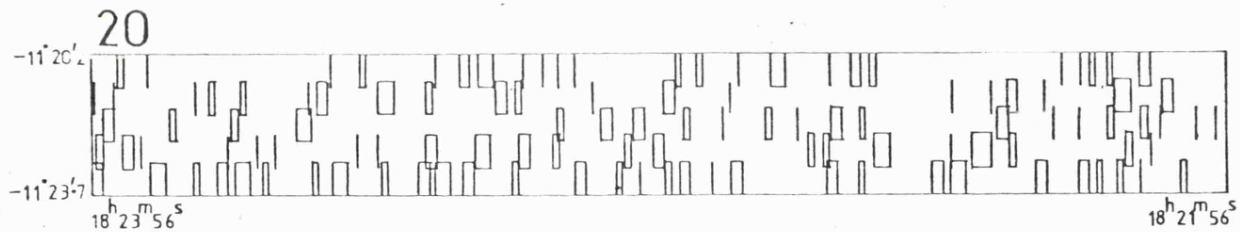


Fig. 4S A map of the sources brighter than $10^m.0$ in the 20^o region.

Figs. 4Q-4W show the distribution of sources in the infrared star count regions. The sources are plotted as boxes; the height of the box indicates the uncertainty of the position of the source due to the length of the slit, and the breadth of the box is proportional to the magnitude of the source, the brighter sources being wider.

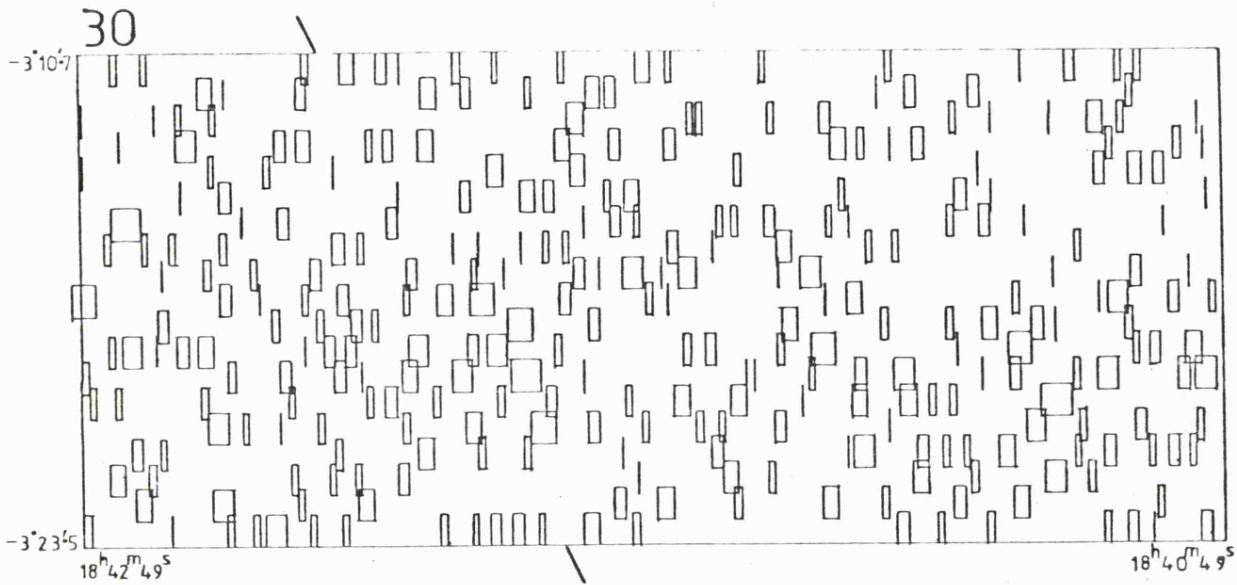


Fig. 4T A map of the sources brighter than $10^m.0$ in the 30° region.

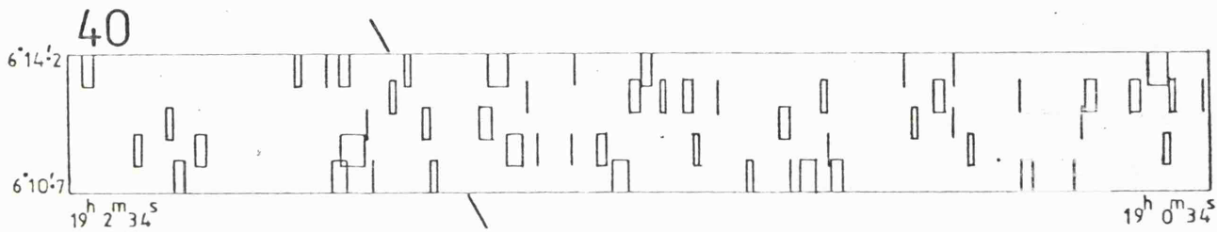


Fig. 4U A map of the sources brighter than $10^m.0$ in the 40° region.

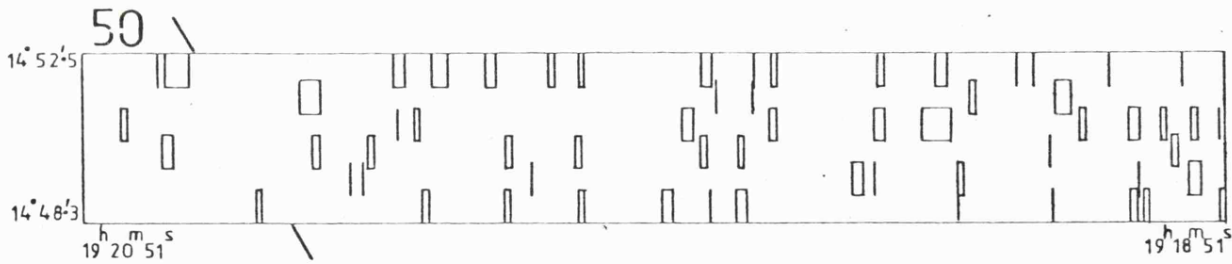


Fig. 4V A map of the sources brighter than $10^m.0$ in the 50° region.

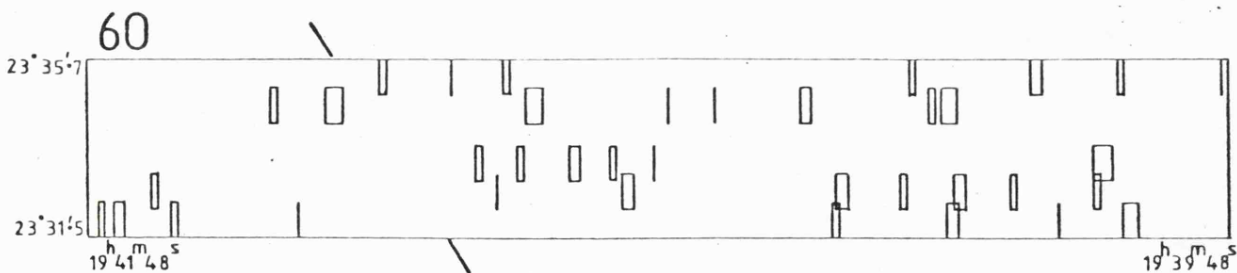


Fig. 4W A map of the sources brighter than $10^m.0$ in the 60° region.

2. DISCUSSION

THE STAR COUNTS

The star counts for all the regions are shown in figures 4H-4P. The results are plotted as error boxes, as discussed earlier. The solid lines indicate the predictions of a model Galaxy which is discussed in the next few sections.

In order that a comparison of the star counts from the regions can be made, they have been plotted on one diagram without error boxes. This is shown in figure 4X. What is immediately apparent from this diagram is that there is no uniform decrease in the counts from 0° out to 60° . Figure 4Y shows the cumulative count at 9th magnitude for each region against longitude, as an example of this non-uniformity. For stars fainter than 9th magnitude the variation of cumulative count with longitude shows a marked resemblance to the distribution of 2.4 micron flux in a large beam.^{8,24} In figure 4Z is shown a simplified version of Ito et al.'s⁸ figure 2 describing the variation of the 2.4 micron flux with longitude in a 2° beam. A more recent map²⁴ at this wavelength shows a very similar longitude dependence and flux levels in a 1.7° beam. The similarity between the star counts and the flux measurements ought to be expected if the 2.4 micron emission is mostly from stars. It might be expected, on the other hand, that since the star count areas are much smaller than the large beam size of the flux measurements, regional variations of say extinction and star density, smoothed in the large beam, could affect the star counts. Such small scale variations may be the reason for the low star counts seen in the 10° region, compared to 20 and 30; no corresponding minimum being seen in the large beam flux at this longitude. The smoothing effect of the large beam observations will be most severe in the galactic centre direction where large gradients in the stellar density can be

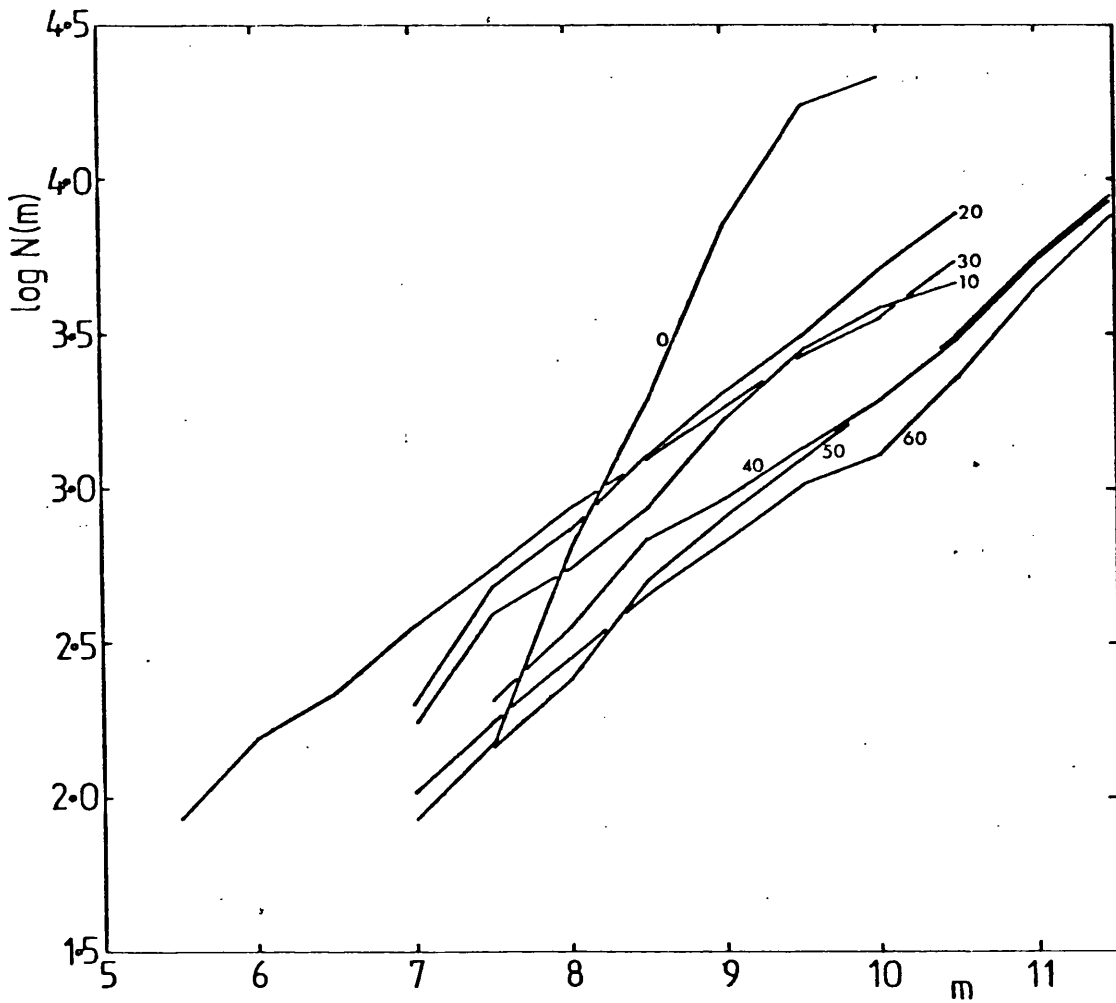


Fig. 4X The cumulative infrared star counts from all seven regions plotted on one diagram without error bars.

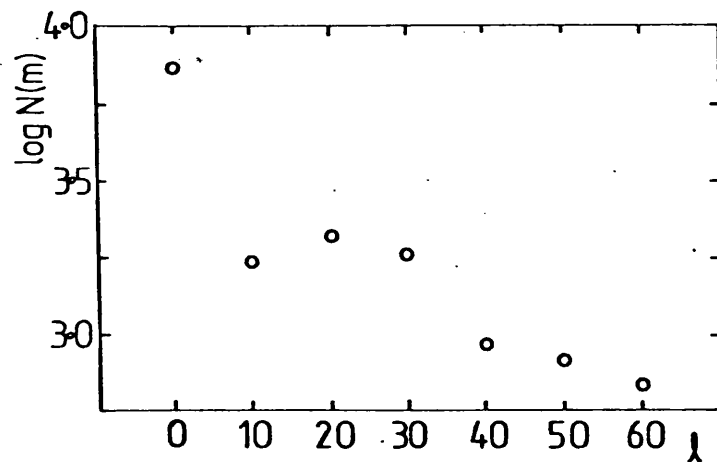


Fig. 4Y The cumulative star count at $m = 9.0$ in each region plotted against longitude l .

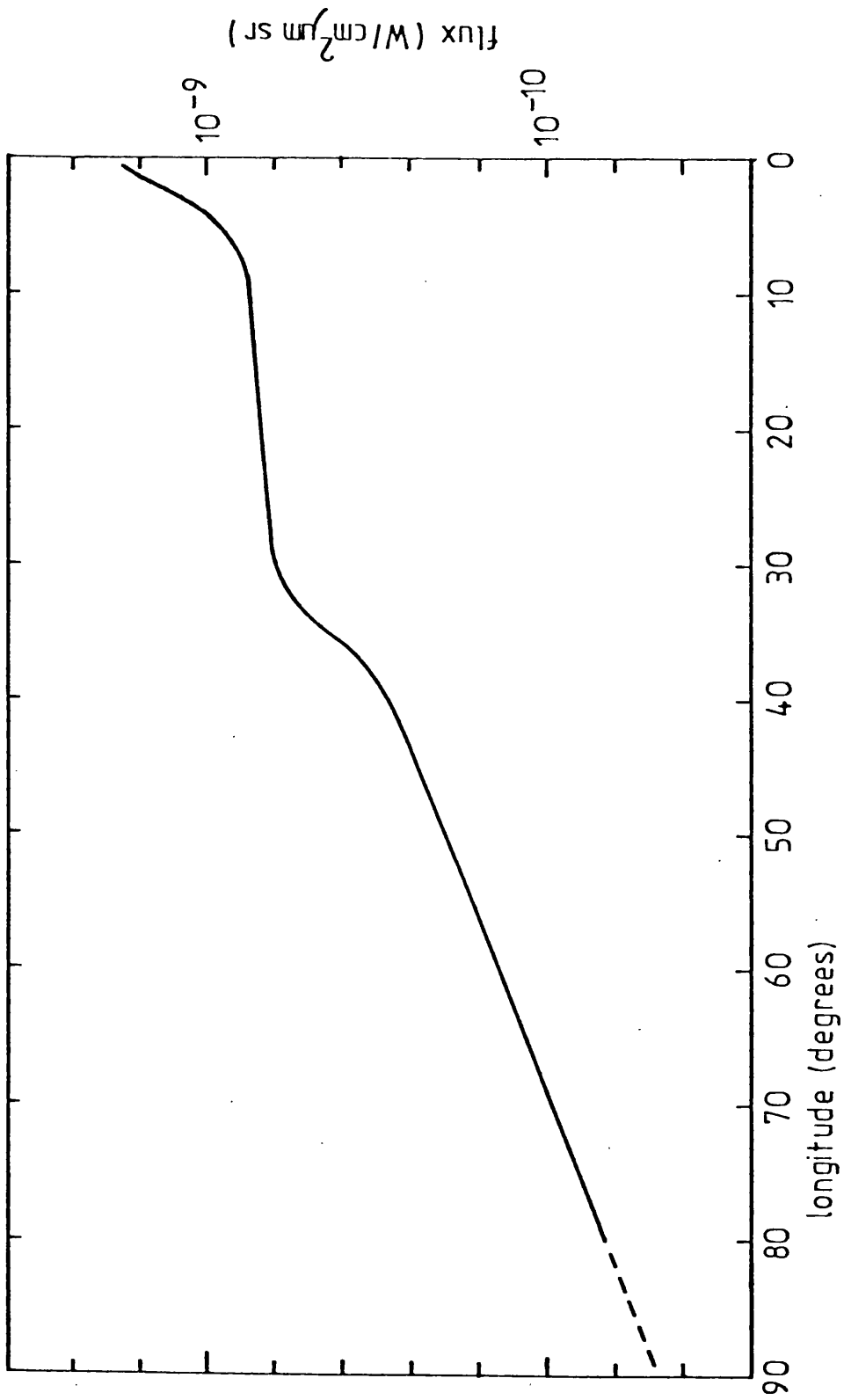


Fig. 4Z The variation of the 2.4 micron flux with galactic longitude in the galactic plane, with a 20 beam (ref. 8).

expected.

For the star counts towards the galactic centre it can be seen that in magnitude intervals brighter than 8th magnitude fewer stars were counted than in almost any other region. The cause of this must be due to increased extinction somewhere along the line of sight at 0° , unless an extraordinary density distribution of stars is implied for the Galaxy. The visible star counts showed that a large cloud of extinction is seen at a distance of about 1700 pc in the direction of the galactic centre. An extinction of $0^m.8$ at K (8^m in the visible) in this cloud, would account for the discrepancy in the 0° counts below 8th magnitude, since a horizontal shift of $0^m.8$ for the 0° curve brings the cumulative star counts at $7^m.0$ and $7^m.5$ in line with those at 10 and 20. Between magnitude intervals 8 and 9 the logarithm of the cumulative count ($\log N(m)$) rises by 1.1 in the observed data. Since this rise is greater than 0.6, which is implied by a model under the three assumptions of no extinction, constant density of stars and infinite distribution of stars, the density of stars must increase somehow along the line of sight. The star counts alone cannot prove where this increase occurs, because of the multiplicity of answers that can be obtained from the fundamental equation of star counts (see Chapter 2). The following model fit section will discuss further this increase in density and where this might occur.

In the 30° region more stars are seen for magnitudes brighter than $8^m.0$ than in any of the other regions. Evidence indicates that these extra stars are due to red giants associated with regions of star formation in the '5 kpc' ring. This is discussed more fully later.

From these star counts the total flux of radiation observed in these regions can be calculated. In table 4III are listed the integrated fluxes for the corrected count in each region. So that a

TABLE 4III

FLUXES OF OBSERVED STARS IN THE IR REGIONS

Region	Flux of Observed Stars with $m < 10.0$ $W_{cm}^{-2} \mu^{-1} sr^{-1}$	Ito et al. Flux ⁸ $W_{cm}^{-2} \mu^{-1} sr^{-1}$	Difference $\overline{[B - A]}$	Model Flux for $m < 10.0$
	$2.2\mu \overline{[A]}$	$\overline{[B]}$		
0	$6.6 \times 10^{-10} \pm 0.7$	$93 \times 10^{-10}^*$ 18.1×10^{-10}	11.5×10^{-10}	8.78×10^{-10}
10	$2.2 \times 10^{-10} \pm 0.4$	7.4	5.2	3.94
20	$2.8 \times 10^{-10} \pm 0.4$	6.9	4.1	3.24
30	$3.9 \times 10^{-10} \pm 0.6$	6.1	2.2	3.97^+
40	$1.5 \times 10^{-10} \pm 0.2$	2.6	1.1	2.13
50	$2.0 \times 10^{-10} \pm 0.3$	2.0	0.0	1.75
60	$0.9 \times 10^{-10} \pm 0.1$	1.3	0.4	1.45

* from EN68²

+ with density enhancement

fair comparison can be made between regions the fluxes of the observed stars have only been calculated for stars brighter than $10^m.0$. The errors are calculated from the possible 0.2 magnitude error in the strength of a source. Also listed in the table are the integrated fluxes measured by Ito et al.⁸; these are likely to be lower limits due to the smoothing effect of the large beam. For the galactic centre a smaller beam flux measurement can be obtained from Becklin and Neugebauer² and this is also listed in table 4III. For the 0° region there is a large discrepancy between the flux from the observed stars and the total integrated flux. This difference is probably due to large numbers of stars in the dense core of the Galaxy with apparent magnitudes fainter than the measured $10^m.0$ limit. (A star with apparent magnitude $10^m.0$ at 8000 parsecs with an extinction of $2^m.7$ has an absolute magnitude of ~ -7). Some of the difference could also be made up from extended emission undetected with the narrow chop, from the 'active' centre of the Galaxy.

Going away from the galactic centre the difference between the fluxes from the observed stars and the total integrated flux becomes less. This convergence suggests that stars fainter than the observed magnitude limit are becoming less important to the total integrated flux further out in the plane.

Maps of all observed sources brighter than $10^m.0$ in the regions are shown in figures 4Q-4W. For the 0° region the sources are seen to be clustered towards the galactic plane but do not appear to have any circular symmetry around the galactic centre. Bailey²⁵ deduced from maps of the galactic centre by Becklin and Neugebauer^{2,6} that the 2.2 micron surface brightness follows a $r^{-0.8}$ power law equivalent to $r^{-1.8}$ for the star density, out to a radius of at least 50 pc. Although this law implies circular symmetry, Bailey had to allow for

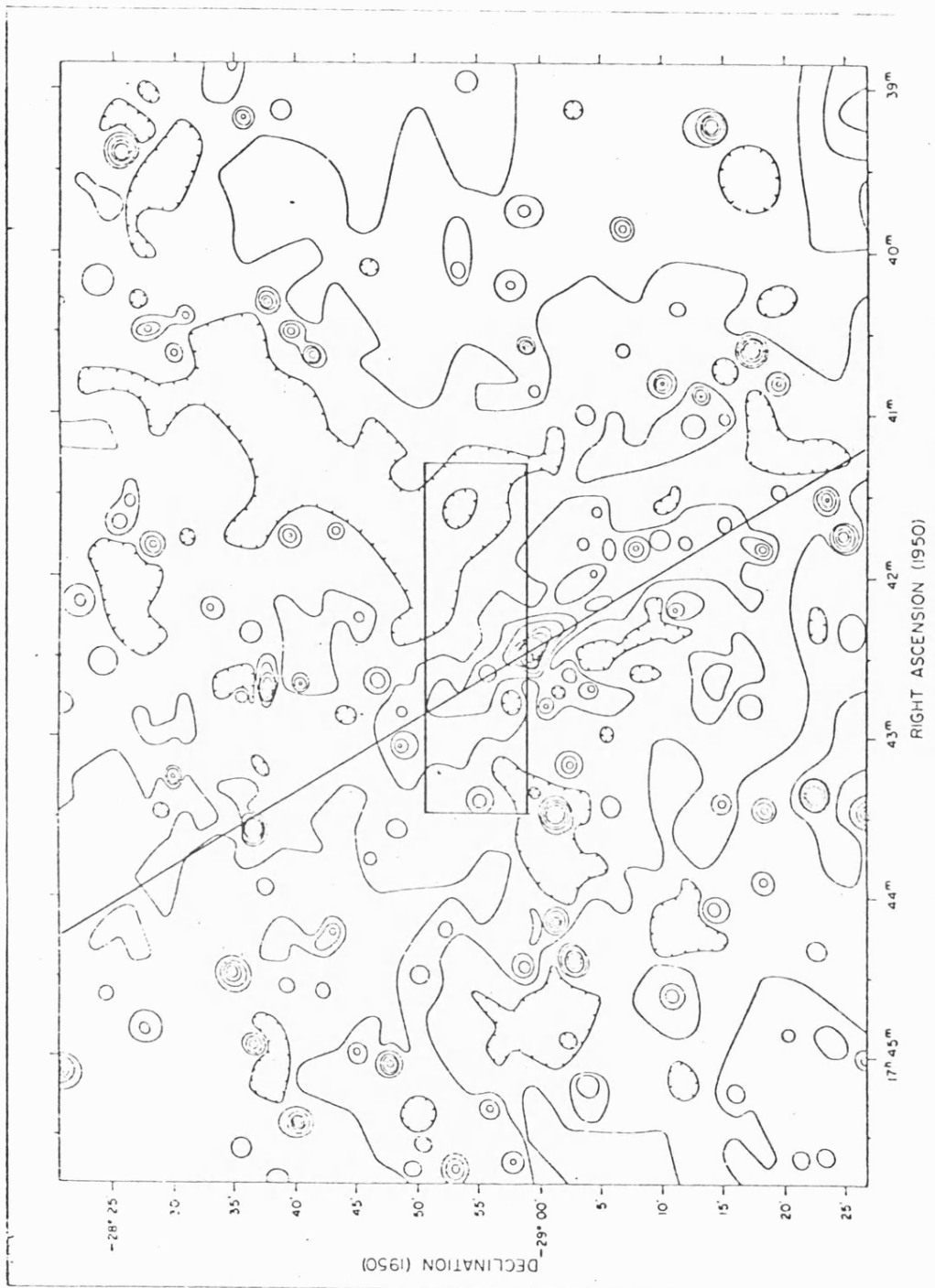


Fig. 4AA Becklin and Neugebauer's low resolution 2.2 micron map of the galactic centre (ref. 7). The box indicates the position of the infrared star count 0^o region.

deviations from circular symmetry in the data to obtain this relation. The star counts at 0° appear to follow the pattern of flux measurements in Becklin and Neugebauer's⁷ low resolution map. Figure 4AA reproduces this map with the star count area overlaid. The low flux levels approximately 2^m west of the nucleus is matched in the star count map with a region where few stars brighter than $10^m .0$ are seen.

The 30° map in relation to the excess of bright sources is discussed in the chapter on obscured sources. The maps of the other regions show a more or less random distribution of infrared stars.

It would be very useful if these maps could be overlaid on a Schmidt sky plate so that the infrared stars could be identified. The resolution of the observations is however insufficient to definitely assign a star to an infrared source. The reliability of the identification could be improved by comparing visible (V) and near-infrared (I) Schmidt plates to pick out candidate stars by their V-I colours. Possible methods for this comparison are discussed in the chapter on obscured sources.

A MODEL GALAXY

As a first step in the analysis of the star counts, a very simple Galaxy model was proposed. The basis of the model came from the work by Bahcall and Soneira²⁶ for visual star counts.

The fundamental star count equation

$$A(m, \ell) = \int_0^{\infty} r^2 \rho(r) \phi(M) dr \quad (4.3)$$

was used to predict the star counts (A) per steradian, in each magnitude interval (dm) in the direction of galactic longitude ℓ . For this simple model the density ρ was assumed to be purely due to the exponential

disc component of the Galaxy. Bahcall and Soneira use a disc density function.

$$\rho_d(r) = \exp(-(x - r_0)/h) \quad (4.4)$$

where x is the radial distance from the galactic centre, r_0 is the Sun - centre distance, and h is the scale length of the disc distribution. The constants were initially set at $r_0 = 8000$ pc, $h = 3500$ pc. The variation of ρ_d with height perpendicular to the plane has been neglected, since all the regions studied are very close to the plane. Hayakawa et al.²⁴ have shown that the near infrared sources are associated with spiral arms, but an axisymmetric model is assumed for simplicity to simulate the gross structure. In the plane of the Galaxy the spheroid density component quoted by Bahcall and Soneira only becomes significant for radii less than 500 pc or directions within $\sim 4^\circ$ of the nucleus.

A 2.2 micron luminosity function was obtained as follows. For magnitudes brighter than $M_k = -1.0$ the spectral parameters listed by Elias⁵ in his luminosity function were integrated over absolute magnitude. For magnitudes fainter than $M_k = -1.0$ the function was obtained by applying the V-K colours of Johnson²⁷ to the spectral types making up the visual luminosity function from Astrophysical Quantities⁴ (p.247). At the join of these two components the function was smoothed by eye. This infrared luminosity function is listed with its visual counterpart from Astrophysical Quantities (p.248) in table 4IV, and shown in figure 2A. For the analysis the luminosity function was assumed to be universally constant. It was shown in Chapter 2 that the dominant contribution to the star count comes from the part of the luminosity function which has a gradient of $10^{0.4}$: steeper than this, the fainter stars dominate : shallower than this, the brighter stars

TABLE 4IV

INFRARED AND OPTICAL LUMINOSITY FUNCTION

(See figure 2A)

Abs. mag	IR	Opt
M	$10 + \log \phi(M)$	
-10	2.65	
- 9	3.12	
- 8	3.50	
- 7	3.95	
- 6	4.37	2.30
- 5	4.78	3.08
- 4	5.18	3.63
- 3	5.62	4.21
- 2	6.02	4.77
- 1	6.41	5.31
0	6.80	5.87
1	7.14	6.36
2	7.42	6.70
3	7.67	6.98
4	7.86	7.19
5	7.96	7.34
6	8.02	7.47
7	8.04	7.53
8	8.04 *	7.61
9	8.04	7.70
10	8.04	7.81
11	8.04	7.90

* The trend of the IR function is uncertain beyond 8th mag, but it appears that a flattening, similar to the optical function at fainter magnitudes does occur.

dominate. The infrared luminosity function has a gradient of $10^{0.42}$ between absolute magnitudes -10 and -3 . This is very close to the critical value of $10^{0.4}$ where all intervals contribute equally. This means that the predicted star counts will be sensitive to the value of the luminosity function at the bright end where the statistics are poor. The bright end of the luminosity function is defined by late type stars which may significantly change the shape of the function in regions where non-disc population stars are significant, for example the galactic centre, or the galactic bulge. The greatest uncertainty in the star counts must be the constancy of the luminosity function, which is the most difficult to verify.

To complete the model an expression for the interstellar extinction has to be defined. As a first approximation it is assumed that the interstellar extinction is uniformly distributed.

The discussion is separated into two sections. All six regions in the galactic plane $10^\circ - 60^\circ$ will be treated together. The galactic centre star counts will be discussed separately because of some of the unique features in this direction.

THE PLANE FIT

In figures 4J to 4P the solid lines show the model prediction for 0.1 magnitudes per kiloparsec of infrared extinction. As can be seen this very simple model of the Galaxy gives a creditable fit for all the regions away from the centre. A constant extinction of $0^{m.1} \text{ kpc}^{-1}$ and a scale length of 3500 parsecs fits the data within the errors of the observations. The 30° region shows an excess of bright stars over the predicted count, but at the faint magnitude end the star counts do match the model predictions.

Maihara et al.²⁹ deduced from the 2.4 micron distribution that

there is a ten-fold concentration of infrared emissivity in a ring midway between the Sun and galactic centre. A simple approximation to this was considered in the model by having a ten-fold density increase between 3500 and 4500 pc. The model prediction from this is shown by the upper curve in figure 4BB. With the general luminosity function, this density enhancement predicts too many faint stars, although it fits the bright end of the star counts reasonably well. To limit the effect of this increase, the model was altered so that only a section of the luminosity function suffered the density enhancement; the exponential disc used the general luminosity function as before. The lower curve in figure 4BB shows the prediction of this model, with only stars of absolute magnitude $M < -7$ having the increase of density. This gives a much improved fit to the observed data. The star counts suggest that the enhancement in the 2.4 micron emissivity towards 30° is produced by stars with a small range of absolute magnitudes. If this is occurring in a tangential 4 kpc ring then the distances imply that M giants or supergiants must be the cause. Puget et al.³⁰ attribute the 2.4 micron distribution to massive red giants associated with regions of rapid star formation in a ring midway between the Sun and the galactic centre, which is compatible with the findings of the star counts. The effect of this ring in the non-tangential 10° and 20° directions is, however, not sufficient to determine whether this 'ring' is seen in these directions, within the errors of the star counts. For this additional modelling the extinction was assumed to be constant with distance, with the value of $0^m.1 \text{ kpc}^{-1}$.

The value of $0^m.1 \text{ kpc}^{-1}$ for the average extinction in the galactic plane ($= 1^m.0 \text{ kpc}^{-1}$ in the visible) is slightly higher than values found from optical studies. Bok and Bok²⁸ (p.194) and Trumpler and Weaver²² (p.452) quote values of $0^m.7 \text{ kpc}^{-1}$ for the average

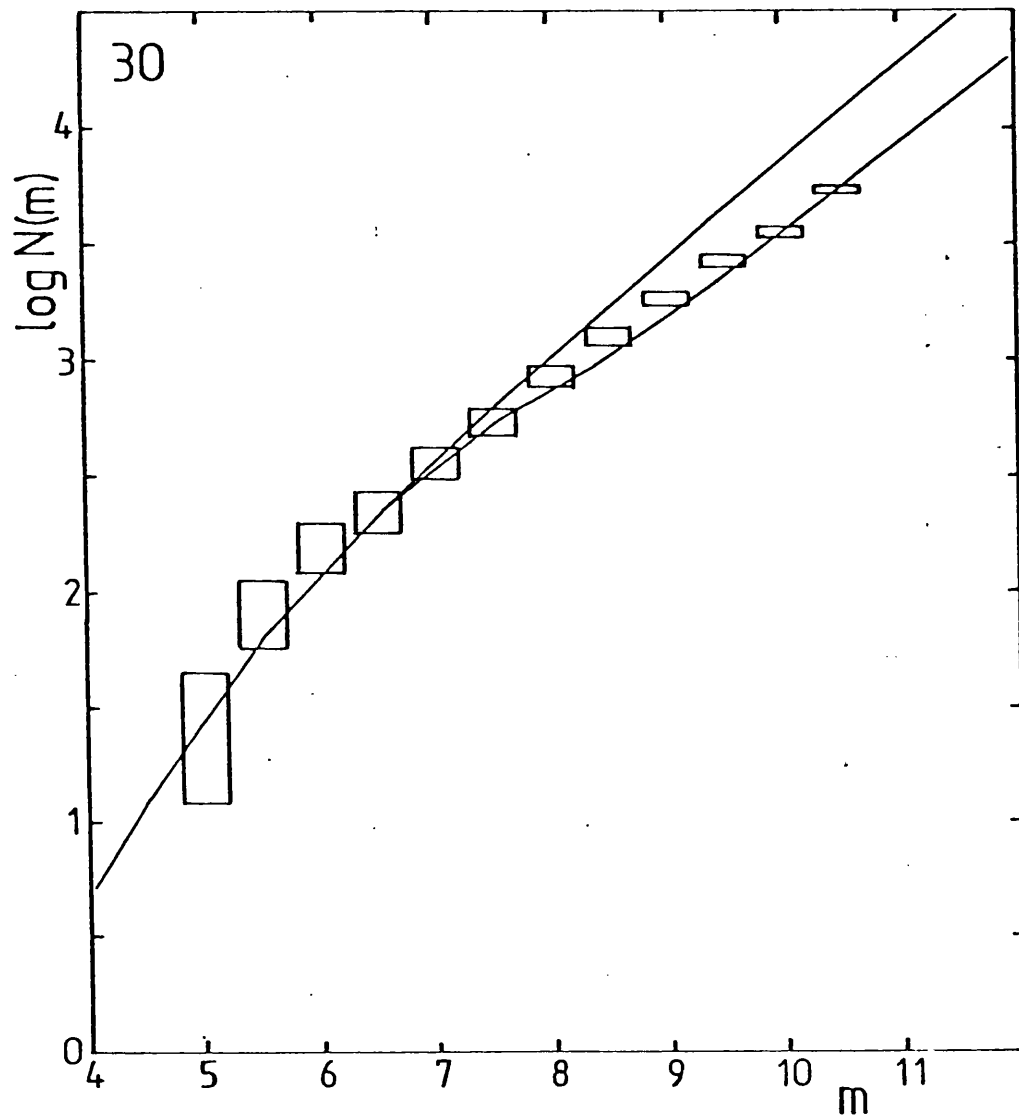
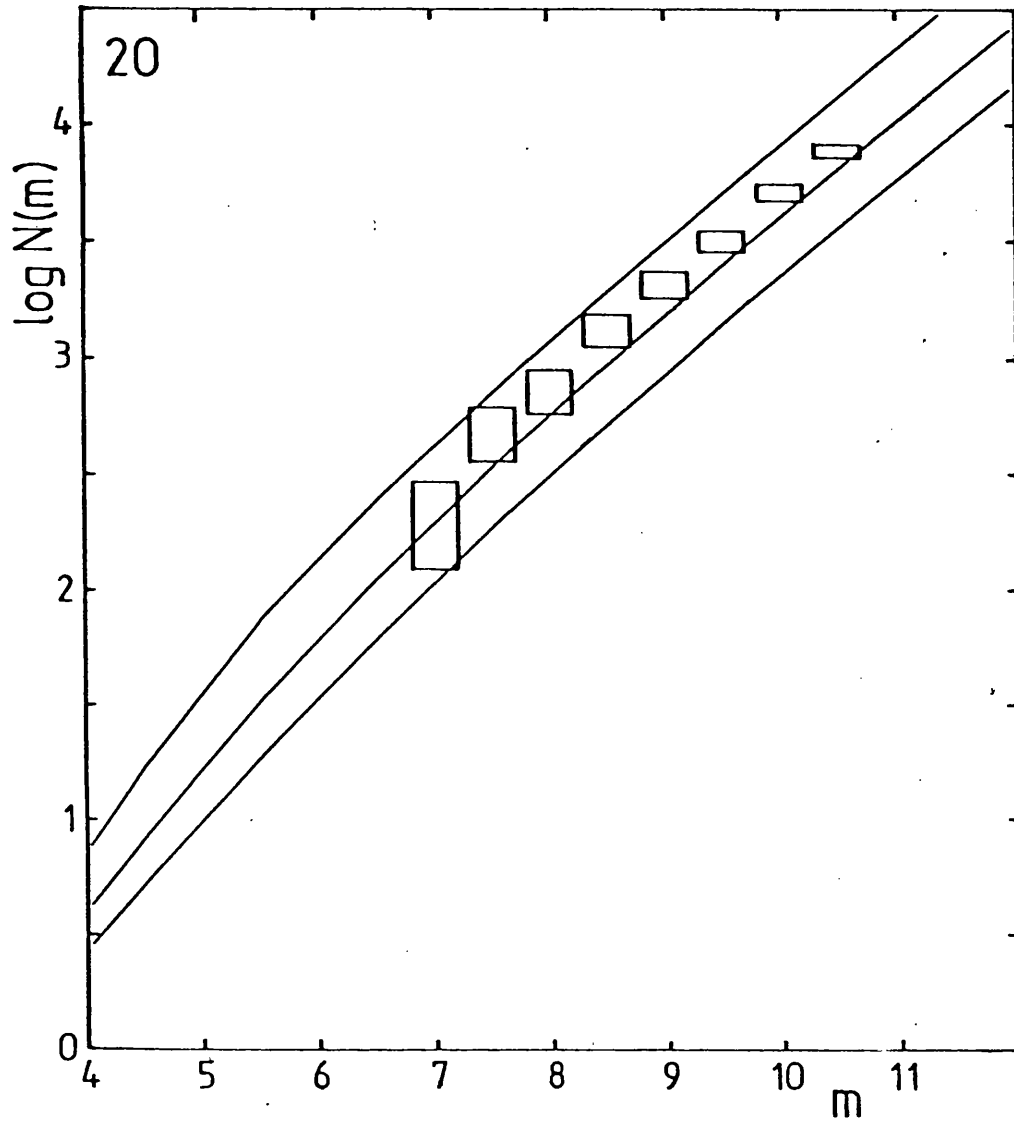


Fig. 4BB The infrared star counts for the 30° region. The model predictions are exponential disc with uniform extinction and a ten times density enhancement at 4000 pc (upper curve), and the same but with the density enhancement only applying to a small section of the luminosity function (lower curve) (see page 4.21).

extinction in the visible ($= 0^m.07$ in the infrared).

As an alternative to the constant extinction model in the plane of the Galaxy, a model in which the extinction varied with the stellar density was also considered. The relative extinction (to the solar neighbourhood) was calculated from an equation similar to that for the stellar density (4.4). A value of $0^m.1 \text{ kpc}^{-1}$ at the Sun predicted too much extinction when integrated along the line of sight. A value of $0^m.05 \text{ kpc}^{-1}$ at the Sun gives a reasonable fit to the data. The dashed lines in figures 4J to 4P represent the model with this exponential extinction. At 30° the two models give almost identical results. The fit with this model is not quite as good as the constant extinction when all six regions are considered.

The properties of the model when some of the parameters are varied are shown in figures 4CC to 4EE for the 20° region. In figure 4CC is shown the variation of uniform extinction from zero to $0^m.2 \text{ kpc}^{-1}$. In figure 4DD is shown the effect of the variation of the scale length of the disc from $h = 3000$ to 4000 pc . As can be seen, the predicted star counts are relatively insensitive to changes in the scale length; a difference of 500 pc can be matched by changing the extinction value by $0^m.03 \text{ kpc}^{-1}$. If the extinction is reduced from $0^m.1 \text{ kpc}^{-1}$ to $0^m.07 \text{ kpc}^{-1}$ to match the visually derived value, the fit to the observed data can be restored by increasing the scale length to $h = 4000 \text{ pc}$. In figure 4EE is shown the effect of steepening the luminosity function, over the sensitive region from $M = -1$ and brighter, by 10%. This reduces the influence of the luminosity function at the bright end where the statistics are poor. The decrease in the predicted count is however noticeable and to bring the model into line with the observed data would require reducing the overall extinction to almost zero. Since, in the infrared, neither the scale



Fig, 4CC The infrared star counts for the 20° region. .
 The model predictions are for the exponential disc with constant scale length and with uniform extinctions of zero (upper curve), 0.1^m kpc^{-1} , and 0.2^m kpc^{-1} (see page 4.22).

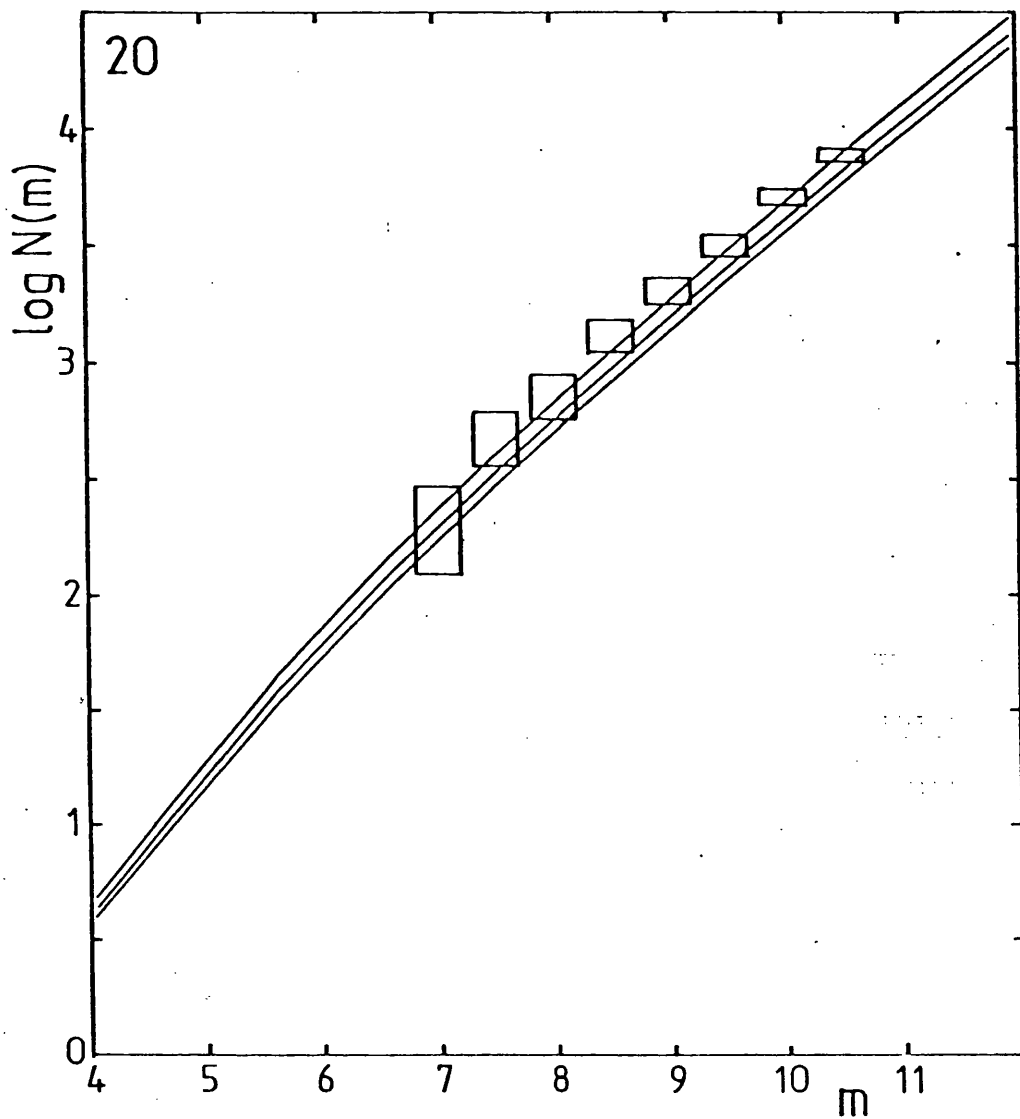


Fig. 4DD The infrared star counts for the 20° region. The model predictions are for the exponential disc with uniform extinction of 0.1^m kpc^{-1} , and with scale lengths of 3000 (upper curve), 3500 and 4000 parsecs (see page 4.22).

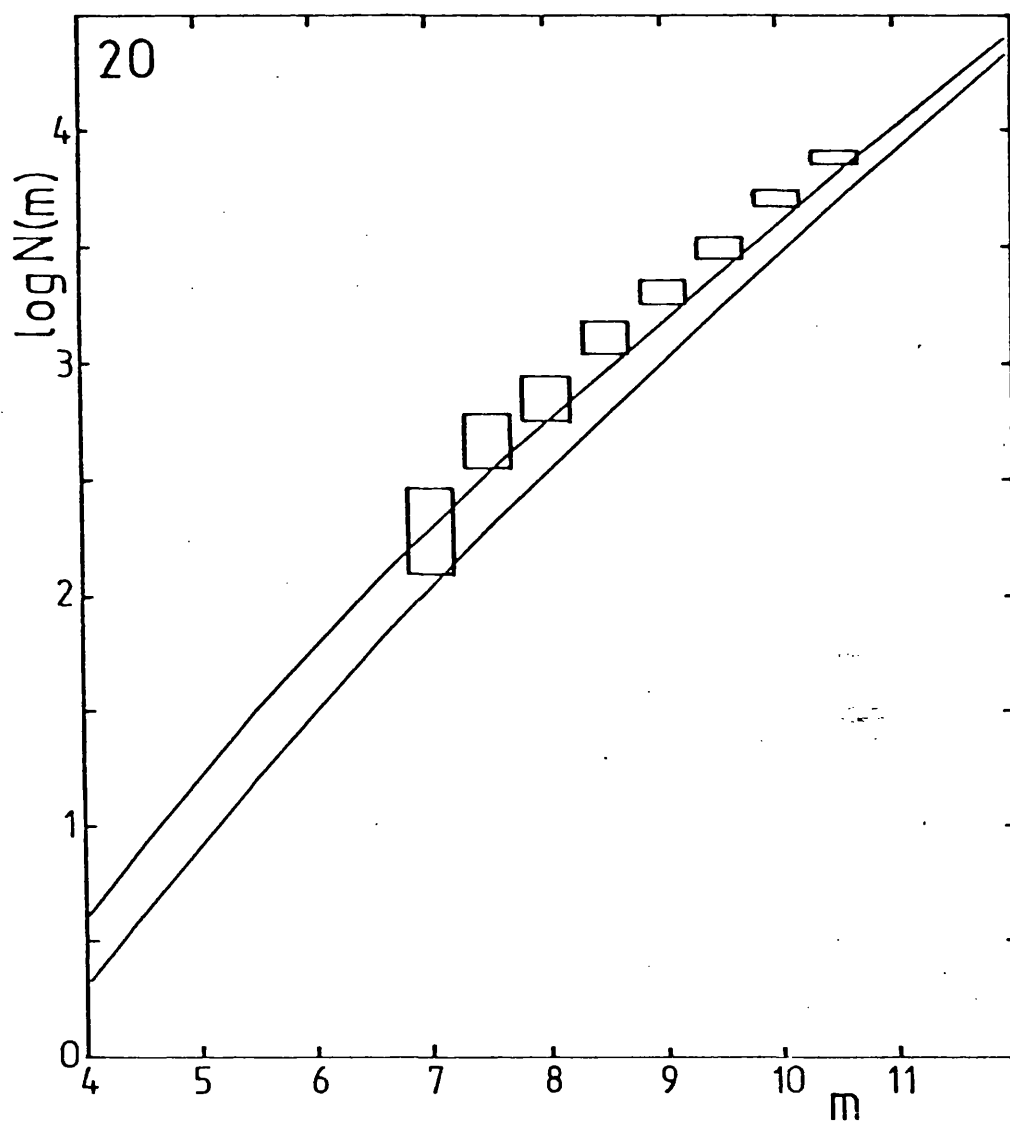


Fig. 4EE The infrared star counts for the 20° region. The model predictions are for the exponential disc with uniform extinction of 0.1^m kpc^{-1} , and the usual luminosity function (upper curve), and the same but with the luminosity function 10% steeper for magnitudes brighter than $M = -1$ (see page 4.22).

length of the disc nor the luminosity function are particularly well known these could be significantly varied in opposition without affecting the predicted count.

From the model the fluxes from the predicted star counts can be calculated. These are listed in table 4III for regions 10 - 60 for $0^{m.1} \text{ kpc}^{-1}$ of uniform infrared extinction, integrated up to the 10.0 magnitude limit. For the 30° region the flux is inclusive of the density enhancement over the limited region of the luminosity function.

THE CENTRE FIT

With the model parameters as above, using a uniform extinction of $0^{m.1} \text{ kpc}^{-1}$, the fit to the galactic centre star counts is very poor. Figure 4H shows the prediction for this model. This misfit is not wholly surprising since the implied extinction to the nucleus is only 0.8 magnitudes ($r_{\odot} = 8000 \text{ pc}$), whereas Becklin and Neugebauer^{2,3} found that there is 2.7 magnitudes of extinction at 2.2 microns, along the path length to the nucleus. With this purely exponential model no pattern of interstellar extinction can predict the shape of the star counts. Consider the effect of extinction on star counts from an unobscured region. Extinction will shift the curve to fainter magnitudes if its effect is sudden, or will flatten the curve for a more uniform distribution. The steep rise seen in the observed counts for the 0° region cannot be produced by this model. Between $8^{m.0}$ and $9^{m.0}$ the logarithm of the cumulative count ($N(m)$) rises by 1.1 in the observed data, but the equivalent change in the model prediction is only 0.42 for zero extinction.

To account for this increase in the star count requires a significant change in the stellar density or the luminosity function

from the model, along the line of sight to the galactic centre. The fact that the star counts rise steeply also implies that with the general luminosity function, the large density increase must occur in a very small space to counteract the smoothing effect of this broad function. An obvious omission from the model is the spheroid component of the Galaxy. Bahcall and Soneira²⁶ quote an expression for the spheroid which is an attempt to quantify the de Vaucouleurs $r^{1/4}$ brightness law. Unfortunately it is known that this approximation becomes inaccurate for the central few hundred parsecs of the Galaxy; just where this component starts to dominate the exponential disc, in the plane. It is also quite likely that the disc component does not extend to the very centre of the Galaxy, and so an expression for the stellar density in the nucleus is needed. By interpreting the infrared surface brightness gradients from the maps of Becklin and Neugebauer, Bailey²⁵ showed that the stellar densities followed a $r^{-1.8}$ law for $r < 500$ pc. This component was set with a relative central density of 1.6×10^6 in a radius of 1 pc. This value was decided by trial and error to explain the steepness of the count. This relative central density when integrated with the general luminosity function implies about 10^5 stars in the central parsec or a mass of $5 \times 10^4 M_{\odot}$.⁴⁴ This is about a factor of 10 down on the value of $4 \times 10^5 M_{\odot}$ quoted by Oort³¹ for the central parsec.

With this component and the assumption of a uniform $0^{m.1} \text{ kpc}^{-1}$ extinction, the model predicts far more stars than are observed. As before this value of the extinction gives a total to the nucleus much less than is quoted from other sources. So far this model has neglected the extinction screen seen in the visible star counts. If this screen contributes $0^{m.8}$ (8^m in the visible) of the total of $2^{m.7^{2,3}}$ of infrared extinction along the path length to the nucleus, and that the rest of the extinction is distributed uniformly along the path length

($0^m.24 \text{ kpc}^{-1}$) then a much better fit is obtained. The fit is slightly improved if this constant extinction is raised to $0^m.275 \text{ kpc}^{-1}$. With the $0^m.8$ screen this implies a total extinction to the nucleus of $3^m.0$. This model prediction is shown in figure 4H.

There is an inconsistency that these star counts are fitted by an extinction value almost three times that needed to explain the other six regions in the plane. How can there be a high interstellar extinction in one direction and a constant value elsewhere in a generally axisymmetric Galaxy? This high extinction value need not be uniformly distributed along the line of sight. Since these star counts seem to be dominated by the dense core then the actual distribution of extinction is unimportant, so long as the majority of the obscuration occurs outside the very centre. There is evidence to suggest that over the central few parsecs the extinction is low and uniform. Gatley et al.³² deduced that this is the case by mapping the nucleus simultaneously at three infrared wavelengths (30, 50 and 100 microns) out to a radius of 15 pc. In contrast the stellar density falls by a factor of more than 100 between 1 and 15 pc ($\rho \propto r^{-1.8}$) Kobayashi et al.³³ found that for the central $7' \times 7'$ ($15 \times 15 \text{ pc}$, $r_0 = 8000 \text{ pc}$), the polarisations are almost uniform in their amplitudes as well as their directions, indicating that they are generated by dust outside the galactic core region. The radial extinction model with $0^m.05 \text{ kpc}^{-1}$ at the Sun, which reasonably fitted the disc counts, predicts too little extinction for the centre count. With $0^m.1 \text{ kpc}^{-1}$ at the Sun this model predicts too much extinction.

The star counts can give very little information on how the extinction to the nucleus is distributed along the line of sight. The low observed counts at $7^m.0$ and $7^m.5$ seem to be explained by the cloud of extinction at 1700 pc. Oda et al.³⁴ deduced from the 2.4 micron

distribution that about one-third of the total extinction to the nucleus occurs in the central 300 pc, with the other two-thirds occurring in the disc. If this were so then the uniform extinction needed to fit the observed star counts could be reduced to under $0^m.2 \text{ kpc}^{-1}$, more in line with the $0^m.1 \text{ kpc}^{-1}$ needed to fit the disc counts.

Even with all of these considerations the fit of the model to the observed count for the 0^0 region is not ideal. The region observed only samples a small section of the galactic core which is known to be complicated. The quality of the data is not good enough to justify consideration of fine structure.

Of course this discussion is complicated if some or all of the density increase occurs along the path length to the centre. The density enhancement implied by Maihara et al.²⁹ midway between the Sun and the galactic centre has little effect on the observed star counts if it is just a ten times increase. If the density increase producing the steepening of the star counts is due to the nucleus then the flux predicted by the model should be of the order of that observed. Becklin and Neugebauer² measured in a 1 arcminute beam centred on their source 7 a flux of $9.3 \times 10^{-9} \text{ W cm}^{-2} \mu^{-1} \text{ sr}^{-1}$. Ito et al.⁸ measured a flux of $1.8 \times 10^{-9} \text{ W cm}^{-2} \mu^{-1} \text{ sr}^{-1}$ in their much larger 2^0 beam. Using the model which best fitted the star counts ($r^{-1.8}$ density in the core and $3^m.0$ of extinction to the centre) and extrapolating the model to an apparent magnitude of $20^m.0$ ($M = +3$ at the centre) the predicted flux is $44.1 \times 10^{-10} \text{ W cm}^{-2} \mu^{-1} \text{ sr}^{-1}$ which is double that seen by Ito et al.⁸ Beyond this magnitude the model flux increases by about $3 \times 10^{-10} \text{ W cm}^{-2} \mu^{-1} \text{ sr}^{-1}$ per magnitude interval. This predicted flux is less than the integrated flux seen by Becklin and Neugebauer which might be expected if even fainter stars are still significant and

if the Becklin and Neugebauer result contains flux from non-stellar sources.

The requirement that the large density enhancement needed to explain the steep star counts should occur in a small space, means that if this does occur outside the galactic centre then a very unusual region must exist, by chance lying in the line of sight to the nucleus. It seems certain that the star counts are under the influence of the dense core of the Galaxy.

CONCLUSIONS

Infrared star counts in the plane of the Galaxy have been presented and are seen to fit in with the structure of the Galaxy derived from different techniques. Away from the nucleus in the plane, the star counts can be described by a simple exponential disc model. At 30° where the line of sight is tangential to a ring of molecular clouds, this disc population appears to be supplemented by an increase in density of late-type giants. Towards the galactic centre the extinction at 2.2 microns is low enough for the dense core to be seen in the star counts; these dominating the star counts from the disc population.

Chapter 4

REFERENCES

1. Neckel, T. and Klare, G., 1980. *Astron. Astrophys. Suppl.* 42, 251.
2. Becklin, E.E. and Neugebauer, G., 1968. *Astrophys. J.* 151, 145.
3. Becklin, E.E., Mathews, K., Neugebauer, G. and Willner, S.D.,
1978. *Astrophys. J.* 220, 831.
4. Allen, C.W., 1973. *Astrophysical Quantities*, Athlone Press, London.
5. Elias, J.H., 1978. *Astrophys. J.* 223, 859.
6. Becklin, E.E. and Neugebauer, G., 1975. *Astrophys. J.* 200, L71.
7. Becklin, E.E. and Neugebauer, G., 1978. *Publ. astr. Soc. Pacif.*
90, 657.
8. Ito, K., Matsumoto, T. and Uyama, K., 1977. *Nature* 265, 517.
9. Okuda, H., Maihara, T., Oda, N. and Sugiyama, T., 1977.
Nature, 265, 515.
10. Grasdalen, G.L., Strom, K.M. and Strom, S.E., 1973. *Astrophys.*
J. 184, L53.
11. Strom, K.M., Strom, S.E. and Vrba, F.J., 1976. *Astron. J.* 81, 308.
12. Strom, S.E., Vrba, F.J. and Strom, K.M., 1976. *Astron. J.* 81, 314.
13. Vrba, F.J., Strom, S.E. and Strom, K.M., 1976. *Astron. J.* 81, 317.
14. Elias, J.H., 1978. *Astrophys. J.* 224, 453.
15. Elias, J.H., 1978. *Astrophys. J.* 224, 857.
16. Jones, T.J., Hyland, A.R., Robinson, G., Smith, R. and Thomas, J.
1980. *Astrophys. J.* 242, 132.
17. Reike, G.H. and Low, F.J., 1973. *Astrophys. J.* 184, 415.
18. Abolins, J., 1980. Ph.D. Thesis, Leicester University.
19. Sherrington, M., 1980. Ph.D. Thesis, Leicester University.
20. Johnson, H.L., Mitchell, R.I., Iriarte, B. and Wisniewski, W.Z.,
1966. *Lun. Plan. Lab. Comm.* 4, 99.

21. Glass, I.S., 1974. Mon. Notes. astr. Soc. Sth. Afr. 33, 53.
22. Trumpler, R.J. and Weaver, H.F., 1953. Statistical Astronomy,
Dover Publications, New York.
23. Giles, A.B., 1981. Mon.Not.R.astr.Soc., in press.
24. Hayakawa, S., Matsumoto, T., Murakami, H., Uyama, K., Thomas,
J.A. and Yamagami, T., 1981. Astron. Astrophys. 100, 116.
25. Bailey, M.E., 1980. Mon.Not.R.astr.Soc. 190, 217.
26. Bahcall, J.N. and Soneira, R.M., 1980. Astrophys. J. Suppl.
39, 411.
27. Johnson, H.L., 1966. Ann. Rev. Astr. Astrophys. 4, 193.
28. Bok, B.J. and Bok, P.F., 1974. The Milky Way, Harvard Univ.
Press, Cambridge, Mass.
29. Maihara, T., Oda, N., Sugiyama, T. and Okuda, H., 1978.
Publ. astr. Soc. Japan 30, 1.
30. Puget, J.L., Serra, G. and Ryter, C., 1978. In IAU Symp. No.
84, Large scale characteristics of the Galaxy, ed.
W.G. Burton, Reidel, Dordrecht Holland, p.105.
31. Oort, J.H., 1977. Ann. Rev. Astr. Astrophys. 15, 295.
32. Gatley, I., Becklin, E.E., Werner, M.W. and Wynn;Williams, C.G.,
1977. Astrophys. J. 216, 277.
33. Kobayashi, Y., Kawara, K., Kozasa, T., Sato, S. and Okuda, H.,
1980. Publ. Astron. Soc. Japan 32, 291.
34. Oda, N., Maihara, T., Sugiyama, T. and Okuda, H., 1979.
Astron. Astrophys. 72, 309.

5

CHAPTER 5

OBSCURED SOURCES IN THE GALACTIC PLANE

DISCOVERY

The plane of the Galaxy at 30° longitude shows some interesting properties. The line of sight is tangential to a ring of high density molecular clouds¹ where the γ -ray production rate² and the H166 α recombination line^{3,4} are particularly high. In the far infrared a maximum of emission is found in this direction^{5,6} and at 2.4 microns there is a plateau of emission extending out to 30 degrees.^{7,8} Puget et al.⁹ attribute this 2.4 micron distribution to massive red giants associated with regions of rapid star formation in a ring midway between the Sun and the galactic centre.

In conjunction with the acquisition of infrared star counts, the Tenerife observations of May 1980 gave the opportunity for studying a region in the 30° direction in the hope of finding some evidence for these unusual properties. The star counts for this region (figure 4L) show indications of an excess of bright infrared sources. A map of the sources brighter than $10^m.0$ is shown in figure 4T. One particularly prominent cluster of sources shows up near the centre of the scanned area. An opportunity to investigate this cluster arose in May 1981 at Tenerife. In this session infrared and optical photometry of individual stars was performed.

PHOTOMETRY

The observations were made using the Leicester Mark I photometer in dual channel mode (see figure 4D). The light from the telescope is split into infrared and optical components by the dichroic mirror. The reflected infrared radiation is then chopped before entering the dewar. The transmitted optical radiation is passed through an aperture and filter onto the photomultiplier tube (EMI 9502S). Mandy Sherrington in her Ph.D. thesis¹⁰ describes the construction and

setting up of this equipment.

The photometry was done using the standard dual beam switching technique, where the source is alternately measured in the positive and negative infrared beams. In this way the optical channel looks alternately at the source and blank sky.

The map produced from the star count scans did not have the spatial resolution to pinpoint the objects of interest, and so the telescope was moved around the area until any of the bright 2.2 micron sources was seen in the preamplifier output on the oscilloscope. When a source had been centred in a 2 mm circular aperture (22 arc-seconds), and checked for no negative beam contamination, it was measured at four wavelengths V, J, H and K (0.55, 1.2, 1.6 and 2.2 microns). Only one of the eight cluster sources (star 4) had a measurable V brightness. (1σ in 10 seconds at V was measured at 17.7 magnitudes, which is fainter than can be seen by eye at Tenerife). Table 5I lists the photometry of the sources and the corresponding infrared colours. Infrared calibrations were from Johnson's list of standards.¹¹ Visible calibrations were from the list of Neckel and Chini.¹² Stars 7 and 8 were measured by Andy Longmore (ROE) and Mandy Sherrington (Leicester) on a subsequent visit. The numbering of the sources was determined by the order of measurement. Star 0 is not part of the cluster, but an obscured source 15 arcseconds north of SAO 142588. It was accidentally discovered because this star was used as the origin for the star count scans.

To ascertain the positions of these stars, the eyepiece field was checked against a photograph from a Palomar survey red plate, and then marked. Back in Leicester these positions were compared with an I plate (0.9 microns) of the UK Schmidt galactic plane survey on which all the sources showed up. The positions listed in table 5I are

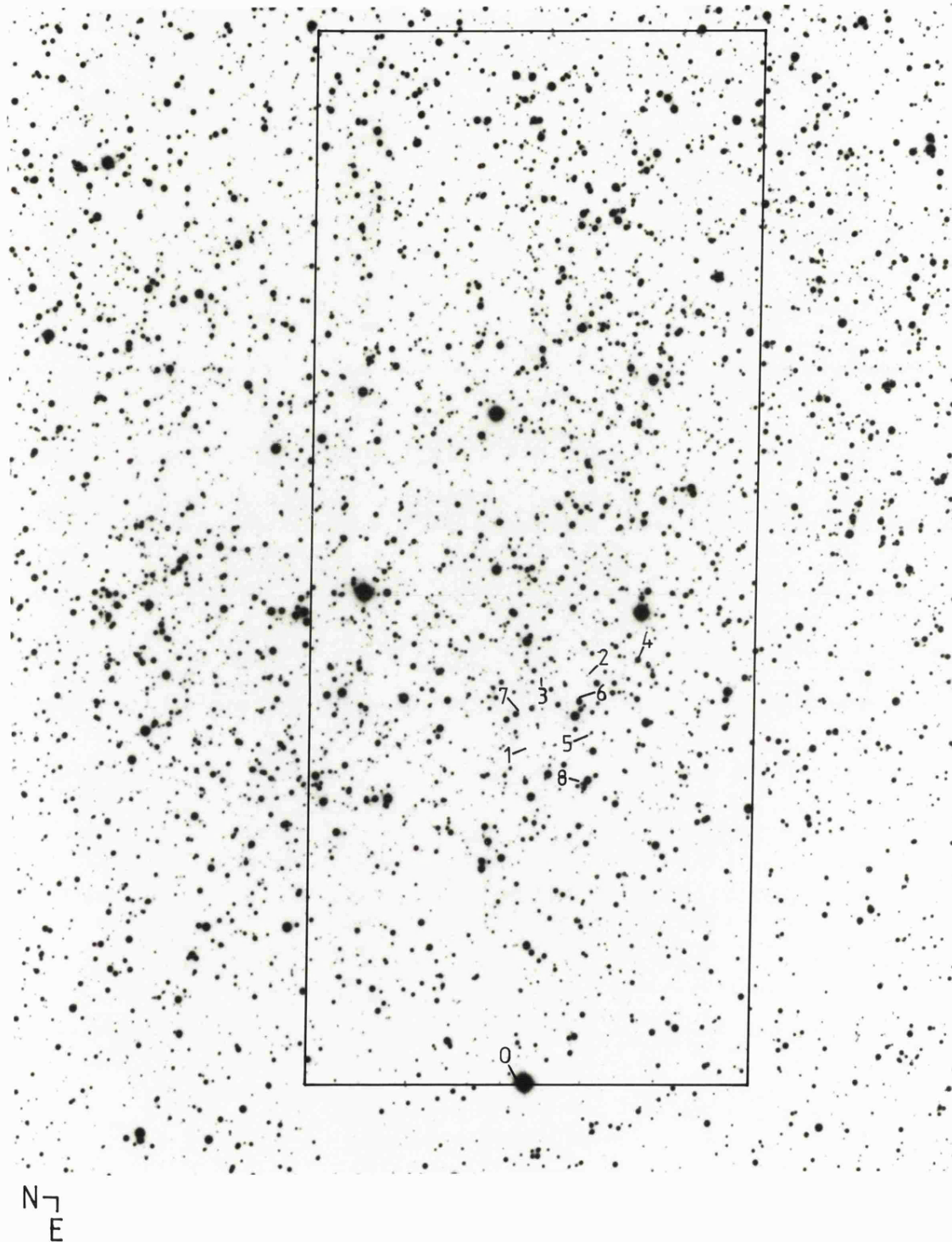


Fig. 5A Finding chart for the obscured sources in the 30° region (see table 5I). The box indicates the limits of the infrared star count scans (see page 4.7).

TABLE 51

JHK PHOTOMETRY OF THE OBSCURED SOURCES

Object	RA 1950	DEC 1950	V	J	J-H	H-K
SAO 142541	18 ^h 40 ^m 40 ^s .5	-3 ^o 14' 20"	8.5*			
SAO 142569	18 ^h 41 ^m 53 ^s .6	-3 ^o 12' 19"	8.5*			
SAO 142570	18 ^h 41 ^m 55 ^s .4	-3 ^o 20' 13"	8.8*			
SAO 142588	18 ^h 42 ^m 49 ^s .2	-3 ^o 17' 5"	8.1*			
Star 0	18 ^h 42 ^m 49 ^s .1	-3 ^o 16' 52"		8.21	2.37 ± .02	1.08 ± .02
Star 1	18 ^h 42 ^m 10 ^s .8	-3 ^o 16' 56"		9.39	1.88	0.82
Star 2	18 ^h 42 ^m 2 ^s .6	-3 ^o 18' 39"		7.39	1.79	0.88
Star 3	18 ^h 42 ^m 3 ^s .0	-3 ^o 17' 19"		8.33	1.95	0.88
Star 4	18 ^h 42 ^m 00 ^s .9	-3 ^o 20' 2"	15.96 ± .05	7.54	1.32	0.61
Star 5	18 ^h 42 ^m 9 ^s .3	-3 ^o 18' 39"		8.82	1.63	1.33
Star 6	18 ^h 42 ^m 5 ^s .2	-3 ^o 18' 23"		9.50 ± .01	1.94 ± .02	0.77 ± .03
Star 7	18 ^h 42 ^m 7 ^s .8	-3 ^o 16' 23"		9.09 ± .02	2.53 ± .02	1.14
Star 8	18 ^h 42 ^m 14 ^s .7	-3 ^o 18' 41"		9.97 ± .02	2.48 ± .03	1.11 ± .02

positions of stars
accurate to 10 arcsec

* from SAO
catalogue

where no error is quoted it
is better than .01

measured from this I plate based on positions of nearby SAO stars.

Figure 5A reproduces the Palomar red plate on which the positions of the sources have been marked, plus the extent of the star count area.

Below are listed details of the sources.

Star 0 - 15 arcseconds north of SAO 142588. Not part of the cluster.

Star 2 - brightest K magnitude of the cluster sources.

Star 4 - measurable visual magnitude.

Star 6 - 7 arcseconds west of visible star.

Star 7 - not coincident with visible star.

Star 8 - 10 arcseconds north of visible star.

DISCUSSION

A two colour diagram (J - H versus H - K) of the stars is shown in figure 5B. The points are plotted on a simplified diagram from Jones and Hyland¹³ (their figure 1). The curved line with letters gives the position in the two-colour diagram for unreddened stars, and the solid line is the reddening line with a gradient of 2.09. All but one of the sources (star 5) lie on this reddening line. Star 5 has an infrared excess which could be due to circumstellar dust or maybe free-free emission. Apart from star 4, which has the measurable visible magnitude, the remainder of the stars fall into two groups on the reddening line. Stars 1, 2, 3 and 6 have an excess $E(J - H)$ of about 0.9 from the end of the unreddened curve, and stars 0, 7 and 8 have an excess $E(J - H)$ of about 1.4 from the end of this curve.

From the position on this reddening line a lower limit to the total visual extinction can be estimated, by assuming that the least reddening occurs for M stars (giants or supergiants) occupying the

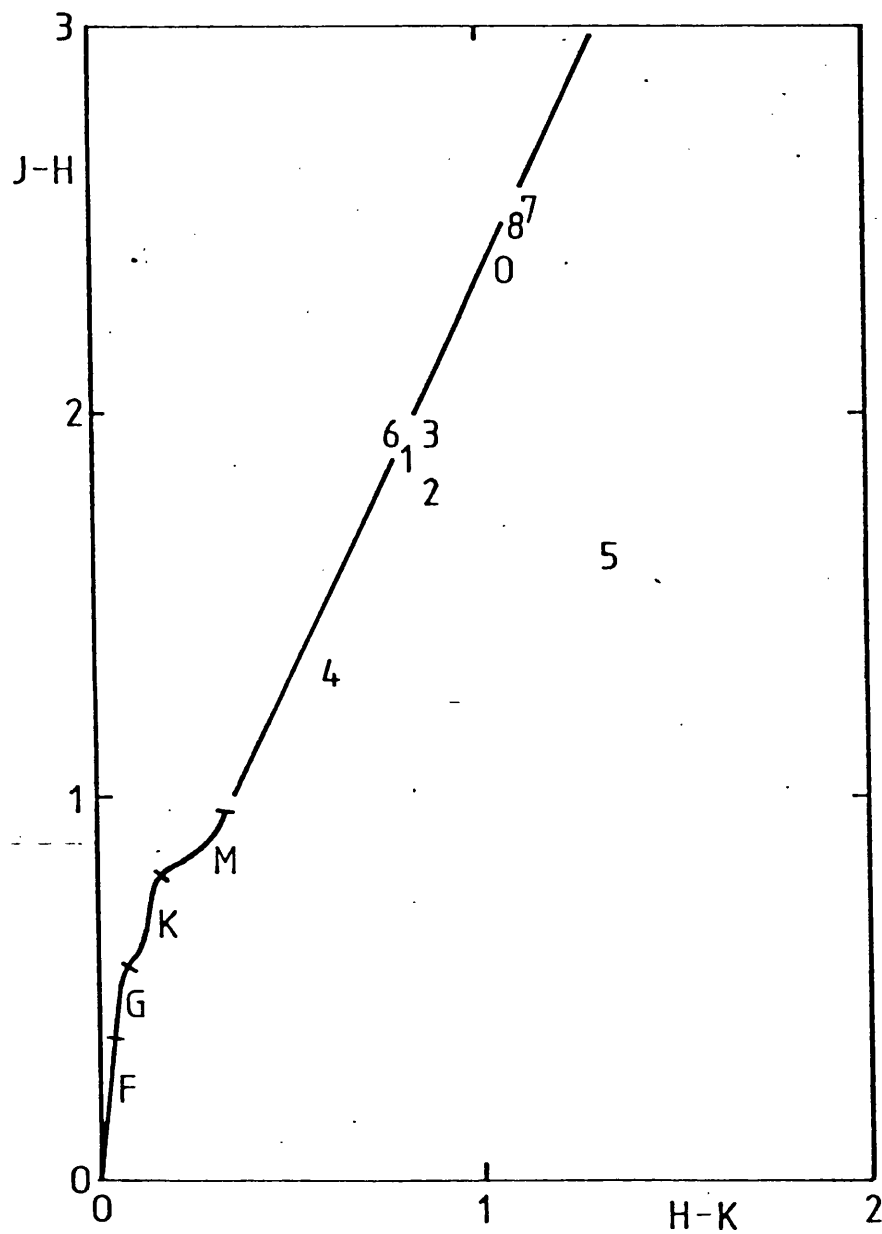


Fig. 5B The two colour diagram (J-H, H-K) of the 'cluster' sources. The curved line with letters shows the position of unreddened stars. The straight line is the reddening line with a gradient of 2.09 (ref. 13).

position marked M on the two colour plot. The standard van de Hulst extinction law¹⁴ (figure 1C) gives the colour excesses for stars.

These are listed below.

	Colour excess ratio
E_{V-R}/E_{B-V}	0.80
E_{V-I}/E_{B-V}	1.62
E_{V-J}/E_{B-V}	2.30
E_{V-H}/E_{B-V}	
E_{V-K}/E_{B-V}	2.78
E_{V-L}/E_{B-V}	2.91

From the observed J - K excess and the above list the visual colour excess E_{B-V} can be calculated

$$\begin{aligned}
 E_{J-K} &= E_{V-K} - E_{V-J} \\
 &= E_{B-V} (2.78 - 2.30) \\
 E_{J-K} &= 0.48 E_{B-V} \qquad (5.1)
 \end{aligned}$$

To work out the excess at J - K, the largest intrinsic J - K (the end of the M line) is taken as the 'worst' case. This gives a value of $(J - K)_{\text{intrinsic}} = 1.4$.

For stars 1, 2, 3, 6 $(J - K)_{\text{observed}} \approx 2.7$

$$E_{J-K} = (J - K)_{\text{observed}} - (J - K)_{\text{intrinsic}}$$

$$\therefore E_{J-K} = 1.3$$

From equation (5.1) $E_{B-V} = E_{J-K}/0.48$

Finally to obtain the visual extinction the equation

$$A_V = R \times E_{B-V}$$

is employed, where A_V is the total visual extinction and R is the ratio of total to selective extinction. Assuming a standard value for $R = 3.1$, this gives an extinction for stars 1, 2, 3 and 6 of

$$A_V = 8.4 \text{ magnitudes.}$$

For stars 0, 7, 8 $(J - K)_{\text{observed}} \approx 3.5$

$$\therefore E_{J-K} = 2.1$$

and $A_V = 13.6$ magnitudes.

If these stars belong to the tangential ring then their distance will be about 5000 to 6000 pc ($r_\phi = 8000$ pc). Assuming a distance of 5000 pc and the extinctions from above, this implies that the stars would have to have absolute K magnitudes of

star	M_K
0	-10.1
1	- 7.6
2	- 9.6
3	- 8.8
6	- 7.5
7	- 9.4
8	- 8.5

Stars of this order of absolute magnitude would have to be very late type giants M6III or later¹⁵ or supergiants.^{16,17}

To further the study of these obscured sources, Andy Longmore kindly measured some of the stars with the infrared circular variable filter (CVF) between wavelengths 1.97 and 2.4 microns on the 3.8m UK

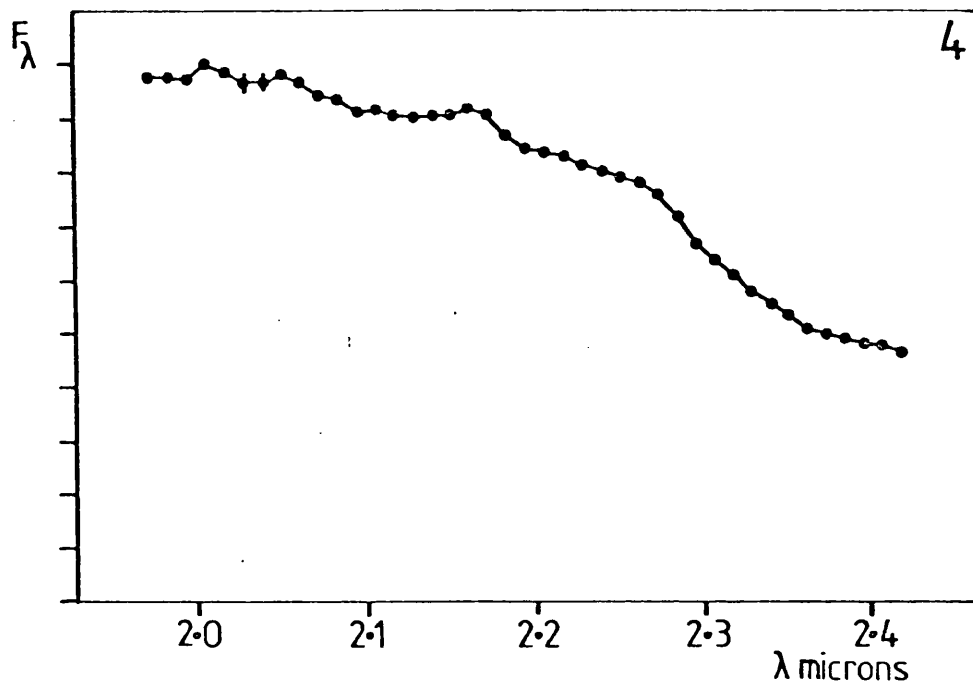


Fig. 5E The 2.0-2.4 micron spectrum of star 4. The CO absorption is apparent beyond 2.3 microns.

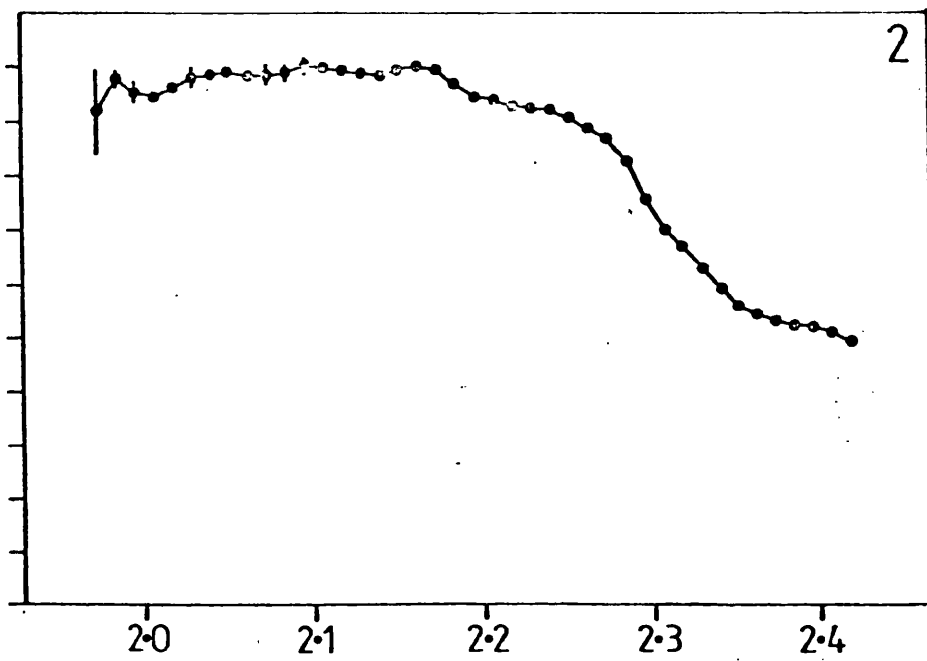


Fig. 5F The 2.0-2.4 micron spectrum of star 2.

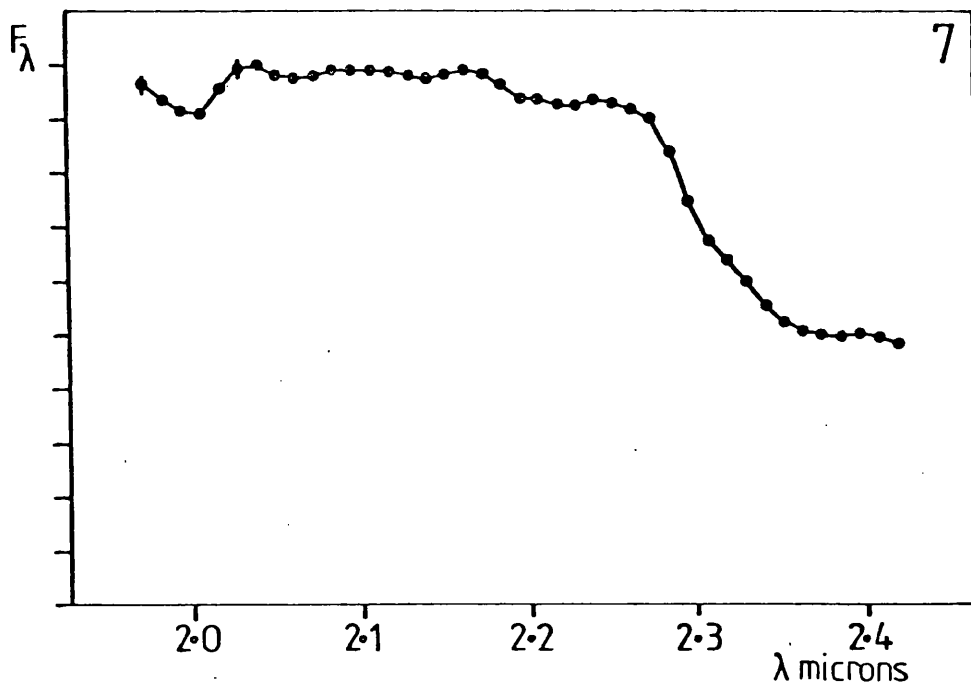


Fig. 5G The 2.0-2.4 micron spectrum of star 7. The CO absorption is apparent beyond 2.3 microns.

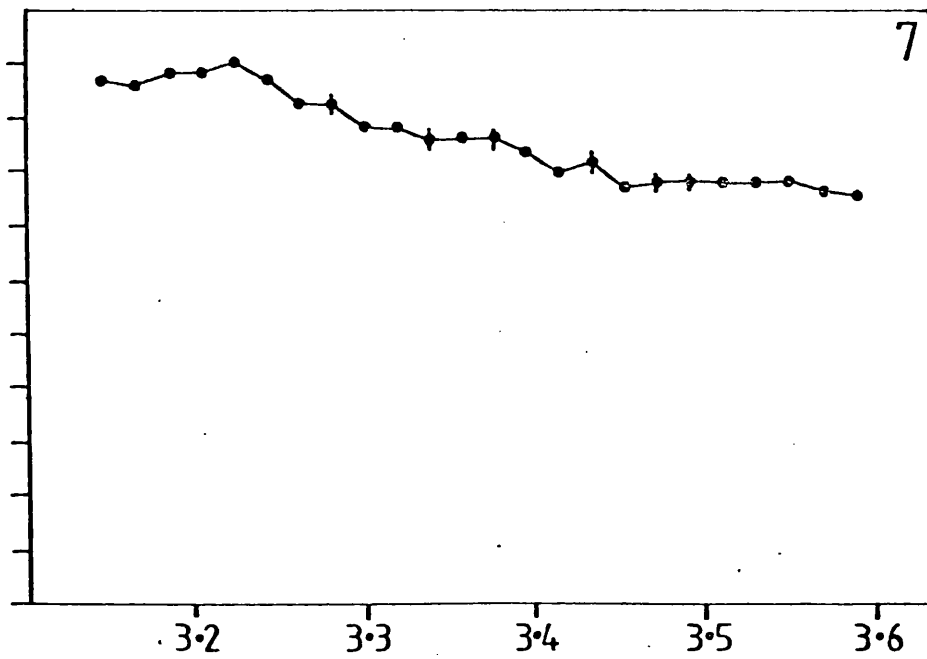


Fig. 5H The 3.2-3.6 micron spectrum of star 7.

infrared telescope on Hawaii. He reports (private communication) that for the three stars measured (2, 4 and 7) all have strong 2.3 micron CO features¹⁸ and are probably supergiants rather than giants, although this is by no means certain. The types are approximately M2⁺²₋₁ with 7 later than 2 later than 4. The spectrum of star 7 between 3.14 and 3.59 microns is essentially flat which confirms that it is not a carbon star.

It would be very tempting to say that these stars are physically associated in an obscured, evolved cluster. One problem is that stars 7 and 8, which appear to be part of the association are much more heavily reddened than stars 1, 2, 3 and 6. Star 4 is less reddened and star 5 is an unusual source. Stars 1, 2, 3 and 6 are thus the strongest candidates for a true cluster. What is the chance of this cluster being made up of a line of sight positioning of sources? The 'cluster' members were chosen on the grounds of their bright K magnitudes, all the sources are brighter than $M_K = 7.0$. The 'cluster' size is approximately four arcminutes square or 1/225 of a square degree. Taking the observed number of stars per square degree in this direction brighter than $M_K = 7$, including these sources, as a generous case, that is 365 per square degree, the mean number of stars in a 4' x 4' square is 1.62. Using a random Poisson distribution then the chance of 8 sources in this area is approximately 1/7000. If the disc model (see Chapter 4) with 0.1 magnitudes per kpc of extinction is used to predict the number of stars, then this gives a mean number in the 4' x 4' square of $156/225 = 0.69$ and the Poisson distribution predicts that the chances of 8 sources occurring in this square is over one in a million.

If stars 1, 2, 3 and 6 are associated and the other four stars

are randomly distributed then the odds against this for the two star counts considered are 1/50 for the generous case and 1/1500 for the disc model prediction.

These 'cluster' sources are also unusual, over the area scanned, in that they are among the very few bright infrared sources without visible counterparts. This can be shown by the overlay technique described in the next section. See figure 5C.

The arguments posed seem to disagree on the question of membership of the cluster. The association of the 8 bright sources, the fact that only one has a visible counterpart and the scarcity of such heavily obscured sources in this area, suggest that these are related. The infrared colours showing that 4 of the 8 are distinct, suggests that the association is a chance alignment. A unifying theory would be of a genuine cluster with heavy internal extinction. The active conditions in the 30° direction enhances the odds of such a cluster occurring.

THE V - I OVERLAY

The discovery of the obscured cluster in the 30° region was very much a matter of chance. The initial discovery came from the map of the star count sources which showed up a region of bright stars grouped together (see figure 4T). This map took over three hours of telescope time to produce, not including the time to set up the scans and to calibrate, and many more hours of analysis back at Leicester. Mapping with a telescope in search for bright infrared stars is time consuming. Depending on the purpose of the project, the use of near-infrared Schmidt plates could produce comparable results for large areas in a more efficient way.

The Palomar and UK Schmidt near-infrared surveys of the Milky Way can be combined with the visual surveys to show up stars with large V - I colours. It is necessary that one of the plates is the negative of the other so that stars which appear on both plates cancel into grey, and stars which only appear on one stand out. The negative could be produced photographically or electronically in a camera viewing system. A viewing system where both plates are viewed together is needed, such as a blink comparator. Horner and Craine¹⁹ used this technique to search error boxes of some IRC (infrared catalogue) sources for identification.

At a less professional level the overlay technique can be set up using photographic equipment. A simple method is to photograph a small section of both Schmidt plates. The photographic negatives have white stars on black sky. From one of these negatives (preferably the visible plate) a normal print is made. The print has black stars on a white sky, like the Schmidt plates. This print is placed under a photographic enlarger, with the other plate (the near infrared) negative in the holder. The negative is projected onto the print, and the enlarger magnification is adjusted until the two plates match. Now any stars which appear on the near infrared plate and not on the visible will show up as white dots, while the sky background, and stars appearing on both plates will cancel into grey. A star much brighter in the infrared but still visible will appear as a white annulus.

For presentation in this thesis, a refinement of this photographic technique is needed. From the negatives in the two colours, large scale transparencies were produced having the same scale. The visible plate had black stars on clear film, and the infrared plate had clear stars on black sky. These two transparencies were overlaid on a light table, and another picture of the combined field was taken,

from which prints could be made. This technique was used to produce the photographs of the 0° and 30° regions in figures 5D and 5C. It can be seen that on both diagrams, the registration between the two plates is not perfect; the visible plate being slightly smaller than the I plate. Around the edges of the pictures the stars are not properly aligned. This is due to the difficulty of perfectly matching the two plate sizes when producing the transparencies.

THE OBSCURED CLUSTER IN V - I

Shown in figure 5C is the V - I overlay for the 30° region containing the obscured cluster. The cluster appears slightly up and right of the centre of the diagram. The large white mark up and left of the centre is caused by a blemish on the I plate. The cluster members can be identified from the finder chart of figure 5A. Sources 1, 2, 3 and 5 are particularly prominent on this picture. In the area covered by the picture ($\sim 2/3$ of the infrared star count box) there are no sources which stand out as clearly as some of the cluster sources.

This technique seems ideal for finding late type stars ($V - I_{\text{int}} > 2$) behind a cloud of about 8 magnitudes of visual extinction (giving a 4 magnitude advantage in I over V) so that V - I is about 6 magnitudes or more. More extinction will give a greater V - I, but such stars are likely to be more distant, and on top of the increased obscuration will probably be too faint on the I plate to stand out prominently. This is the case for star 7 of the measured sources. Its K magnitude is slightly brighter than star 3, but its image on the I plate and the V - I overlay is much less prominent. (Star 7 is just south and west of a star, seen on both plates, about 1 cm north and east of star 3 in figure 5C).

This overlay technique may be of use for identifying some of the IRAS (Infrared Astronomical Satellite) sources. The shortest wavelength observable by the satellite is in the 5 to 8 micron Short Wavelength Channel (SWC). This instrument has a small field of view (15 arcseconds, an equivalent beam area to our galactic centre observations) and so should not be too confused in the galactic plane.

THE GALACTIC CENTRE IN V - I

Shown in figure 5D is the V - I overlay for the 0° region, including the line of sight to the galactic centre, and covering about 2/3 of the infrared star count box. The galactic centre direction is in the top right sector about $6\frac{1}{2}$ cm from the top of the picture and about $2\frac{1}{2}$ cm from the right hand edge. The apparent increase in infrared stars to the right of the picture is due to a deterioration of image quality on the V overlay transparency, making the I stars stand out.

This region shows a number of very red stars, and invisible stars scattered over the area. For late type stars the difference in V - I behind 8 magnitudes of extinction (see Chapter 3) is about 6 magnitudes or more. The overlay technique in this direction could possibly be used to obtain star counts behind the obscuring cloud.

With 27 magnitudes of visual extinction and 13 magnitudes at I to the galactic centre, the dense nucleus is not seen with this technique, but star counts at I could reach the '5 kpc ring' to see if there is an increase in the density of stars, over the disc population as postulated by Maihara et al.

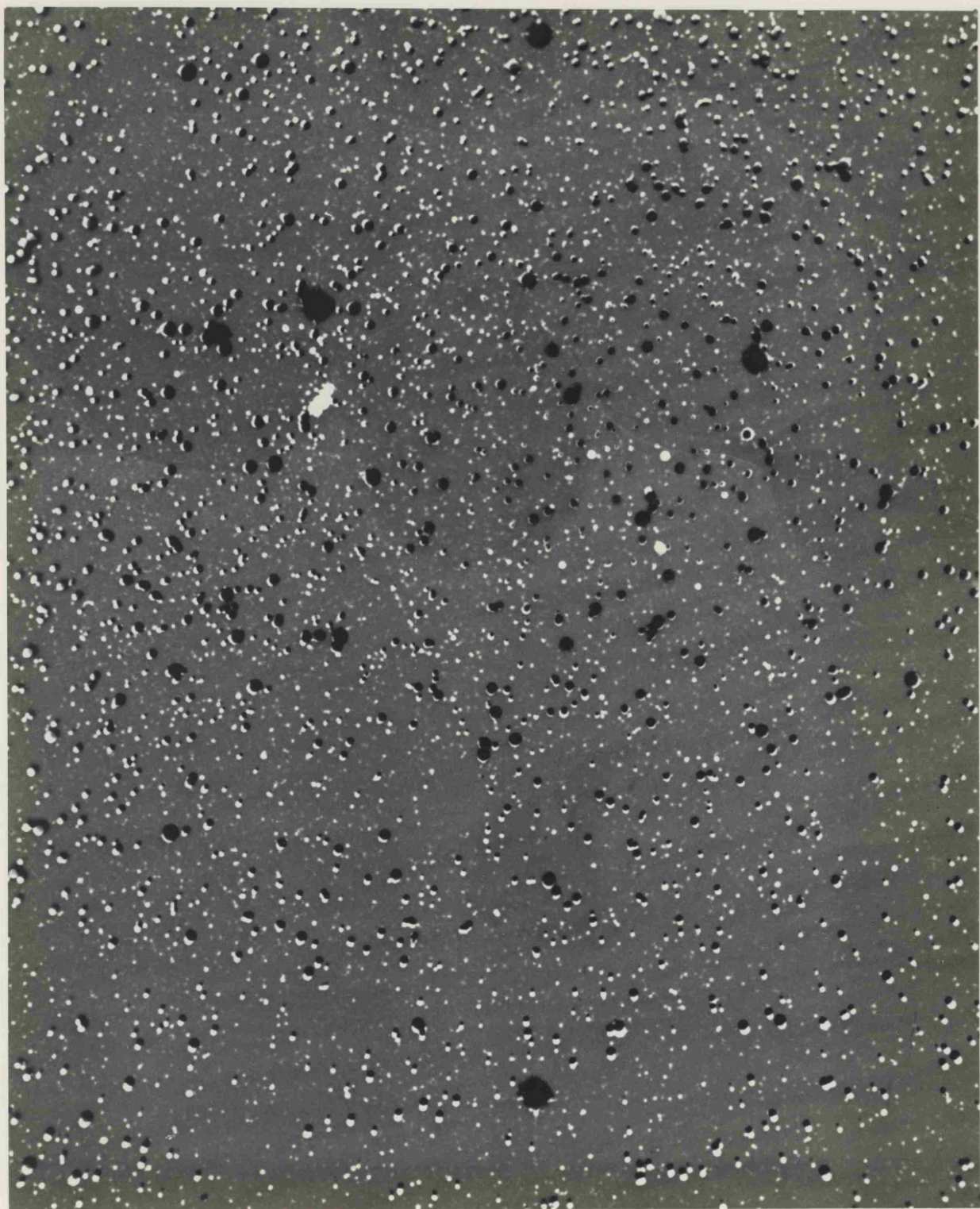


Fig. 5C The V-I overlay for the 30° region. The V plate is shown by black stars, and the I plate by white. Figure 5A indicates the observed sources (see page 5.9).

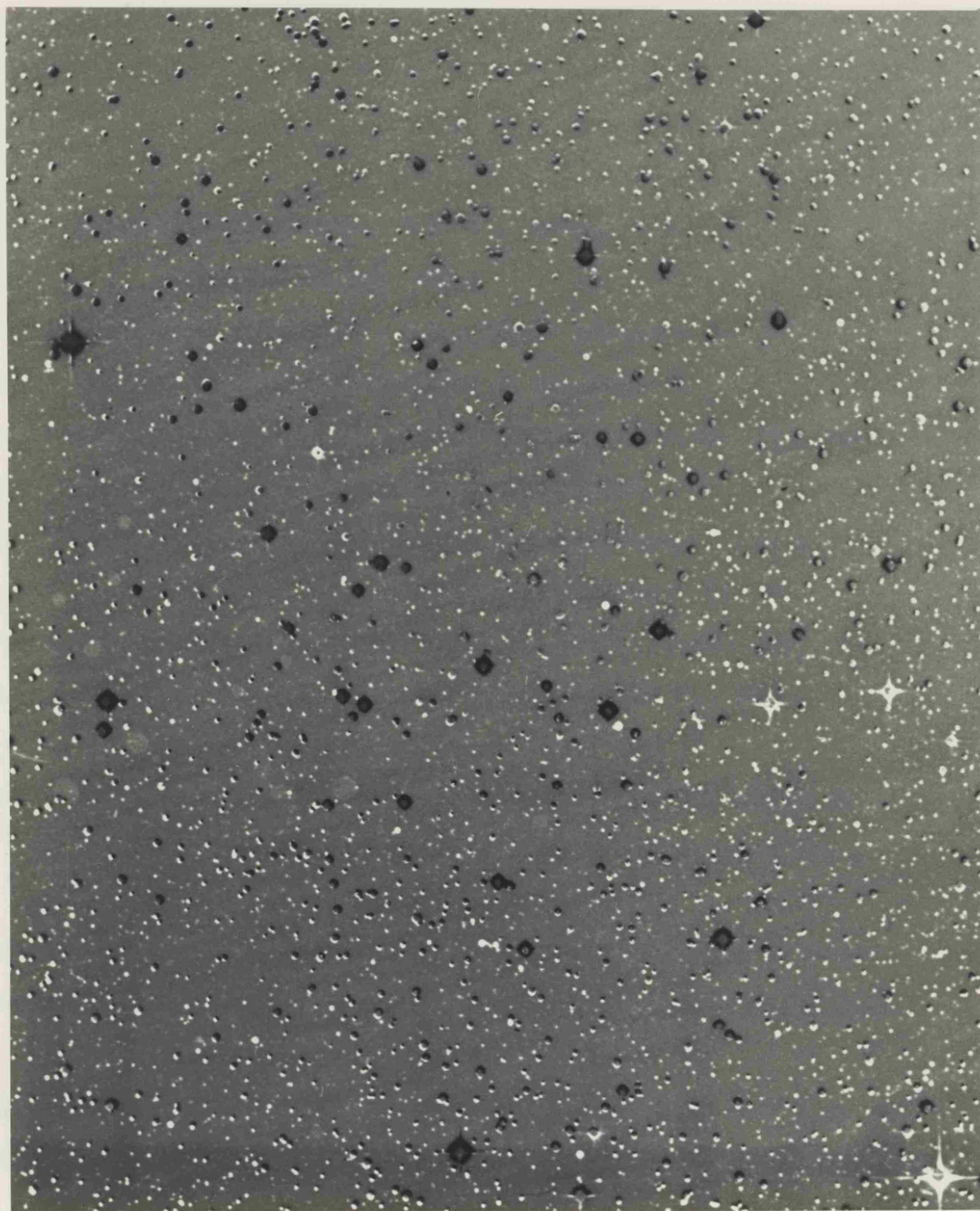


Fig. 5D The V-I overlay for the 0° region. The V plate is shown by black stars, and the I plate by white (see page 5.10).

Chapter 5

REFERENCES

1. Solomon, P.M., Scoville, N.Z. and Sanders, D.B., 1979.
Astrophys. J. 232, L89.
2. Puget, J.L. and Stecker, F.W., 1974. Astrophys. J. 191, 323.
3. Lockman, F.J. 1976. Astrophys. J. 209, 429.
4. Hart, L. and Pedlar, A., 1976. Mon.Not.R.astr.Soc. 176, 547.
5. Drapatz, S., 1979. Astr. Astrophys. 75, 26.
6. Serra, G., Boisse, P., Gispert, R., Wijnbergen, J., Ryter, C.
and Puget, J.L., 1979. Astr. Astrophys. 76, 259.
7. Ito, K., Matsumoto, T. and Uyama, K., 1977. Nature 265, 517.
8. Okuda, H., Maihara, T., Oda, N. and Sugiyama, T., 1977.
Nature 265, 515.
9. Puget, J.L., Serra, G. and Ryter, C., 1978. In IAU Symp. No.
84 'Large scale characteristics of the Galaxy', ed.
W.G. Burton, Reidel, Dordrecht, p.105.
10. Sherrington, M., 1980. Ph.D. Thesis, University of Leicester.
11. Johnson, H.L., Mitchell, R.I., Iriarte, B. and Wisniewski, W.Z.,
1966. Lun. Plan. Lab. Comm. 4, 99.
12. Neckel, T. and Chini, R., 1980. Astr. Astrophys. Suppl. 39, 411.
13. Jones, T.J. and Hyland, A.R., 1980. Mon.Not.R.astr.Soc. 192, 359.
14. Johnson, H.L., 1968. In 'Nebulae and Interstellar Matter', eds.
B.M. Middlehurst and L.H. Aller, Univ. of Chicago, Chicago.
15. Elias, J.H., 1978. Astrophys. J. 223, 859.
16. Allen, C.W., 1973. Astrophysical Quantities, Athlone Press, London.
17. Lee, T.A., 1970. Astrophys. J. 162, 217.
18. Baldwin, J.R., Frogel, J.A. and Persson, S.E., 1973. Astrophys.
J. 184, 427.

19. Horner, V.M. and Craine, E.R., 1980. Publ. Astron. Soc. Pacific 92, 209.
20. Maihara, T., Oda, N., Sugiyama, T., Okuda, H., 1978. Publ. Astron. Soc. Japan 30, 1.

APPENDIX A

All the sources detected from the infrared scanning are listed by region and scan. The information at the top of each list indicates the right ascension of the first and last integration bin of a scan, and the declination of the centre of the top and bottom scan. A source is identified by its position, given by the integration bin corresponding to the positive peak, and its K magnitude. The scans are listed from south to north, each scan separated by a negative number.

608 numbers = 29.9 arcminutes
 0 = 18h 42m 40.5
 608 = 18h 42m 40.5
 19 scans = 12.0 arcminutes
 scan 1 = 1.1
 scan 19 = 1.1

```

****
**
***
***
***
****
****
****
****
****

```

POSN	MAG	POSN	MAG
399	9.79	10	10.41
410	9.97	10	10.41
463	8.89	10	10.41
481	8.29	10	10.41
502	9.59	10	10.41
576	9.97	10	10.41
1133		10	10.41
53	9.83	10	10.41
77	8.19	10	10.41
161	10.74	10	10.41
169	9.70	10	10.41
205	7.98	10	10.41
238	8.33	10	10.41
249	8.29	10	10.41
281	8.30	10	10.41
294	7.33	10	10.41
322	8.14	10	10.41
373	8.14	10	10.41
406	8.53	10	10.41
448	8.14	10	10.41
467	8.30	10	10.41
470	9.58	10	10.41
485	9.53	10	10.41
516	8.14	10	10.41
571	8.14	10	10.41
599	9.97	10	10.41
14		10	10.41
1	8.7	10	10.41
70	8.88	10	10.41
100	9.48	10	10.41
135	8.33	10	10.41
157	8.14	10	10.41
163	8.14	10	10.41
221	8.53	10	10.41
226	7.47	10	10.41
251	8.48	10	10.41
278	8.14	10	10.41
478	8.33	10	10.41
542	8.00	10	10.41
559	8.53	10	10.41
622	8.53	10	10.41
74	8.53	10	10.41
15		10	10.41
8	10.14	10	10.41
21	9.97	10	10.41
57	8.88	10	10.41
87	8.34	10	10.41
107	8.22	10	10.41
119	7.44	10	10.41
154	9.14	10	10.41
164	8.32	10	10.41
184	7.33	10	10.41
257	9.53	10	10.41
285	7.71	10	10.41
315	8.29	10	10.41
403	8.26	10	10.41
407	8.55	10	10.41
417	8.59	10	10.41
432	8.97	10	10.41
447	8.26	10	10.41
448	8.97	10	10.41
584	8.97	10	10.41
597	8.97	10	10.41
116		10	10.41
1	9.90	10	10.41
11	8.22	10	10.41
40	8.53	10	10.41
53	8.15	10	10.41
71	8.22	10	10.41
90	8.00	10	10.41

Acknowledgements

I would firstly like to thank Dave Adams for giving the impetus to, and for supervising this work. I extend grateful thanks to Barry Giles, now halfway round the world, for his valuable contributions.

I am indebted to those who assisted with the observations: Phil Lawson, Andy Adamson, Richard Jameson, Mandy Sherrington and Andy Longmore. I would also like to thank the members of the Astronomy Department who made my term so enjoyable. To the Prof. I extend my condolences for asking me to stay on in a 'professional' capacity. The usual congratulations go to Norma Corby for an excellent typing job.

To the anonymous members of the UK Schmidt and COSMOS units of the Royal Observatory Edinburgh, I thank for their courteous and helpful assistance. The members of the Computer Lab. and the Central Photographic Unit at Leicester also deserve mention. Of course this thesis would never have begun but for the financial contributions of the Science Research Council.

I have a special regard for all those friends and acquaintances who have shared with me the last six years at Leicester.

Last but definitely not least go my heartfelt thanks to Enid and John, my parents. Not only did they conceive me, but gave moral and financial support to my education. Only time will tell if it was for the good.

N.E. March 1982

NICHOLAS EATON

INFRARED AND OPTICAL STAR COUNTS IN THE PLANE OF THE GALAXY

Infrared and optical star counts have been obtained to investigate the stellar distribution in the plane of the Galaxy. The discovery of an obscured infrared cluster of sources is presented and a search technique for finding such obscured sources using visible and near-infrared plates is discussed. The techniques and mathematical treatment of star counting are described and, as an introduction, a literature review of the galactic structure is given.

Optical star counts in a strip across the dark rift of the Galaxy, containing the line of sight to the galactic centre, indicate that the extinction in this direction starts to increase significantly at a distance of about 1500 pc, approximately at the distance of the Sagittarius arm. Counting the stars into resseau squares shows that the direction of the thickest extinction in the visible, for star counts to $18^m.0$, is not coincident with the plane of the Galaxy but about $+1^\circ$ in latitude away.

Infrared star counts at 2.2 microns have been obtained for seven regions, spaced at 10° intervals, in the galactic plane. Away from the nucleus the star counts seem to fit a simple exponential disc model. At a longitude of 30° where the line of sight is tangential to a ring of molecular clouds, the disc population appears to be supplemented by an increase in density of late-type giants. Towards the galactic centre the extinction at 2.2 microns is low enough for the dense core to be seen in the star counts, these dominating the star counts from the disc population.